USGS
science for a changing world

Prepared in cooperation with the U.S. Department of Energy, National Nuclear Security Administration Nevada Site Office, Office of Environmental Management, under Interagency Agreement DE-EM0004969

Permeable Groundwater Pathways and Tritium Migration Patterns from the HANDLEY Underground Nuclear Test, Pahute Mesa, Nevada

Scientific Investigations Report 2021–5032

U.S. Department of the Interior
U.S. Geological Survey

Cover. Pahute Mesa, looking northeast toward the Nevada National Security Site, Nevada. Photograph by Steven R. Reiner, U.S. Geological Survey, 2021.

Permeable Groundwater Pathways and Tritium Migration Patterns from the HANDLEY Underground Nuclear Test, Pahute Mesa, Nevada

By Tracie R. Jackson

Prepared in cooperation with the U.S. Department of Energy, National Nuclear Security Administration Nevada Site Office, Office of Environmental Management, under Interagency Agreement DE-EM0004969

Scientific Investigations Report 2021–5032

U.S. Department of the Interior
U.S. Geological Survey

U.S. Geological Survey, Reston, Virginia: 2021

Suggested citation:
Jackson, T.R., 2021, Permeable groundwater pathways and tritium migration patterns from the HANDLEY underground nuclear test, Pahute Mesa, Nevada: U.S. Geological Survey Scientific Investigations Report 2021–5032, 49 p., https://doi.org/10.3133/sir20215032.

Associated data for this publication:
Jackson, T.R., 2021, MODFLOW-2005 and MT3DMS models and supplemental data used to simulate groundwater flow and tritium transport from the HANDLEY underground nuclear test, Pahute Mesa, southern Nevada: U.S. Geological Survey data release, https://doi.org/10.5066/P9YRDQSN.

ISSN 2328-0328 (online)

Contents

Figures

Tables

Conversion Factors

U.S. customary units to International System of Units

Multiply	By	To obtain
	Length	
inch (in.)	25.4	millimeter (mm)
foot (ft)	0.3048	meter (m)
mile (mi)	1.609	kilometer (km)
	Area	
square foot (ft^2)	0.09290	square meter (m^2)
	Volume	
gallon (gal)	3.785	liter (L)
cubic foot (ft^3)	0.02832	cubic meter (m^3)
cubic mile (mi^3)	4.168	cubic kilometer (km^3)
	Flow rate	
gallon per minute (gal/min)	0.06309	liter per second (L/s)
cubic foot per day (ft^3/d)	0.02832	cubic meter per day (m^3/d)
acre-foot per year (acre-ft/yr)	1,233	cubic meter per year (m^3/yr)
	Velocity	
foot per day (ft/d)	0.3048	meter per day (m/d)
	Hydraulic conductivity	
foot per day (ft/d)	0.3048	meter per day (m/d)
	Hydraulic gradient	
foot per foot (ft/ft)	1	meter per meter (m/m)
	Transmissivity	
foot squared per day (ft^2/d)	0.09290	meter squared per day (m^2/d)
	Concentration	
grams per foot cubed (g/ft^3)	23,543.11	picocuries per liter

Temperature in degrees Fahrenheit (°F) may be converted to degrees Celsius (°C) as follows:

$$°C = (°F - 32) / 1.8.$$

Datums

Vertical coordinate information is referenced to the National Geodetic Vertical Datum of 1929 (NGVD 29).

Horizontal coordinate information is referenced to the North American Datum of 1983 (NAD 83).

Altitude, as used in this report, refers to distance above the vertical datum.

Supplemental Information

Transmissivity: The standard unit for transmissivity is cubic foot per day per square foot times foot of aquifer thickness ([ft^3/d]/ft^2)ft. In this report, the mathematically reduced form, foot squared per day (ft^2/d), is used for convenience.

Abbreviations

BFCU	Bullfrog confining unit
BRA	Belted Range aquifer
CHLFA5	Calico Hills lava flow aquifer #5
CHZCM	Calico Hills zeolitic composite unit
HSU	Hydrostratigraphic unit
LCA	lower carbonate aquifer
LPCU	lower Paintbrush confining unit
mBZ	modified brecciated zone
mCHLFA5	modified Calico Hills lava flow aquifer #5
mCHZCM	modified Calico Hills zeolitic composite unit
mHFM	modified hydrostratigraphic framework model
MODFLOW	U.S. Geological Survey modular finite-difference groundwater model
mPBRCUd	modified pre-Belted Range confining unit–deep
mPBRCUs	modified pre-Belted Range confining unit–shallow
mPBRLFA	modified pre-Belted Range lava flow aquifer
MT3DMS	three-dimensional multispecies transport model
mUPCUd	modified upper Paintbrush confining unit–deep
mUPCUs	modified upper Paintbrush confining unit–shallow
NNSS	Nevada National Security Site
PBRCM	pre-Belted Range composite unit
PEST	Parameter ESTimation code
PMOV	Pahute Mesa–Oasis Valley
PMOV HFM	Pahute Mesa–Oasis Valley hydrostratigraphic framework model
TCA	Tiva Canyon aquifer
TMLVTA	Timber Mountain lower vitric tuff aquifer
TMWTA	Timber Mountain welded tuff aquifer
UPCU	upper Paintbrush confining unit
USGS	U.S. Geological Survey
WLM	Water-level model

Permeable Groundwater Pathways and Tritium Migration Patterns from the HANDLEY Underground Nuclear Test, Pahute Mesa, Nevada

By Tracie R. Jackson

Abstract

The HANDLEY nuclear test was detonated at about 2,700 feet below the water table on March 26, 1970, in Pahute Mesa, south-central Nevada. Measured tritium concentrations in boreholes *ER-20-12* and *PM-3* indicate that a shallow tritium plume has migrated more than 1 mile (mi) downgradient from the HANDLEY test within a semi-perched aquifer and deeper tritium plumes have migrated 4.5 miles (mi) within underlying regional aquifers. Boreholes *ER-20-12* and *PM-3* are in an area of moderate-to-low transmissivity, but observation of tritium moving 4.5 mi within 40 years of the detonation indicates that high-transmissivity intervals exist. However, the location of these permeable pathways is unknown.

This report integrates geologic, hydrologic, and tritium data to infer the location of permeable pathways near and downgradient from the HANDLEY test. Numerical groundwater-flow and tritium-transport models were developed to estimate hydraulic and transport properties between the HANDLEY test and boreholes *ER-20-12* and *PM-3*. Recharge, hydraulic-conductivity, specific-yield, specific-storage, and effective-porosity distributions were estimated with the numerical models by fitting simulated water-level altitudes, vertical-head differences, aquifer-test transmissivities, tritium concentrations, and drawdowns in wells *PM-3-1* and *PM-3-2* to measured equivalents. Drawdowns were estimated in wells *PM-3-1* and *PM-3-2* in response to groundwater withdrawals during the drilling of borehole *ER-20-12*. A modified hydrostratigraphic framework model (mHFM) was developed that incorporates hydrostratigraphic units (HSUs) from the Pahute Mesa–Oasis Valley hydrostratigraphic framework model (PMOV HFM). HSUs in the mHFM were modified from the PMOV HFM by grouping HSUs that, conceptually, are hydraulically similar and splitting HSUs based on water-level, aquifer-test, and tritium data.

Shallow and deeper tritium plumes have migrated to borehole *ER-20-12* from the HANDLEY test. The shallow plume migrated from the HANDLEY test through the Timber Mountain welded tuff aquifer, whereas the deeper plumes moved through the Belted Range aquifer (BRA) and modified pre-Belted Range lava flow aquifer (mPBRLFA). Simulated tritium concentrations indicate that the leading edges of tritium plumes reached borehole *ER-20-12* by 1990. From 1970 to 2020, the simulated tritium load mostly occurs between borehole *ER-20-12* and the HANDLEY test.

An unmapped permeable feature was simulated between borehole *ER-20-12* and the downgradient Ribbon Cliff structural zone. This permeable feature hydraulically connects the BRA and mPBRLFA with the Tiva Canyon aquifer (TCA). The TCA is the most transmissive unit in the study area. Simulated tritium from the deeper plumes moves through the permeable feature downgradient from borehole *ER-20-12* and then migrates toward well *PM-3-1* through the TCA. The leading edge of the deeper simulated tritium plumes reaches well *PM-3-1* by 2010.

The mHFM and PMOV HFM do not include a permeable HSU at the water table near borehole *PM-3*, which is necessary for numerical flow and transport models to match measured water levels, transmissivities, and tritium concentrations in well *PM-3-2*. Consistently higher measured tritium concentrations in shallow well *PM-3-2*, compared to deeper well *PM-3-1*, and a downward vertical gradient between these wells indicate that a permeable feature exists near the water table that causes faster tritium migration toward the shallow well. Reevaluation of the PMOV HFM and geologic investigations, such as drilling another well, are needed to more precisely understand the shallow permeable pathway from the Handley test to well *PM-3-2*.

Introduction

The HANDLEY nuclear test was detonated underground on March 26, 1970, in the Pahute Mesa–Oasis Valley (PMOV) groundwater basin, southern Nevada (fig. 1). This large-yield (greater than 1 megaton) nuclear test was detonated at about 2,700 ft below the water table in borehole *U-20m*. The HANDLEY test was detonated farther below the water table than any other nuclear test on the Nevada National Security Site (NNSS; U.S. Department of Energy, 2015).

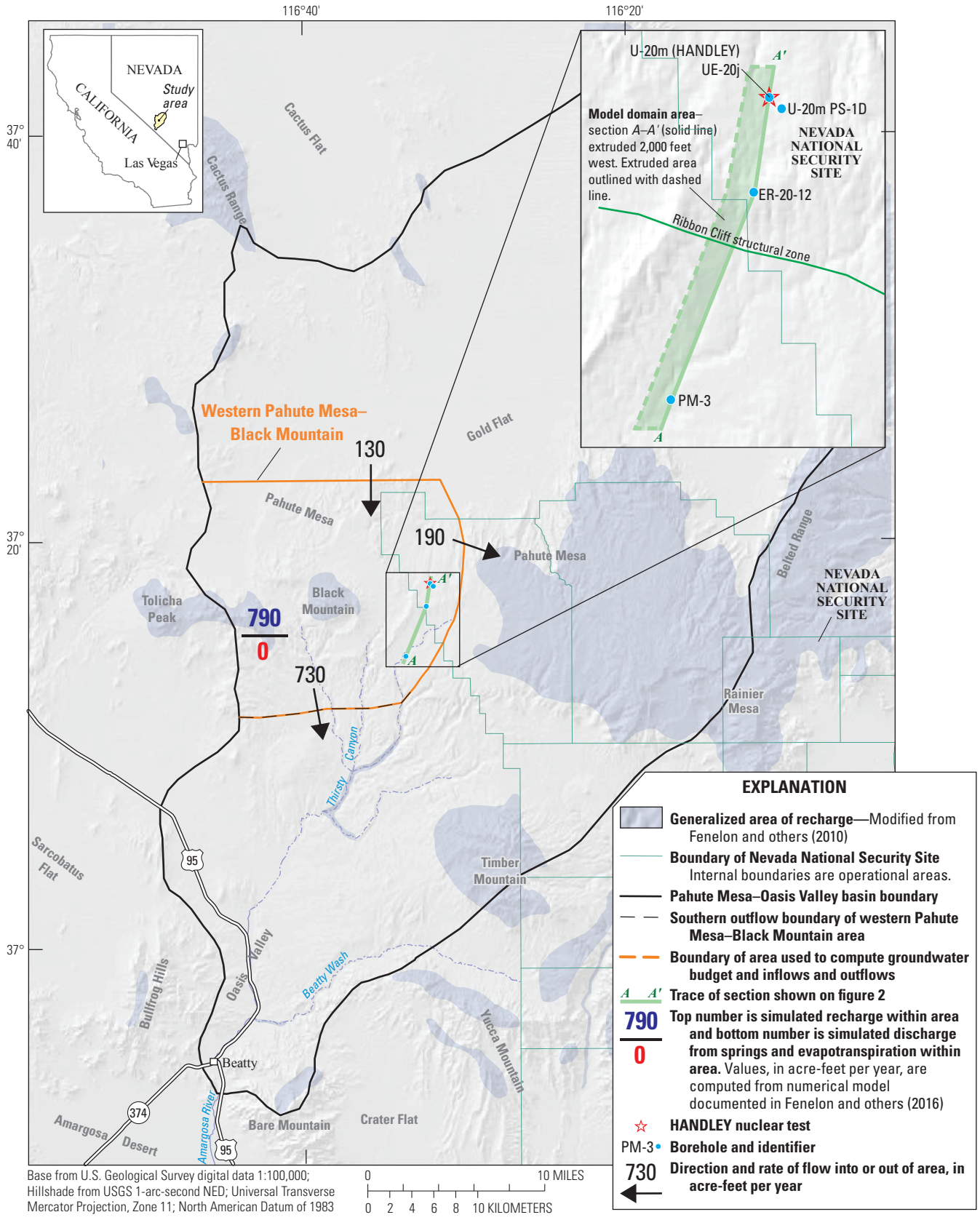

Figure 1. Inflows, outflows, and groundwater budget in the western Pahute Mesa–Black Mountain area; and physiography, recharge areas, and selected boreholes in the Pahute Mesa–Oasis Valley groundwater basin, southern Nevada (modified from Jackson and others, 2021).

Tritium has been detected from the HANDLEY nuclear test in downgradient boreholes *ER-20-12* and *PM-3* (fig. 1; Navarro-Intera, LLC, 2015). Tritium-plume migration is complex because the HANDLEY test occurred in an area with semi-perched[1] and regional aquifers. Measured tritium concentrations in boreholes *ER-20-12* and *PM-3* indicate that tritium migrated more than 1 mile downgradient from the test within the semi-perched aquifer and several miles within underlying regional aquifers.

Measured tritium concentrations in boreholes downgradient of the HANDLEY test indicate relatively fast transport; however, single-well aquifer-test results indicate that boreholes *ER-20-12* and *PM-3* are in an area of moderate-to-low transmissivity. Transmissivities of less than 300 and 600 ft^2/d have been estimated in boreholes *ER-20-12* and *PM-3*, respectively (Frus and Halford, 2018; Navarro, 2018). However, tritium concentrations greater than 100 picocuries per liter (pCi/L) were measured 4.5 mi downgradient from the HANDLEY nuclear test in borehole *PM-3* within 40 years of the detonation (Navarro-Intera, LLC, 2015). Observation of tritium moving 4.5 mi in 40 years (1.6 ft/d) indicates fast transport through high-transmissivity intervals, ranging from 1,280 to 12,800 ft^2/d. The high-transmissivity range of 1,280 to 12,800 ft^2/d was estimated using a modified Darcy equation (Freeze and Cherry, 1979) with fractured-rock effective porosities that range from 0.005 to 0.05 (Winograd and Thordarson, 1975), an assumed aquifer thickness of 1,600 ft (Jackson and others, 2021), and a measured hydraulic gradient between the HANDLEY nuclear test and borehole *PM-3* of 0.01 ft/ft. Therefore, a tritium transport velocity of 4.5 mi in 40 years indicates that high-transmissivity intervals exist, but the location of these permeable pathways within volcanic units is unknown.

A numerical model can be used to reconcile areas with moderate-to-low transmissivities and fast tritium transport to infer the location of permeable pathways between the HANDLEY nuclear test and downgradient boreholes *ER-20-12* and *PM-3*. Geologic data, water-level altitudes, vertical-head differences, aquifer-test results, and tritium concentrations are available in boreholes *ER-20-12*, *PM-3*, and *UE-20j* (Frus and Halford, 2018; Navarro-Intera, LLC, 2015; U.S. Department of Energy, 2018a; 2020; Jackson, 2021). Borehole *UE-20j* is 75 ft southwest of the HANDLEY nuclear test and provides information about hydrologic conditions prior to the nuclear detonation.

[1]Semi-perched groundwater is a localized, unconfined volume of groundwater that is separated from the underlying regional groundwater system by a zone of saturated, low-permeability rocks near the water table. These low-permeability rocks have vertical hydraulic conductivities that are less than the local recharge rate; therefore, recharge is impeded from moving downward, causing water levels in the semi-perched aquifer to be elevated above regional water levels (Jackson and others, 2021).

Results of this numerical study will aid in the understanding of tritium migration in a complex hydrologic setting that can be applied to flow and transport modeling at a groundwater-basin scale. Hydraulic- and transport-property estimates from this study can be used to forecast transport from nuclear tests in other areas of Pahute Mesa where data are limited.

Purpose and Scope

This report integrates geologic, hydrologic, and tritium data to infer the location of permeable pathways downgradient from the HANDLEY nuclear test. Geologic data include lithologic well logs from boreholes *UE-20j*, *ER-20-12*, and *PM-3* and the three-dimensional distribution of hydrostratigraphic units (HSUs), which was extracted from a preexisting hydrostratigraphic framework model of the Pahute Mesa–Oasis Valley groundwater basin (U.S. Department of Energy, 2020). Hydrologic data include static water-level altitudes from 10 wells; static vertical-head differences between 5 well pairs; 9 single-well aquifer-test transmissivity estimates from wells in boreholes *UE-20j*, *ER-20-12*, and *PM-3*; and drawdown estimates in wells *PM-3-1* and *PM-3-2* from groundwater withdrawals at borehole *ER-20-12*. Tritium data include tritium concentrations measured in 7 wells within boreholes *U-20m PS-1D*, *ER-20-12*, and *PM-3*.

Numerical groundwater-flow and tritium-transport models were developed to estimate hydraulic and transport properties between the HANDLEY test and borehole *PM-3*. The models simulate a 2,000-ft-wide and 28,400-ft-long flow path (streamtube) that begins 2,000 ft upgradient from the HANDLEY test at borehole *U-20m* and extends 2,600 ft downgradient from borehole *PM-3* (fig. 2). Recharge, hydraulic-conductivity, specific-yield, specific-storage, and effective-porosity distributions were estimated with the numerical models by fitting simulated water-level altitudes, vertical-head differences, aquifer-test transmissivities, tritium concentrations, and transient water-level declines in wells *PM-3-1* and *PM-3-2* to measured equivalents. The estimated hydraulic-conductivity, specific-yield, specific-storage, and effective-porosity distributions were used to infer permeable pathways. Simulated tritium-concentration distributions and tritium breakthrough curves in wells within boreholes *U-20m PS-1D*, *ER-20-12*, and *PM-3* are shown from the date of the HANDLEY nuclear test detonation (March 26, 1970) to 2020. The numerical models and analyses discussed in this report are documented in a separate USGS data release (Jackson, 2021).

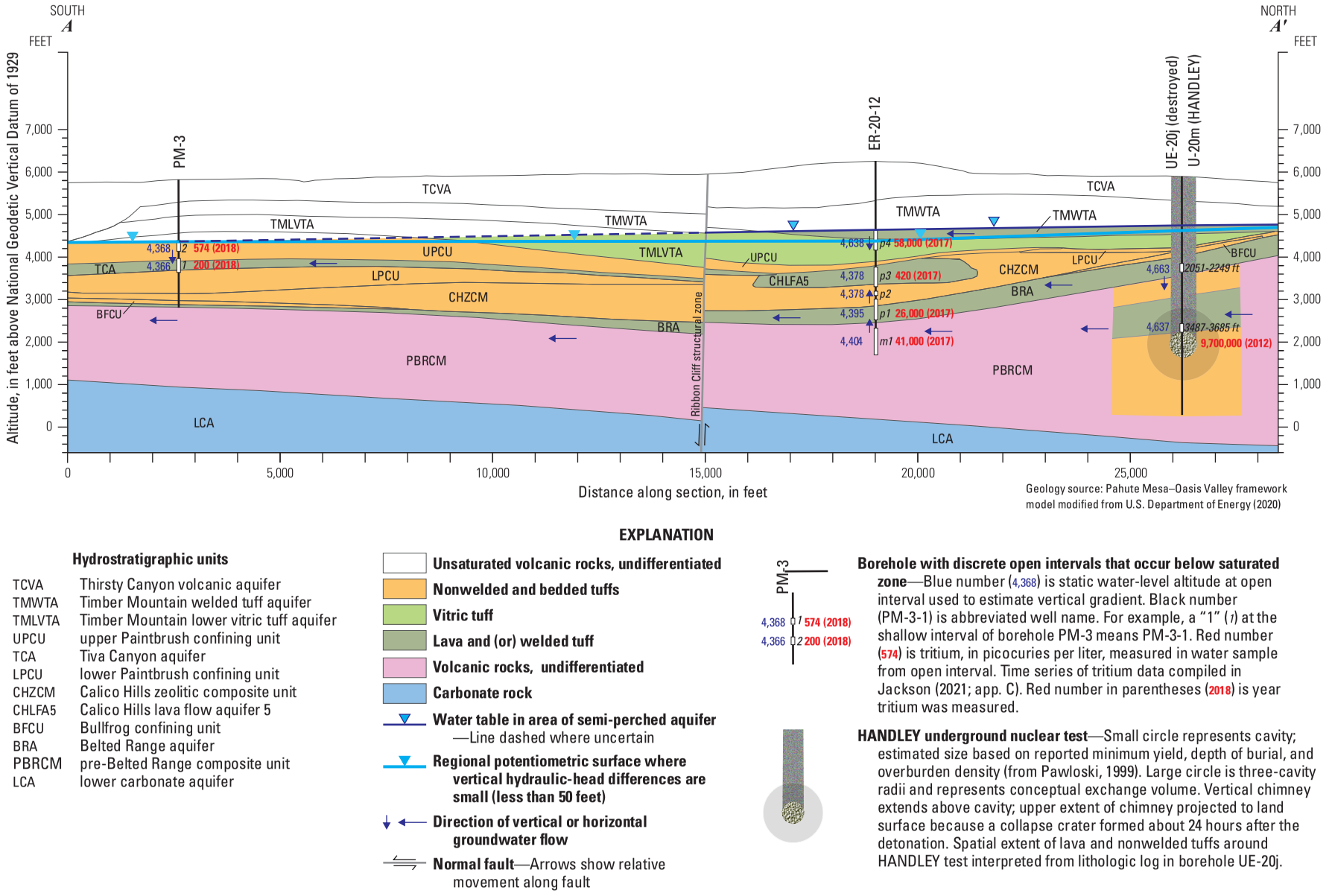

EXPLANATION

Hydrostratigraphic units

TCVA	Thirsty Canyon volcanic aquifer
TMWTA	Timber Mountain welded tuff aquifer
TMLVTA	Timber Mountain lower vitric tuff aquifer
UPCU	upper Paintbrush confining unit
TCA	Tiva Canyon aquifer
LPCU	lower Paintbrush confining unit
CHZCM	Calico Hills zeolitic composite unit
CHLFA5	Calico Hills lava flow aquifer 5
BFCU	Bullfrog confining unit
BRA	Belted Range aquifer
PBRCM	pre-Belted Range composite unit
LCA	lower carbonate aquifer

- **Unsaturated volcanic rocks, undifferentiated**
- **Nonwelded and bedded tuffs**
- **Vitric tuff**
- **Lava and (or) welded tuff**
- **Volcanic rocks, undifferentiated**
- **Carbonate rock**
- **Water table in area of semi-perched aquifer**—Line dashed where uncertain
- **Regional potentiometric surface where vertical hydraulic-head differences are small (less than 50 feet)**
- **Direction of vertical or horizontal groundwater flow**
- **Normal fault**—Arrows show relative movement along fault

PM-3
4,368 1 574 (2018)
4,366 2 200 (2018)

Borehole with discrete open intervals that occur below saturated zone—Blue number (4,368) is static water-level altitude at open interval used to estimate vertical gradient. Black number (PM-3-1) is abbreviated well name. For example, a "1" (*1*) at the shallow interval of borehole PM-3 means PM-3-1. Red number (574) is tritium, in picocuries per liter, measured in water sample from open interval. Time series of tritium data compiled in Jackson (2021; app. C). Red number in parentheses (2018) is year tritium was measured.

HANDLEY underground nuclear test—Small circle represents cavity; estimated size based on reported minimum yield, depth of burial, and overburden density (from Pawloski, 1999). Large circle is three-cavity radii and represents conceptual exchange volume. Vertical chimney extends above cavity; upper extent of chimney projected to land surface because a collapse crater formed about 24 hours after the detonation. Spatial extent of lava and nonwelded tuffs around HANDLEY test interpreted from lithologic log in borehole UE-20j.

Figure 2. Geologic and hydrostratigraphic cross section from the HANDLEY nuclear test to borehole *PM-3*, showing potentiometric surfaces, groundwater-flow directions, and tritium in wells, Pahute Mesa, southern Nevada (modified from Jackson and others, 2021).

Naming Convention of Wells

As used in this report, a well is defined as a single, temporary, or permanent completion in a borehole, where the completion defines a unique open interval. Based on this definition, boreholes *ER-20-12*, *PM-3*, and *UE-20j* have multi-well completions. Boreholes *ER-20-12* and *PM-3* have permanent completions, which include multiple monitoring tubes installed within the annulus. For example, borehole *ER-20-12* has five nested wells, which are listed in order from shallowest to deepest: (1) *ER-20-12 p4*; (2) *ER-20-12 p3*; (3) *ER-20-12 p2*; (4) *ER-20-12 p1*; and (5) *ER-20-12 m1* (fig. 2). Borehole *PM-3* has two nested wells: deep well *PM-3-1* and shallow well *PM-3-2* (fig. 2). Borehole *UE-20j*, which was destroyed by the HANDLEY nuclear detonation on March 26, 1970, was an open borehole that consisted of temporary completions, where water-level measurements were made in packer-isolated intervals. Wells in borehole *UE-20j* are differentiated by names that use a parenthetical expression added after the borehole name—for example: *UE-20j (2051-2249 ft)*. The two numbers in the parenthetical expression separated by a dash refer to the depth of the top and bottom of the open interval in the well. All borehole and well names in this report are consistent with those used in the U.S. Geological Survey National Water Information System (NWIS) database (U.S. Geological Survey, 2020) and are italicized in the text for clarity.

Description of Study Area

The study area is the 28,400-ft by 2,000-ft shaded area of the model domain shown in figure 1, which is within the western Pahute Mesa–Black Mountain area of the PMOV groundwater basin. The study area encompasses a conceptualized groundwater-flow path from the HANDLEY nuclear test through downgradient boreholes *ER-20-12* and *PM-3* (section *A–A′* on fig. 1). Pahute Mesa and Black Mountain are part of an extensive volcanic plateau that encompasses the study area. Land-surface altitudes range from 6,258 ft at borehole *ER-20-12* to about 5,700 ft at the southern extent of the study area downgradient from borehole *PM-3* (fig. 2).

The climate of the study area is arid to semi-arid, characteristic of a high desert region. The climate is characterized by hot summers and mild winters, large fluctuations in daily and annual temperatures, and low precipitation and humidity. Average summertime maximum temperatures on Pahute Mesa are about 84 °F, whereas average wintertime minimum temperatures on Pahute Mesa are about 25 °F (Soulé, 2006). Annual precipitation in the study area is about 8 in. (Soulé, 2006). Precipitation occurs primarily in late autumn through early spring and in mid-summer. Precipitation falls primarily as rain, and during the winter months as snow.

Geology

Depositional, volcanic, and tectonic processes have juxtaposed geologic units into a complex three-dimensional framework that affects groundwater flow. The geologic history is divided into three periods of deposition and tectonic deformation: (1) Early Paleozoic marine deposition, which formed thick sequences of carbonate rocks; (2) Cenozoic volcanism; and (3) Cenozoic normal and strike-slip faulting (Winograd and Thordarson, 1975; Laczniak and others, 1996).

Cenozoic volcanic rocks are the dominant rock type in the study area. From the Oligocene to Miocene, multiple eruptions occurred from at least seven calderas centered on Pahute Mesa, Timber Mountain, and Black Mountain in the southwestern Nevada volcanic field (U.S. Department of Energy, 2020). Caldera-forming eruptions deposited rhyolitic-to-dacitic lava flows; ash-flow, ash-fall, and reworked tuffs; and tectonic, eruptive, and flow breccias (Winograd and Thordarson, 1975; Laczniak and others, 1996; Faunt and others, 2010). Volcanic rocks are more than 10,000 ft thick (Sawyer and others, 1994; U.S. Department of Energy, 2020). The estimated volume of rock erupted from these calderas exceeds 3,000 cubic miles (Sawyer and others, 1994).

Large-scale normal faulting occurred during and after the period of Cenozoic volcanism (Faunt and others, 2010; U.S. Department of Energy, 2020). From the mid-Tertiary to Quaternary, normal faults formed the Basin and Range topography of the Great Basin province. Normal faults are the most common structural feature in the study area (Winograd and Thordarson, 1975). Mid-to-late Cenozoic extensional faulting resulted in northwest- to northeast-striking, high-angle normal faults with as much as 1,000 ft of vertical offset on Pahute Mesa (U.S. Department of Energy, 2020).

Hydrostratigraphy

A three-dimensional hydrostratigraphic framework model was developed of the PMOV basin and vicinity (U.S. Department of Energy, 2020) and is referred to as the Pahute Mesa–Oasis Valley hydrostratigraphic framework model (PMOV HFM). Geologic units in the PMOV HFM have been classified as aquifers, confining units, or composite units based on lithology and on fracture and matrix properties (Winograd and Thordarson, 1975; Laczniak and others, 1996; Prothro and others, 2009). Aquifers consist of rocks with assumed high fracture permeability or high matrix porosity and permeability. Rocks with minimal fracturing or assumed low matrix porosity and permeability are classified as confining units. A composite unit is defined as a grouping of rocks composed of aquifers and confining units and is assumed to have a large range in transmissivity that spans several orders of magnitude (Jackson and others, 2021).

Geologic units previously designated as aquifers, confining units, or composite units are organized into hydrostratigraphic units (HSUs) in the PMOV HFM (Prothro and others, 2009; U.S. Department of Energy, 2020). The HSU classification scheme integrates stratigraphic information into aquifer and confining unit designations. For example, welded tuffs of the Tiva Canyon tuff are conceptualized as aquifers and are mapped as the Tiva Canyon aquifer (TCA). Bedded tuffs of the Paintbrush Group, which directly overlie the TCA, are conceptualized as confining units and are mapped as part of the upper Paintbrush confining unit (UPCU). Mapped HSUs in figure 2 were extracted from the PMOV HFM.

Volcanic rocks form the principal aquifers and confining units in the study area because of their widespread distribution (Blankennagel and Weir, 1973; Fenelon and others, 2010). Rhyolitic-to-dacitic lavas and densely welded tuffs are the principal aquifers. Lavas can have high permeabilities where fractured, but the lavas are restricted areally and in thickness (Prothro and Drellack, 1997). Densely welded tuffs can have well-connected fracture networks and are widespread, which can provide lateral continuity for water to move through the flow system. Partially welded, nonwelded, and bedded tuffs have limited fracture networks and, as a result, have been classified as confining units, especially where they are zeolitized (Blankennagel and Weir, 1973). Vitric tuffs are assumed to have high matrix porosity and permeability and have been classified as aquifers in the PMOV HFM (U.S. Department of Energy, 2020).

Carbonate rocks are grouped into the lower carbonate aquifer (LCA) in the PMOV HFM. The LCA is a regionally extensive aquifer with high fracture permeability east of the study area (Winograd and Thordarson, 1975). However, in the study area, the LCA probably is a minimal component of the groundwater-flow system. This is because the LCA occurs at estimated depths of 6,000 ft below land surface near the HANDLEY nuclear test (fig. 2), where rocks at this depth typically have low transmissivity (Halford and Jackson, 2020). The LCA in the study area also is not expected to be an aquifer because this unit is discontinuous and likely has been altered by volcanic activity (U.S. Department of Energy, 2020). Therefore, the LCA is conceptualized to function as a confining unit in the study area.

Conceptual Framework

Geologic, hydrologic, and tritium data were integrated to develop a conceptual framework of groundwater flow and tritium migration near and downgradient from the HANDLEY nuclear test. The relation of transmissivity with depth was used to determine the active part of the groundwater system where nearly all flow occurs. Transmissivities were estimated for HSUs in boreholes *UE-20j*, *PM-3*, and *ER-20-12* from single-well aquifer tests. Drawdowns were estimated in wells *PM-3-1* and *PM-3-2*, where water levels only responded to groundwater withdrawals during the drilling of borehole *ER-20-12*. Transmissivity estimates from aquifer tests, estimated drawdowns, water-level altitudes, vertical gradients, and measured tritium concentrations were used to infer permeable HSUs and tritium-migration pathways within semi-perched and regional aquifers near and downgradient from the HANDLEY nuclear test. Nuclear testing locally alters the physical properties of the surrounding rocks and affects tritium-migration patterns. A modified hydrostratigraphic framework was developed in this study that integrates the conceptual understanding of groundwater flow and tritium transport through permeable units near and downgradient from the HANDLEY nuclear test.

Transmissivity Variations with Depth

Jackson and others (2021) analyzed transmissivity variations with depth in the PMOV basin using transmissivity estimates compiled from a hydraulic-properties database (Frus and Halford, 2018). The relation between transmissivity and depth was well defined for volcanic rocks because discrete depth intervals were slug tested consecutively from the water table to the bottom of 17 Pahute Mesa boreholes, which have total depths ranging from 3,705 to 13,686 ft below land surface (Blankennagel, 1967; Blankennagel and Weir, 1973; Frus and Halford, 2018). These slug tests cumulatively tested about 45,000 ft of volcanic rock beneath Pahute Mesa. Jackson and others (2021) showed that greater than 98 percent of the transmissivity in volcanic rocks occurs within 1,600 ft of the water table. Transmissive intervals can occur at depths greater than 1,600 ft below the water table but are more common at shallower depths (Frus and Halford, 2018). In this study, the transmissivity with depth relation is used as a justification to assign low transmissivities (less than 10 ft^2/d) to rocks greater than 3,000 ft below the water table in areas where data are absent.

Transmissivity Estimates from Aquifer Tests

Transmissivities were estimated for HSUs in boreholes *UE-20j*, *PM-3*, and *ER-20-12* from single-well aquifer tests (fig. 3). Constant-rate aquifer tests were used to estimate the bulk transmissivity of all saturated HSUs in boreholes *UE-20j* and *PM-3*. The bulk transmissivity estimated from the constant-rate tests was distributed to HSUs using slug-test results from discrete-depth intervals in the open boreholes. Drilling and aquifer-test data were used to estimate transmissivities for HSUs open to wells *ER-20-12 m1*, *ER-20-12 p1*, and *ER-20-12 p4*. Aquifer-test data and analyses are documented in a separate USGS data release (Jackson, 2021, app. A).

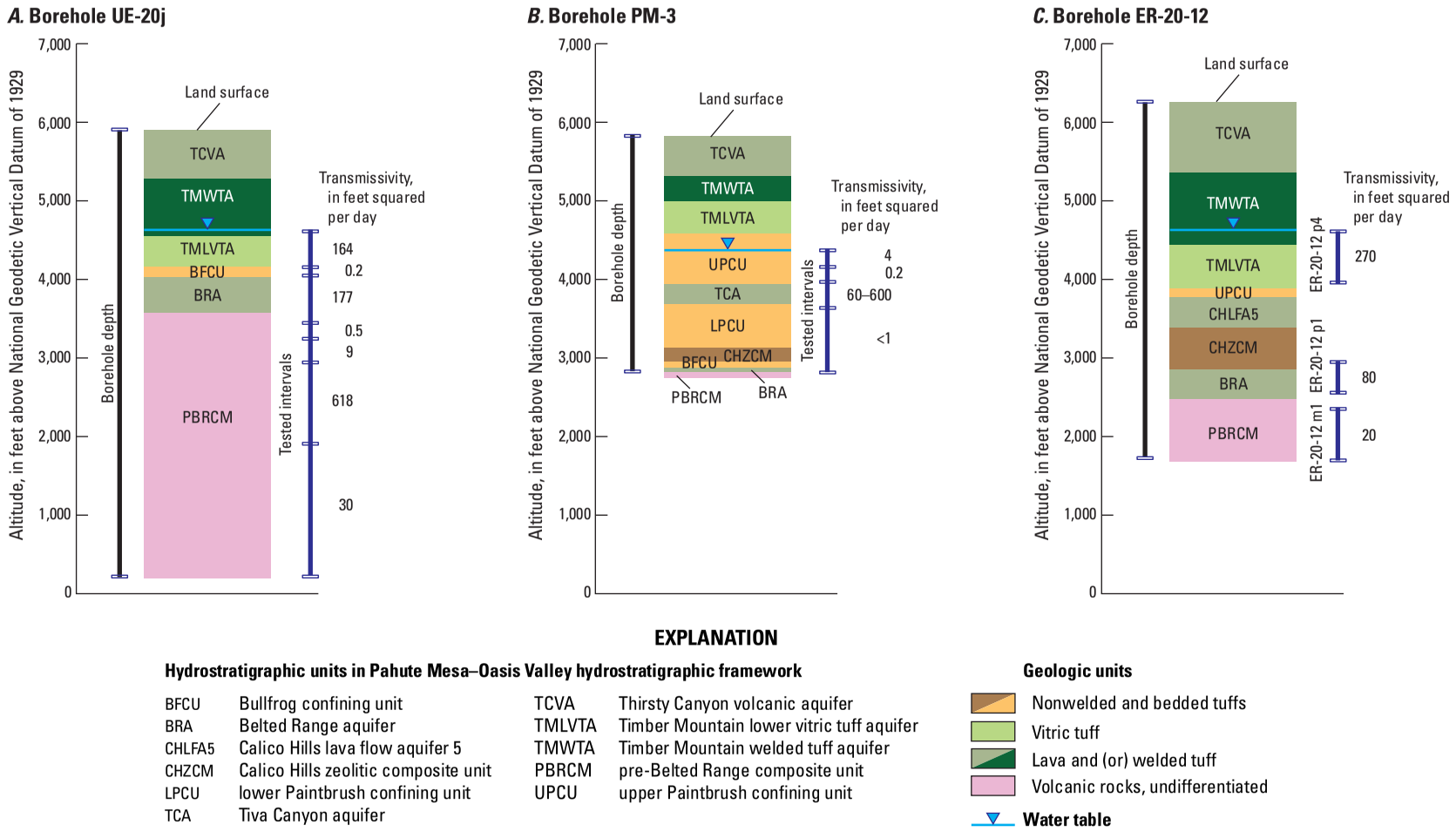

Figure 3. Geologic units, hydrostratigraphic units, and transmissivity estimates at discrete depths in boreholes *UE-20j (A), PM-3 (B)*, and *ER-20-12 (C)*, Pahute Mesa, southern Nevada.

Borehole UE-20j

Borehole *UE-20j* is 75 ft southwest of the HANDLEY nuclear test and provides information about hydrologic conditions prior to the nuclear detonation. Borehole *UE-20j* was drilled to a depth of 5,690 ft from August 24 to November 11, 1964 (Hasler, 1965). The borehole was cased from land surface to a depth of 1,740 ft, where the bottom of the casing was about 470 ft below the static water table (Hasler, 1965). The borehole was uncased from 1,740 to 5,690 ft below land surface so that volcanic rocks open to the hole could be hydraulically tested in 1964 (Hasler, 1965). The borehole was plugged in 1969, in preparation for the detonation of the HANDLEY nuclear test (U.S. Department of Energy, 2015).

A constant-rate aquifer test was done in borehole *UE-20j* during October 21–22, 1964 (Frus and Halford, 2018). The constant-rate test hydraulically tested all saturated units in the open borehole. The average pumping rate was 56 gal/min during the 23-hour, constant-rate test and the estimated transmissivity is 1,000 ft^2/d (Frus and Halford, 2018).

Vertical variations in transmissivity with depth were estimated from slug-test analyses in borehole *UE-20j* (Frus and Halford, 2018). The slug tests were done at discrete-depth intervals within borehole *UE-20j* during October 24–26, 1964 (fig. 3*A*; Blankennagel and Weir, 1973; Frus and Halford, 2018). Straddle packers were used to isolate and slug test the discrete-depth intervals, which typically were about 200 ft. The suite of packer-isolated intervals spanned from about 470 ft below the water table to the bottom of the borehole in *UE-20j*.

Summed transmissivity from slug-test results of all depth intervals in a borehole theoretically should equal the transmissivity estimated from the constant-rate test of the open borehole. In actuality, the sum of slug-test transmissivities was about 560 ft^2/d, which is less than the constant-rate test transmissivity (1,000 ft^2/d) because highly permeable intervals could not be quantified by slug tests (Frus and Halford, 2018, p. 19). An integrated borehole analysis was done by Frus and Halford (2018) to reconcile differences between slug-test and constant-rate test transmissivities. Permeable intervals in each borehole were identified based on extensive geophysical logging (temperature, salinometer, and radioactive tracer logs) and minimally raised water levels during slug-test injection (Blankennagel, 1967; Blankennagel and Weir, 1973). The integrated borehole analysis methodology is described as follows:

> "*Differences between transmissivity estimates from pumping tests and summed slug-test results are referred to as excess transmissivity and used to make corrections to hydraulic conductivity estimates from slug tests in permeable intervals…A single hydraulic conductivity estimate was added to all identified permeable intervals in a borehole to include the excess transmissivity calculated for that borehole. Added hydraulic conductivity was calculated as excess transmissivity divided by the length of the sum of permeable intervals*" (Frus and Halford, 2018, p. 19).

Slug-test results in borehole *UE-20j* indicate that the Belted Range aquifer (BRA) and an 800-ft interval within the pre-Belted Range composite unit (PBRCM) are the most transmissive intervals in the borehole (Frus and Halford, 2018). However, the upper 470 ft of saturated borehole, which includes the Timber Mountain welded tuff aquifer (TMWTA), was not packer isolated and slug tested. The TMWTA is inferred to be a transmissive interval in borehole *UE-20j* because this unit is the most likely pathway for a shallow tritium plume to migrate from the HANDLEY nuclear test to well *ER-20-12 p4*, which has a high measured tritium concentration and is open to TMWTA (fig. 2). An approximate transmissivity was estimated for the TMWTA in borehole *UE-20j* by revising the integrated borehole analysis by Frus and Halford (2018). The revised analysis (Jackson, 2021, app. A) used the same methodology from Frus and Halford (2018) but assumed that the BRA, an 800-ft interval within the PBRCM, and the TMWTA at borehole *UE-20j* are high-permeability intervals (fig. 3*A*). Results of the revised analysis indicate that the TMWTA, BRA, and 800-ft interval of PBRCM have estimated transmissivities of 164, 177, and 618 ft^2/d, respectively (fig. 3*A*).

Borehole PM-3

Borehole *PM-3* was drilled to a depth of 3,019 ft during September 1–19, 1988 (Kilroy and Savard, 1996). The borehole was cased from land surface to a depth of 1,473 ft, where the bottom of the casing was about 20 ft below the static water table. The borehole was uncased from 1,473 to 3,019 ft below land surface so that volcanic rocks open to the hole could be hydraulically tested (Kilroy and Savard, 1996). During hydraulic testing, debris fell into the open hole between 2,605 and 3,019 ft below land surface, which may have blocked flow into the borehole from deeper HSUs. Therefore, estimated transmissivities may be biased low for the lower Paintbrush confining unit (LPCU), Calico Hills zeolitic composite unit (CHZCM), Bullfrog confining unit (BFCU), BRA, and PBRCM in borehole *PM-3* (fig. 3*B*).

A constant-rate aquifer test was done in borehole *PM-3* during September 26–27, 1988 (U.S. Department of Energy, 1996). The constant-rate test hydraulically tested all saturated units from the water table to the bottom of the borehole (fig. 3*B*). The average pumping rate was 169 gal/min during the 31-hour, constant-rate test (Kilroy and Savard, 1996; U.S. Department of Energy, 1996) and the estimated transmissivity was 600 ft^2/d (Frus and Halford, 2018).

Vertical variations in transmissivity with depth were estimated from slug-test analyses in borehole *PM-3* (U.S. Department of Energy, 1996; Frus and Halford, 2018). The slug tests were done at discrete-depth intervals within borehole *PM-3* during October 4–20, 1988 (fig. 3*B*; U.S. Department of Energy, 1996). The discrete-depth intervals were isolated with straddle packers and slug tested consecutively from near the water table to the bottom of the borehole (U.S. Department of Energy, 1996). Depth intervals averaged 225 ft.

Transmissive units in borehole *PM-3* were determined from slug-test results and from borehole flow, temperature, and tracer-test logs (Kilroy and Savard, 1996). The borehole logs indicate that the TCA contributes most of the flow to borehole *PM-3* (Kilroy and Savard, 1996), and slug-test results indicate that the TCA is the most transmissive unit open to the borehole (Frus and Halford, 2018). The estimated slug-test transmissivity of the TCA is 60 ft^2/d, whereas all other slug-tested units had transmissivities of less than 5 ft^2/d (fig. 3*B*; Frus and Halford, 2018). The estimated transmissivity from the constant-rate test, which hydraulically tested all units in borehole *PM-3*, is 600 ft^2/d.

Differences in transmissivity between the sum of slug-test results (less than 65 ft^2/d) and the constant-rate test (600 ft^2/d) occur because of measurement device failures and insufficient slug-test data (Kilroy and Savard, 1996). For example, during slug testing of the shallowest interval in borehole *PM-3*, from 1,473 to 1,667 ft below land surface, the pressure transducer was positioned too high in the access port, which resulted in the pressure transducer becoming dry within 19 minutes of the slug injection and caused irregular "jumps" in measured water-level recovery data (Kilroy and Savard, 1996; Frus and Halford, 2018). During slug testing of the next shallowest interval, from 1,665 to 1,865 ft below land surface, communication problems between the pressure transducer and data logger resulted in no recorded data between 12 and 188 minutes after slug injection, which degraded data quality for slug-test analyses (Kilroy and Savard, 1996; Frus and Halford, 2018). The most transmissive interval, from 1,934 to 2,134 ft below land surface, contains the TCA (fig. 3*B*). The estimated slug-test transmissivity of the TCA (60 ft^2/d) likely is biased low because the measurement frequency of the pressure transducer was inadequate for measuring the rapid water-level recovery in the TCA (Kilroy and Savard, 1996; Frus and Halford, 2018). Because the TCA is the only transmissive unit in borehole *PM-3*, the transmissivity estimate from the constant-rate test of 600 ft^2/d was assigned to the TCA (fig. 3*B*).

Borehole ER-20-12

Transmissivities were estimated for HSUs open to wells *ER-20-12 m1*, *ER-20-12 p1*, and *ER-20-12 p4* using water-level and discharge data measured during *ER-20-12* well completion or aquifer testing. Drilling and completion of borehole *ER-20-12* occurred from October 8, 2015 to January 6, 2016 (Navarro, 2016). The borehole was drilled by conventional circulation using an air-foam drilling fluid that was not reused. The air foam was mixed at the surface, pumped down the drill stem, returned to the surface through the annulus while lifting drill cuttings and formation water, and discharged to a sump. The air-foam lift conventional circulation method is effectively a pumping stress on the aquifer system because the drilling method allows formation water to flow naturally to the borehole (Navarro, 2016).

Well ER-20-12 m1

Aquifer testing of well *ER-20-12 m1*, the deepest completion in borehole *ER-20-12* (fig. 3*C*), was done from August 11–18, 2016. Because of the low production rate of well *ER-20-12 m1*, a series of short-duration (0.5–1.5 hour) pumping tests were done at an average pumping rate of 30 gal/min (Navarro, 2018). Well *ER-20-12 m1* is open to lava and nonwelded tuff of the PBRCM and the estimated transmissivity is about 20 ft^2/d (fig. 3*C*; Jackson, 2021, app. A). During aquifer testing at well *ER-20-12 m1*, water levels were monitored in the following observation wells and HSUs: *ER-20-12 p1* (BRA), *ER-20-12 p2* (CHZCM), *PM-3-1* (TCA), and *PM-3-2* (UPCU). Drawdowns were not detected in these observation wells from pumping in well *ER-20-12 m1* (Navarro, 2018). However, drawdown was detected in wells *PM-3-1* and *PM-3-2* from groundwater withdrawals during drilling of borehole *ER-20-12* (see section, "Drawdowns in Borehole PM-3," for details).

Well ER-20-12 p1

A transmissivity was estimated for the BRA open to well *ER-20-12 p1* using a bulk transmissivity estimated from drilling activities. The bulk transmissivity was approximated from 2,515 to 4,352 ft below land surface, or from the Calico Hills lava flow aquifer #5 (CHLFA5) to the bottom of borehole *ER-20-12* on figure 3*C*. The bulk transmissivity was approximated using discharge measurements made during drilling as the borehole was advanced and water-level recovery data after drilling ceased in borehole *ER-20-12*. Discharge of formation water from land surface to a depth of 2,515 ft was excluded from the analysis because a 20-in. casing was installed and cemented in place from land surface to a depth of 2,503 ft during November 21–24, 2015 (Navarro, 2016). From November 24 to December 1, 2015, the borehole was advanced from 2,515 to 4,352 ft below land surface. During this borehole advancement, about 3 million gallons of groundwater were withdrawn from borehole *ER-20-12*. Therefore, the average "pumping" rate was 276 gal/min (Jackson, 2021, app. A).

After drilling ceased on December 1, 2015, three water-level measurements were recorded during December 4–6, 2015, in daily drilling reports for borehole *ER-20-12* (Navarro, 2016, table 6-1). Analysis of water-level recovery data using the Cooper and Jacob (1946) recovery method resulted in an estimated transmissivity of 100 ft^2/d (Jackson, 2021, app. A). The water-production log during drilling of borehole *ER-20-12* showed that the BRA contributes most of the flow within the open borehole between 2,515 and 4,352 ft below land surface (Navarro, 2016). Because aquifer-test results of well *ER-20-12 m1* indicated that the PBRCM has an estimated transmissivity of 20 ft^2/d, the excess transmissivity from the drilling analysis was assigned to the BRA. Therefore, the estimated transmissivity of the BRA is about 80 ft^2/d (fig. 3*C*).

Well ER-20-12 p4

A transmissivity was estimated for the TMWTA open to well *ER-20-12 p4* using slug-test data collected during cementation of the 20-in. casing on November 22, 2015. Well *ER-20-12 p4* is a 1.9-in. slotted piezometer tube that was installed in the annular space between the 20-in. casing and 26-in. borehole of *ER-20-12* (Navarro, 2016). About 2,226 gallons of fresh water and 360 ft^3 of cement were injected through a stab-in style float shoe at the base of the 20-in. casing. The float shoe has a one-way valve that closes after fluids and cement are injected so that these fluids and cement do not flow back into the casing (Navarro, 2016). A pressure transducer was installed in well *ER-20-12 p4* to monitor the rise in water levels caused by the injection of fluids and cement into the annular space (Navarro, 2016, fig. 6-2). Analysis of the water-level rise using the Bouwer and Rice (1976) method resulted in an estimated transmissivity of about 270 ft^2/d for the TMWTA (fig. 3*C*; Jackson, 2021, app. A).

Effect of Groundwater Withdrawals in Borehole ER-20-12 on Water Levels in Borehole PM-3

Pressure transducers were used to measure water levels in wells *PM-3-1* and *PM-3-2* from October 1, 2015 to September 12, 2016 (Navarro, 2018). This water-level monitoring period spanned the duration of *ER-20-12* drilling, well-completion activities, and aquifer testing. Water levels in wells *PM-3-1* and *PM-3-2* only responded to groundwater withdrawals in borehole *ER-20-12* during drilling operations (Navarro, 2018). Analysis of water-level declines (drawdowns) in wells *PM-3-1* and *PM-3-2* requires estimated groundwater-withdrawal rates from borehole *ER-20-12* during drilling.

Estimation of Groundwater-Withdrawal Rates During ER-20-12 Drilling

Groundwater-withdrawal rates were estimated from tabulated injection and water-production rates provided in Navarro (2016, table F-1). Injection and water-production rates were estimated previously by Navarro (2016) using a lithium-bromide tracer mixed with the air-foam drilling fluid. Samples were collected simultaneously from the injected drilling fluid and discharged drilling fluid from the flow line. Water-production rates were calculated by subtracting lithium-bromide concentrations from injected and discharged drilling fluid at each sample time.

A simplified time history of groundwater-withdrawal rates during drilling of borehole *ER-20-12* was constructed from tabulated injection and water-production rates (Navarro, 2016, table F-1). Groundwater-withdrawal rates were computed by subtracting time series of injection rates from water-production (discharge) rates during drilling from November 22 to December 1, 2015 (Jackson, 2021, app. B). Seven withdrawal periods were estimated and are shown in table 1.

Table 1. Estimated groundwater-withdrawal rates in borehole *ER-20-12* during drilling, Pahute Mesa, southern Nevada, November 22–December 1, 2015.

[**Date and time:** month (mm)-day (dd)-year (yyyy) hour (hh):minute (mm):second (ss). **Groundwater withdrawal rate:** gal/min, gallons per minute. **Remarks:** Hydrostratigraphic unit definitions—BRA, Belted Range aquifer; CHLFA5, Calico Hills lava flow aquifer #5; CHZCM, Calico Hills zeolitic composite unit; PBRCM, pre-Belted Range composite unit; TMWTA, Timber Mountain welded tuff aquifer. **Abbreviations:** ft, feet; gal, gallons; in., inch]

Date and time (mm-dd-yyyy hh:mm:ss)	Groundwater-withdrawal rate (gal/min)	Remarks
11-22-2015 01:14:00 – 11-22-2015 01:31:40	107	Cementation of 20-in. casing; 1,890 gal of fresh water injected; activity used primarily to slug test the TMWTA.
11-22-2015 01:31:50 – 11-22-2015 01:33:10	0	Drilling activities ceased.
11-22-2015 01:33:20 – 11-22-2015 01:48:50	174	Cementation of 20-in. casing; 2,693 gal of cement injected; activity used primarily to slug test the TMWTA.
11-22-2015 01:49:00 – 11-22-2015 01:50:00	336	Cementation of 20-in. casing; 336 gal of cement injected; activity used primarily to slug test the TMWTA.
11-22-2015 01:50:05 – 11-24-2015 06:59:00	0	Drilling activities ceased.
11-24-2015 07:00:00 – 12-01-2015 20:00:00	276	Borehole ER-20-12 advanced from 2,515 to 4,352 ft below land surface; about 3 million gal of water cumulatively withdrawn from CHLFA5, CHZCM, BRA, and PBRCM.
12-01-2015 20:00:00 – 07-01-2016 00:00:00	0	Drilling activities ceased.

Estimation of Drawdown with Water-Level Models

Drawdowns in wells *PM-3-1* and *PM-3-2* were estimated with a water-level modeling approach (Halford and others, 2012) because environmental (non-pumping) water-level fluctuations partially masked drawdown from groundwater withdrawals in borehole *ER-20-12*. The water-level modeling approach uses an analytical model to fit a synthetic curve to measured water-level data. The synthetic curve is the sum of one or more time-series components that explain water-level fluctuations in the measured data. Water-level models (WLMs) were used to estimate drawdowns masked by environmental noise by removing environmental water-level fluctuations caused by barometric pressure, tidal forces, and long-term recharge from the measured data. The WLMs were generated using SeriesSEE, a Microsoft Excel® add-in (Halford and others, 2012), and are documented in a USGS data release (Jackson, 2021, app. B).

Drawdowns in wells *PM-3-1* and *PM-3-2* were analytically modeled with a Theis transform of groundwater withdrawals in borehole *ER-20-12*, where water-level changes from multiple withdrawal rates (table 1) were simulated by superimposing multiple Theis (1935) solutions. Theis transforms serve as simple transform functions, where step-wise withdrawal records are translated into approximate water-level responses. Numerical experiments have confirmed that superimposed Theis transforms closely approximate water-level responses, even in hydrogeologically complex aquifer systems (Garcia and others, 2013).

Synthetic water levels in the WLM represent summed time series of water-level fluctuations resulting from earth tides, gravity tides, barometric pressure, other environmental fluctuations (such as recharge), and groundwater-withdrawal responses. Earth and gravity tides were computed functions based on well-established theoretical equations (Harrison, 1971). Hourly-to-weekly fluctuations in barometric pressure were simulated with moving averages of barometric-pressure data measured at wells *PM-3-1* and *PM-3-2*. Hourly-to-weekly fluctuations in background water levels were simulated with moving averages of high-frequency, water-level data measured with a pressure transducer in nearby background well *ER-20-7 m1*. The background well is 4.8 mi southeast of borehole *PM-3* and this background well is assumed to be close enough to borehole *PM-3* to be affected by similar environmental fluctuations, yet distant enough to be unaffected by groundwater withdrawals from borehole *ER-20-12*. Water levels from the background well were critical because they were affected by tidal potential–rock interaction, barometric pressure, and seasonal and long-term climatic trends. These environmental effects also are assumed to be present in wells *PM-3-1* and *PM-3-2*.

Synthetic water levels were fit to measured water levels by minimizing the root-mean-square error of differences between synthetic and measured water levels (Halford and others, 2012). Amplitude and phase were adjusted in each time series used to simulate environmental water-level fluctuations (barometric pressure, tides, and background water levels). Transmissivity and the storage coefficient were adjusted in the Theis transform model. The drawdown estimates at wells *PM-3-1* and *PM-3-2* are the summation of Theis transforms minus residual differences between synthetic and measured water levels (Halford and others, 2012). The summation of all Theis transforms is the direct estimate of the pumping signal. Residuals (measured minus synthetic water levels) represent all unexplained water-level fluctuations. These fluctuations primarily are random (noise) during non-pumping periods but can contain unexplained components of the pumping signal during pumping periods.

Drawdowns in Borehole PM-3

Estimated drawdowns are nearly identical in wells *PM-3-1* and *PM-3-2* (fig. 4). The timings of the drawdowns are nearly synchronous, and both wells have the same maximum drawdown of 0.75 ft. Estimation of similar drawdowns in both wells within borehole *PM-3* provides confidence that the "pumping" signal from drilling activities in borehole *ER-20-12* propagated about 16,500 ft southward to borehole *PM-3*.

Estimated drawdowns in wells *PM-3-1* and *PM-3-2* have root-mean-square errors of 0.04 ft. Fluctuations in residual errors, especially during the groundwater-withdrawal period, occurred because (1) water-production rates were estimated indirectly from lithium-bromide concentrations (Navarro, 2016, p. 88–89); (2) water-production rates were used to develop a simplified "pumping" history of groundwater-withdrawal rates during drilling of borehole *ER-20-12*; and (3) the open interval(s) contributing water to borehole *ER-20-12* changed with time as the borehole was advanced from land surface to a depth of 4,352 ft. Despite these data limitations, estimated drawdowns and the associated groundwater-withdrawal rates (table 1) can be used in numerical models to approximate hydraulic properties between boreholes *ER-20-12* and *PM-3*.

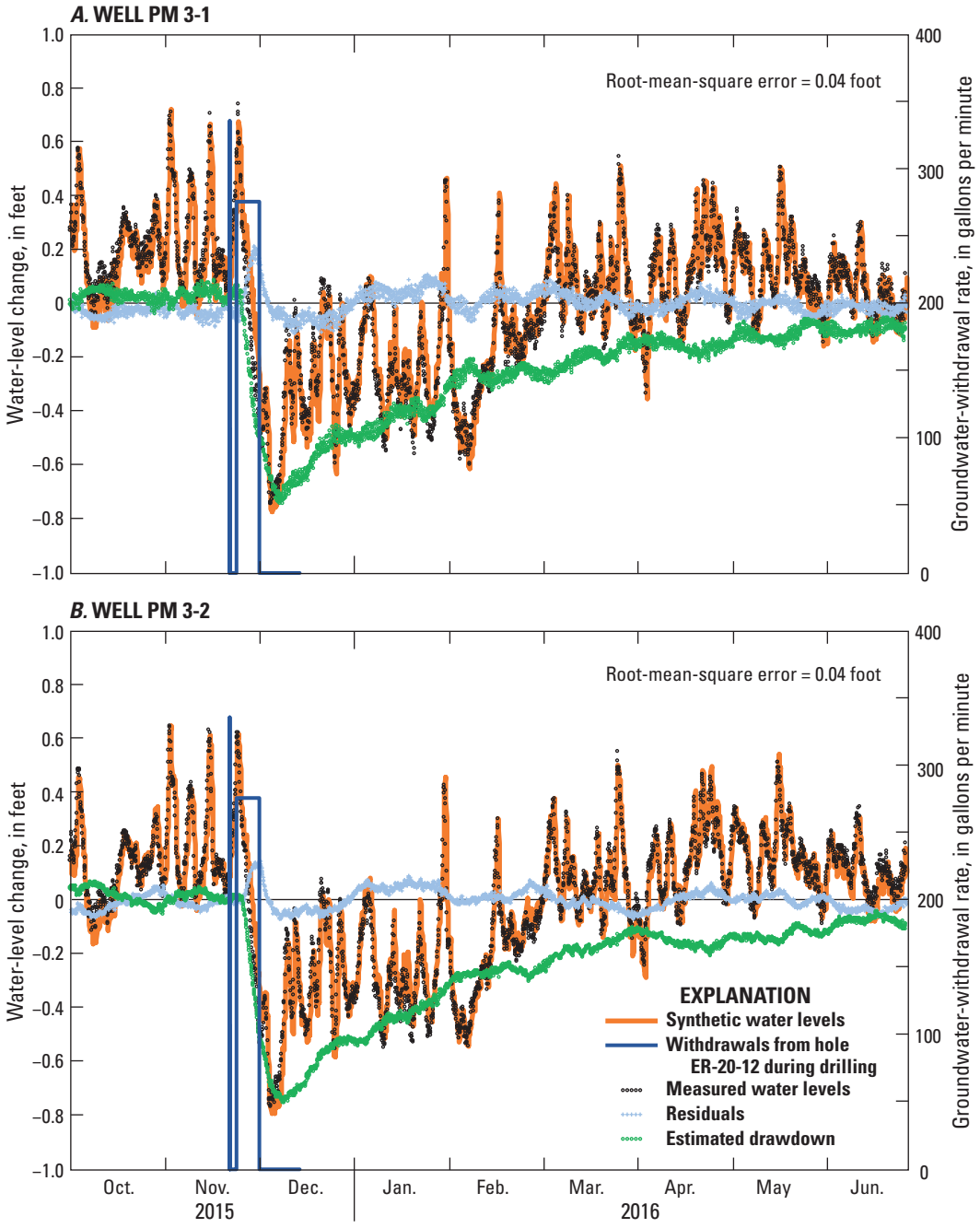

Figure 4. Measured water levels, synthetic water-level curve, residuals (measured minus synthetic water levels), groundwater withdrawals in borehole *ER-20-12* during drilling, and estimated drawdowns from a water-level model in wells (*A*) *PM-3-1* and (*B*) *PM-3-2*, Pahute Mesa, southern Nevada, October 2015–June 2016.

Nuclear-Test Effects on Surrounding Rock

Detonation of a nuclear device underground locally alters the surrounding rock, creating a cavity-chimney system (fig. 2). The cavity is an open, approximately spherical void in the rocks surrounding the detonation location and is formed when high temperatures and pressures from the nuclear detonation vaporize and compress the surrounding rocks (Carroll, 1981). Formation of the open cavity is generally followed by a collapse of overburden material and the generation of a rubble-filled vertical chimney hours to days after the nuclear test. The chimney of the HANDLEY nuclear test is computed to extend from the cavity to above the water table (fig. 2; Pawloski, 1999; Stoller-Navarro Joint Venture, 2009,

table 4-3). The rubble-filled chimney is a potential permeable pathway that connects previously isolated aquifers above the cavity. Upward movement of groundwater and radionuclides through the cavity-chimney system is driven by residual test heat, which causes a convectively (buoyancy) driven recirculation process (Pawloski and others, 2001) that transports radionuclides upward and outward, away from the cavity through permeable intervals in the surrounding rock (Carle and others, 2003).

Groundwater Flow and Tritium Migration

Groundwater flows south-southwest from the HANDLEY nuclear test to downgradient boreholes *ER-20-12* and *PM-3* (fig. 1). In this study, boreholes *U-20m*, *UE-20j*, *ER-20-12*, and *PM-3* are assumed to occur along the same flow path, where groundwater flows from right to left in section *A–A'* (fig. 2). The HANDLEY nuclear test occurs in an area with semi-perched and regional aquifers, which are both contaminated with tritium from this nuclear test (fig. 2). Tritium concentrations in wells within borehole *ER-20-12* indicate the presence of a shallow plume in the semi-perched aquifer and deeper plumes within regional aquifers (fig. 2; Russell and others, 2017; Navarro, 2018). Permeable pathways within semi-perched and regional aquifers are inferred from water-level altitudes, vertical gradients, tritium data, and aquifer-test results in boreholes *UE-20j*, *ER-20-12*, and *PM-3*.

Semi-Perched Aquifer

A semi-perched aquifer was encountered during completion of borehole *ER-20-12* in 2016 (fig. 2; Navarro, 2018). The semi-perched aquifer is composed of the TMWTA and Timber Mountain lower vitric tuff aquifer (TMLVTA) (fig. 2). The water level in the semi-perched TMWTA at well *ER-20-12 p4* is elevated, with a measured water-level altitude of 4,638 ft above the National Geodetic Vertical Datum of 1929 (NGVD 29; fig. 2). This elevated water level is about 260 ft higher than water levels in underlying regional aquifers open to borehole *ER-20-12*.

An examination of the HSUs between boreholes *UE-20j* and *ER-20-12* indicates that several HSUs hydraulically separate the semi-perched aquifer from the regional system (fig. 2). Limited aquifer-test data from wells on the NNSS suggest that the TMLVTA has low transmissivity (Jackson and others, 2021), but probably not low enough to fully isolate the TMWTA from deeper aquifers, such as the CHLFA5 and BRA. The semi-perched TMWTA and TMLVTA are hydraulically separated from the CHLFA5 by UPCU, which consists of nonwelded and bedded tuff and is conceptualized to function as a confining unit (fig. 2). North of borehole *ER-20-12*, the UPCU connects with three conceptual confining units: LPCU, BFCU, and CHZCM[2]. Combined, the UPCU, LPCU, BFCU, and CHZCM likely isolate the semi-perched aquifer (TMWTA and TMLVTA) from deeper aquifers, such as the BRA and CHLFA5.

The semi-perched aquifer is assumed to be supplied by a small amount of recharge that is sufficient to elevate hydraulic heads. The UPCU is the primary HSU that hydraulically isolates the semi-perched aquifer from underlying regional aquifers near borehole *ER-20-12*. To form a shallow, semi-perched aquifer, the recharge rate to the TMWTA must exceed the vertical hydraulic conductivity of the UPCU. Recharge rates likely are less than 1×10^{-4} ft/d, whereas the vertical hydraulic conductivity of the UPCU likely is greater than 1×10^{-6} ft/d (Jackson and others, 2021).

The semi-perched aquifer extends at least from the HANDLEY test to borehole *ER-20-12* because tritium from the test was detected at 58,000 pCi/L in the TMWTA at well *ER-20-12 p4* (fig. 2; Navarro, 2018; U.S. Department of Energy, 2018a). Downgradient migration of tritium could have occurred by upward propagation of tritium from the HANDLEY cavity into the chimney and subsequent lateral migration within the TMWTA to well *ER-20-12 p4* (fig. 2). The TMWTA at borehole *UE-20j*, adjacent to the HANDLEY test, is hydraulically isolated by BFCU. The BFCU is the functional equivalent of UPCU and LPCU in this area. The southern extent of the semi-perched aquifer is unknown.

Regional Aquifers

The BRA and an 800-ft transmissive interval in the PBRCM are the primary regional aquifers near the HANDLEY nuclear test (fig. 2). The 800-ft interval in the PBRCM is composed predominantly of lava flow (U.S. Department of Energy, 2020) and is conceptualized as an aquifer because this interval has a high estimated transmissivity (618 ft^2/d) in borehole *UE-20j* (fig. 3*A*). The BRA and 800-ft interval of transmissive PBRCM are hydraulically separated by a 530-ft interval of low-transmissivity (9.5 ft^2/d) PBRCM (fig. 3*A*) that functions as a confining unit. A downward vertical gradient of 0.02 ft/ft (26-ft vertical-head difference) was estimated between wells *UE-20j (2051-2249 ft)* and *UE-20j (3487-3685 ft)*, which are open to the BRA and transmissive PBRCM, respectively (fig. 2). This downward vertical gradient was estimated in 1964—6 years before the HANDLEY nuclear test was detonated.

Regional groundwater near the HANDLEY test is conceptualized to move southward predominantly through the BRA and transmissive PBRCM toward borehole *ER-20-12*. Regional flow between the HANDLEY test and borehole

[2]Lava flows, such as the CHLFA5, were delineated and extracted from the CHZCM in the PMOV HFM (U.S. Department of Energy, 2020). Because lava flow aquifers were removed from this composite unit, the CHZCM is dominated by nonwelded tuffs and is conceptualized in the PMOV HFM as a confining unit.

ER-20-12 is inferred from tritium data. Two tritium plumes likely migrated from the HANDLEY test cavity through permeable intervals in the BRA and PBRCM toward the lowermost openings in borehole *ER-20-12* (fig. 2). Two tritium plumes are hypothesized because the measured tritium concentration in well *ER-20-12 m1* (PBRCM) was 41,000 pCi/L in 2017, which is about 1.6 times greater than the measured tritium concentration in well *ER-20-12 p1* (BRA) (fig. 2; Jackson, 2021, app. C).

At borehole *ER-20-12*, vertical gradients indicate that groundwater moves from the shallowest and deepest open intervals toward the CHLFA5 (well *ER-20-12 p3*) near the center of the borehole (fig. 2). An upward vertical gradient of 0.01 ft/ft (9-ft vertical-head difference) was estimated from well *ER-20-12 m1* (PBRCM) to well *ER-20-12 p1* (BRA), indicating that nonwelded tuff in the PBRCM hydraulically separates permeable intervals in the PBRCM from the overlying BRA. An upward vertical gradient of 0.04 ft/ft (17-ft vertical-head difference) was estimated from the BRA (well *ER-20-12 p1*) to the CHLFA5 (well *ER-20-12 p2*), indicating that the intervening CHZCM hydraulically separates these aquifers. The downward vertical gradient of 0.3 ft/ft (260-ft vertical-head difference) from the TMWTA (well *ER-20-12 p4*) to the CHLFA5 (well *ER-20-12 p2*) indicates that the intervening UPCU hydraulically separates these aquifers.

Tritium data from well samples collected from borehole *ER-20-12* in 2017 indicate that HSUs surrounding the CHLFA5 provide a degree of hydraulic isolation. The highest tritium concentrations of 58,000 and 41,000 pCi/L occur in the shallowest (*ER-20-12 p4*) and deepest (*ER-20-12 m1*) wells in borehole *ER-20-12*, respectively, whereas the lowest tritium concentration of 420 pCi/L occurs in the CHLFA5 (*ER-20-12 p3*) (fig. 2; Jackson, 2021, app. C). The CHLFA5 tritium concentration is about 1 percent of the tritium concentration in the shallow (TMWTA) and deeper (BRA and PBRCM) HSUs, indicating that tritium migration toward the CHLFA5 largely is impeded by the low permeability of surrounding HSUs, such as the UPCU and CHZCM.

The TCA likely is the primary pathway for regional groundwater to move southwestward from borehole *ER-20-12* to borehole *PM-3*, based on aquifer-test results. Borehole flow, temperature, and tracer-test logs indicate that the TCA contributes most of the flow to borehole *PM-3* (Kilroy and Savard, 1996) and slug-test results indicate that the TCA is the most transmissive unit open to the borehole (fig. 3*B*; Frus and Halford, 2018).

Near the Ribbon Cliff structural zone, regional groundwater is conceptualized to move upward predominantly from the BRA into the TCA, based on results of drilling and aquifer testing at borehole *ER-20-12*. Maximum drawdowns of 0.75 ft were estimated in wells *PM-3-1* and *PM-3-2* from groundwater withdrawals in borehole *ER-20-12* during drilling operations (fig. 4). Drawdowns were observed in wells PM-3-*1* and *PM-3-2* only after groundwater was withdrawn from the CHLFA5, CHZCM, and BRA in hole ER-20-12 (table 1; fig. 4). This result was confirmed by the lack of a drawdown response in wells *PM-3-1* and *PM-3-2* prior to November 22, 2015 (table 1), when borehole ER-20-12 was advanced from land surface through shallow, saturated HSUs (TMWTA, TMLVTA, and UPCU). Drawdown also was not detected in wells *PM-3-1* and *PM-3-2* during later aquifer testing of the PBRCM (ER-20-12 *m1)* (Navarro, 2018).

At borehole *PM-3*, a 2-ft, downward, vertical-head difference (0.004 ft/ft vertical gradient) exists between shallow well *PM-3-2* (UPCU) and deeper well *PM-3-1* (TCA). The downward vertical gradient likely is caused by a small recharge mound near borehole *PM-3*. A probable local source of recharge is surface-water infiltration along an ephemeral tributary of Thirsty Canyon, which is less than 1,000 ft northwest of borehole *PM-3* (fig. 1). The UPCU has low transmissivity (4 ft^2/d or less; fig. 3*B*) and a small amount of recharge along the tributary could elevate the head in the UPCU 2 ft above the underlying TCA.

Tritium has migrated at least 4.5 mi south of the HANDLEY test to borehole *PM-3* (fig. 2). Low concentrations of tritium (less than 50 pCi/L) were detected in well *PM-3-2* in 2000 and 2004 (fig. 5*A*), but the detections were flagged as uncertain (Navarro-Intera, LLC, 2015). In 2011, low levels of tritium were detected again, but with a high level of certainty in wells *PM-3-1* and *PM-3-2* (fig. 5). Tritium concentrations continued to increase from 2011 to 2018, where tritium concentrations were consistently higher in shallow well *PM-3-2* compared to deeper well *PM-3-1* (fig. 5; Jackson, 2021, app. C).

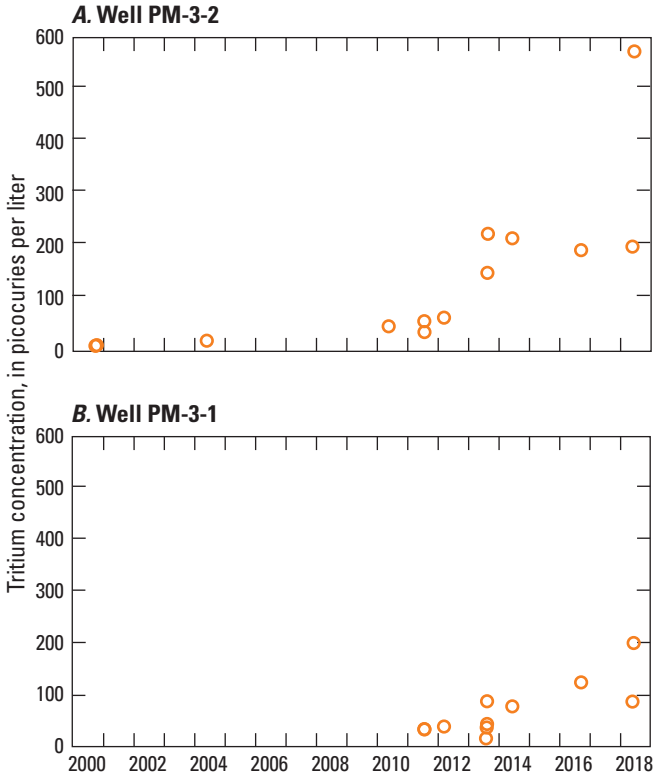

Figure 5. Measured tritium concentrations in wells (*A*) *PM-3-2* and (*B*) *PM-3-1*, Pahute Mesa, southern Nevada, 2000–18. Size of marker represents error range.

Groundwater flow and tritium migration between boreholes *ER-20-12* and *PM-3* are not well understood because of contradictory data. A shallow conceptual flow path to well PM-3-2 is inferred from measured tritium concentrations and vertical-head differences in wells *PM-3-1* and *PM-3-2*. However, a deeper conceptual flow path to well PM-3-1 is inferred from transmissivity estimates of HSUs in borehole *PM-3* and from estimated drawdowns in wells *PM-3-1* and *PM-3-2* during the drilling of borehole *ER-20-12*.

Higher tritium concentrations in shallow well *PM-3-2*, especially after 2013 (fig. 5), and a downward, vertical gradient in borehole *PM-3* suggest lateral tritium migration through shallow HSUs toward well *PM-3-2* and downward groundwater flow to well *PM-3-1* from shallower HSUs. This shallow conceptual flow path suggests that the tritium plume may have migrated laterally through the TMWTA, TMLVTA, and UPCU to well *PM-3-2* (fig. 2) and then migrated downward into underlying HSUs, causing lower measured tritium concentrations in well *PM-3-1* compared to well *PM-3-2* (fig. 5).

A shallow conceptual flow path is inconsistent with the conceptualization of the UPCU as a confining unit and the TMLVTA as a zeolitically altered, low-transmissivity aquifer. Conceptualizing the UPCU as a confining unit between boreholes *ER-20-12* and *PM-3* is justified because (1) in borehole *ER-20-12*, low transmissivity of the UPCU causes the water level in the semi-perched TMWTA to be about 260 ft higher than water levels in the underlying CHLFA5, BRA, and PBRCM (fig. 2); and (2) in borehole *PM-3*, the UPCU has low transmissivity (4 ft^2/d or less; figure 3*B*).

A deep conceptual flow path is inferred from aquifer-test results. Drawdowns were not observed in wells *PM-3-1* and *PM-3-2* from groundwater withdrawals in shallow, saturated HSUs (TMWTA, TMLVTA, and UPCU) during the drilling of borehole *ER-20-12*, which indicates that a strong hydraulic connection does not exist between the TMWTA, TMLVTA, and UPCU north of the Ribbon Cliff structural zone and the UPCU south of the structural zone. Instead, drawdown results indicate that a hydraulic connection exists between the TCA south of the Ribbon Cliff structural zone and the BRA north of the structural zone (figs. 2, 4). Therefore, drawdown results and transmissive intervals inferred from aquifer-test results suggest that the tritium plume migrated laterally in the BRA to borehole *ER-20-12*, moved upward near the Ribbon Cliff structural zone into the TCA, and then migrated laterally in the TCA toward well *PM-3-1* (fig. 2). Nearly identical estimated drawdowns in wells *PM-3-1* and *PM-3-2* indicate that the TCA and UPCU at borehole *PM-3* are hydraulically connected to the regional system. However, the permeable pathway for upward migration of tritium from the TCA into the UPCU and subsequent lateral movement in the UPCU toward well *PM-3-2* is unknown and cannot be inferred from the orientation of HSUs in the PMOV HFM (fig. 2).

Modified Hydrostratigraphic Framework

A modified hydrostratigraphic framework model (mHFM) was developed for this study using the previously published PMOV HFM (U.S. Department of Energy, 2020). The PMOV HFM is not entirely consistent with the conceptual model developed in this study of groundwater flow and tritium migration near and downgradient from the HANDLEY nuclear test. Modifications to the PMOV HFM are based on the conceptual understanding of permeable pathways within semi-perched and regional aquifers, as inferred from water-level altitudes, vertical gradients, tritium data, and aquifer-test results in boreholes *UE-20j*, *ER-20-12*, and *PM-3*.

The PMOV HFM is an ungridded hydrostratigraphic framework model that extends across the entire PMOV groundwater basin. HSUs shown on the cross section in figure 6*A* were extracted from the PMOV HFM and mapped to a 200-ft by 131-ft (61-m by 40-m) grid in the vertical dimension (fig. 6*B*). HSUs in the PMOV HFM (fig. 6*B*) were modified in the mHFM (fig. 6*C*) by grouping HSUs that conceptually are hydraulically similar and splitting HSUs based on water-level, aquifer-test, and tritium data, as discussed below. There are 13 HSUs in the mHFM as compared to 11 HSUs in the PMOV HFM (table 2). The mHFM is documented in Jackson (2021, app. D).

Spatial extents of the TMWTA and TMLVTA remained unchanged between the PMOV HFM and mHFM (fig. 6). The TMWTA and TMLVTA constitute the semi-perched aquifer. The TMWTA provides the primary pathway for the shallow tritium plume to migrate from the HANDLEY nuclear test to well *ER-20-12 p4*. The TMLVTA is conceptualized to function as an aquifer but is expected to have lower transmissivity (0.1–10 ft^2/d) compared to the TMWTA (1–300 ft^2/d), based on aquifer-test data (Frus and Halford, 2018; Jackson and others, 2021). The lithologic log of borehole *ER-20-12* indicates that intervals within the TMLVTA are zeolitically altered, which reduces the matrix porosity and permeability of the vitric tuff (U.S. Department of Energy, 2020).

The CHLFA5 was modified into the mCHLFA5 by extending the unit deeper so that wells *ER-20-12 p3* and *ER-20-12 p2* are open to the same unit. Wells *ER-20-12 p3* and *ER-20-12 p2* are open to the CHLFA5 and CHZCM, respectively (fig. 6*B*). However, these wells have the same water-level altitude (4,378 ft; fig. 2), which suggests that they are hydraulically connected and that the units open to these wells can be modeled as one modified unit. Therefore, the mCHLFA5 includes the CHLFA5 and some permeable intervals in the underlying nonwelded tuff that are part of the CHZCM.

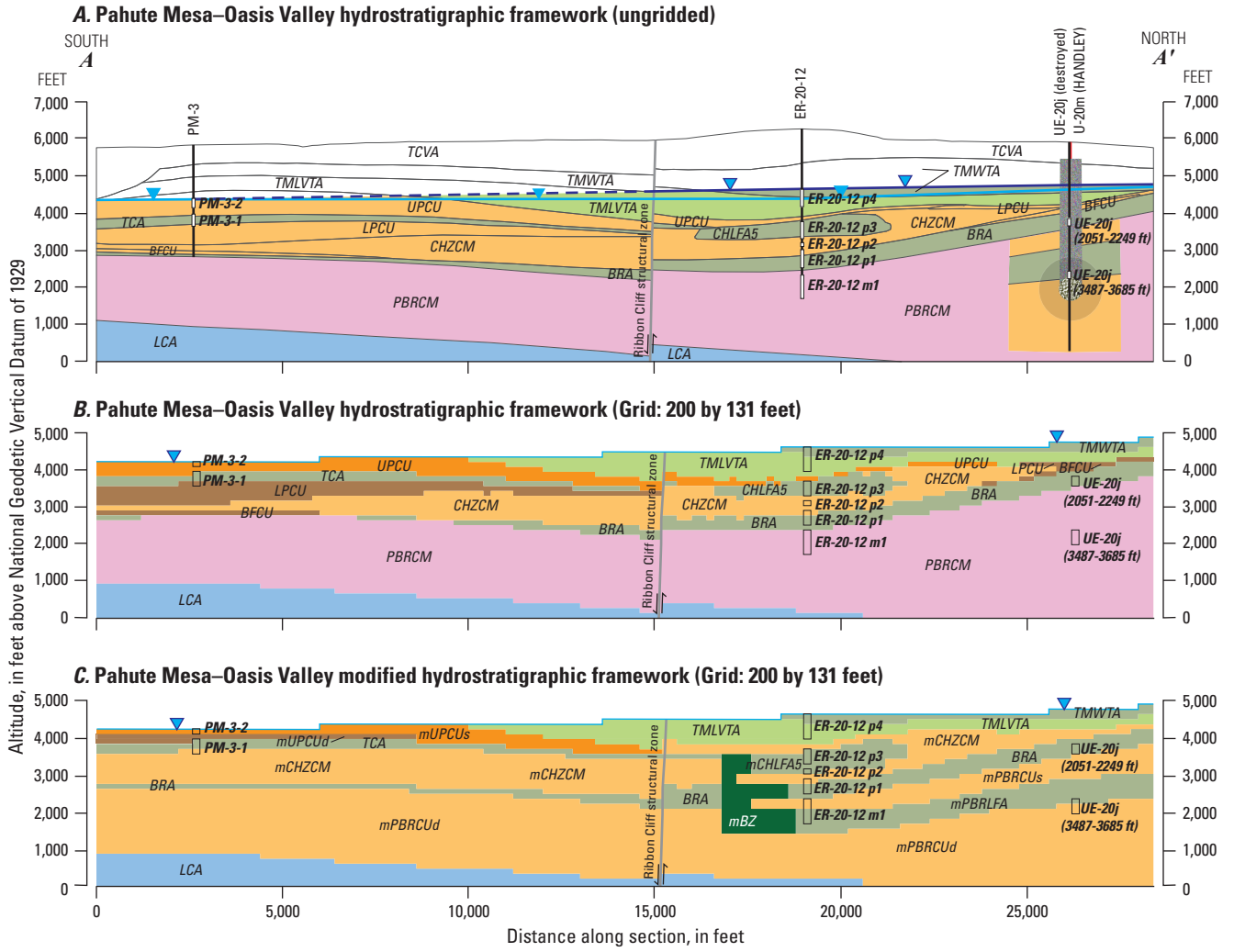

EXPLANATION

Geologic units

- Nonwelded and bedded tuffs
- Vitric tuff
- Lava and (or) welded tuff
- Volcanic rocks, undifferentiated
- Carbonate rock

- **Water table in numerical models**
- **Water table in area of semi-perched aquifer** —Line dashed where uncertain
- **Regional potentiometric surface where vertical hydraulic-head differences are small (less than 50 feet)**
- **Normal fault**—Arrows show relative movement along fault
- PM-3 **Borehole and identifier**
- *PM-3-2* **Well and identifier**

- **HANDLEY underground nuclear test**—Small circle represents cavity; estimated size based on reported minimum yield, depth of burial, and overburden density (from Pawloski, 1999). Large circle is three-cavity radii and represents conceptual exchange volume. Vertical chimney extends above cavity; upper extent of chimney projected to land surface because a collapse crater formed about 24 hours after the detonation. Spatial extent of lava and nonwelded tuffs around HANDLEY test interpreted from lithologic log in borehole UE-20j.
- *LPCU* **Hydrostratigraphic units in Pahute Mesa–Oasis Valley hydrostratigraphic framework (sections A and B)**—see table 2 for list of unit names
- *mCHZCM* **Hydrostratigraphic units in modified hydrostratigraphic framework of numerical models (section C)**—see table 2 for list of unit names

Figure 6. Hydrostratigraphic cross sections showing geologic units, hydrostratigraphic units (HSUs), and well locations in boreholes *PM-3*, *ER-20-12*, and *UE-20j*, Pahute Mesa, southern Nevada. *A*, Cross section showing HSUs extracted from the Pahute Mesa–Oasis Valley hydrostratigraphic framework model (PMOV HFM; U.S. Department of Energy, 2020). *B*, Cross section showing HSUs from the PMOV HFM that are mapped to a grid with cell sizes in the lateral (x) and vertical (y) dimensions of 200 and 131 feet, respectively. *C*, Cross section showing modified HSUs that were used in the modified hydrostratigraphic framework of numerical models. Grid cell sizes in the lateral (x) and vertical (y) dimensions are 200 and 131 feet, respectively.

Table 2. Saturated hydrostratigraphic units in the Pahute Mesa–Oasis Valley hydrostratigraphic framework (U.S. Department of Energy, 2020) and modified hydrostratigraphic framework used in the numerical models of this study, Pahute Mesa, southern Nevada.

[**Hydraulic significance:** ft^2/d, foot squared per day. **Abbreviation:** NA, not applicable]

Hydrostratigraphic units in Pahute Mesa–Oasis Valley hydrostratigraphic framework		Hydrostratigraphic units in modified hydrostratigraphic framework of numerical models		
Abbreviation	**Name**	**Abbreviation**	**Name**	**Hydraulic significance**
Structures				
NA	NA	mBZ	Modified brecciated zone	Unit extends through CHLFA5, CHZCM, BRA, and PBRCM between the Ribbon Cliff structural zone and borehole *ER-20-12*. The mBZ is a conceptualized permeable pathway related to the structural zone that induces upward flow at borehole *ER-20-12*. Permeable mBZ also is conceptualized to connect BRA and CHLFA5 near borehole *ER-20-12* to the TCA, which creates a hydraulic connection for the propagation of the pumping (well drilling) signal from borehole *ER-20-12* to borehole *PM-3*.
Aquifers				
BRA	Belted Range aquifer	BRA	Belted Range aquifer	BRA is composed mostly of lavas and welded tuffs, which are conceptualized as aquifers, with lesser amounts of nonwelded and bedded tuffs. BRA is a transmissive unit in borehole *UE-20j* based on aquifer-test results (Frus and Halford, 2018). High measured tritium concentration in BRA at borehole *ER-20-12* indicates that tritium from the HANDLEY test migrated relatively fast (1.5 miles in 46 years).
CHLFA5	Calico Hills lava flow aquifer #5	mCHLFA5	Modified Calico Hills lava flow aquifer #5	Unit is composed predominantly of lava from the CHLFA5, which is conceptualized as an aquifer. Unit contains minor nonwelded tuff from the CHZCM.
TCA	Tiva Canyon aquifer	TCA	Tiva Canyon aquifer	TCA is the most transmissive unit in borehole *PM-3* based on aquifer-test results (Frus and Halford, 2018). TCA also is most likely unit that propagates the pumping (well drilling) signal from the CHLFA5 and BRA at borehole *ER-20-12* to borehole PM-3.
TMLVTA	Timber Mountain lower vitric tuff aquifer	TMLVTA	Timber Mountain lower vitric tuff aquifer	TMLVTA is composed of vitric tuff. TMLVTA and TMWTA are conceptualized to form a semi-perched aquifer between boreholes *UE-20j* and *ER-20-12*. TMLVTA is conceptualized to have lower transmissivity compared to overlying TMWTA based on aquifer-test data (Jackson and others, 2021).
TMWTA	Timber Mountain welded tuff aquifer	TMWTA	Timber Mountain welded tuff aquifer	TMWTA is composed of welded tuff. TMWTA and TMLVTA are conceptualized to form a semi-perched aquifer. High measured tritium concentration in TMWTA at borehole *ER-20-12* indicates that tritium from the HANDLEY test migrated relatively fast (1.5 miles in 46 years).
PBRCM	Pre-Belted Range composite unit	mPBRLFA	Modified pre-Belted Range lava flow aquifer	Unit is composed predominantly of lava flows, which are conceptualized as aquifers. This is the most transmissive unit in borehole *UE-20j* based on aquifer-test results (Frus and Halford, 2018).

Table 2. Saturated hydrostratigraphic units in the Pahute Mesa–Oasis Valley hydrostratigraphic framework (U.S. Department of Energy, 2020) and modified hydrostratigraphic framework used in the numerical models of this study, Pahute Mesa, southern Nevada.—Continued

[**Hydraulic significance:** ft^2/d, foot squared per day. **Abbreviation:** NA, not applicable]

Hydrostratigraphic units in Pahute Mesa–Oasis Valley hydrostratigraphic framework		Hydrostratigraphic units in modified hydrostratigraphic framework of numerical models		
Abbreviation	**Name**	**Abbreviation**	**Name**	**Hydraulic significance**
Confining units				
PBRCM	Pre-Belted Range composite unit	mPBRCUd	Modified pre-Belted Range confining unit–deep	Unit is composed predominantly of nonwelded tuffs, which are conceptualized as confining units. This is a low transmissivity unit in borehole *UE-20j* based on aquifer-test results (Frus and Halford, 2018).
		mPBRCUs	Modified pre-Belted Range confining unit–shallow	Unit is composed predominantly of nonwelded tuffs, which are conceptualized as confining units. This is a low transmissivity unit in borehole *UE-20j* based on aquifer-test results (Frus and Halford, 2018).
BFCU	Bullfrog confining unit	mCHZCM	Modified Calico Hills zeolitic composite unit	BFCU, CHZCM, LPCU, and UPCU are composed of nonwelded or bedded tuffs, which are conceptualized as confining units. UPCU downgradient from Ribbon Cliff structural zone was not grouped into mCHZCM to allow for potential variability between mCHZCM and UPCU when estimating hydraulic and transport properties.
CHZCM	Calico Hills zeolitic composite unit			
LPCU	Lower Paintbrush confining unit			
UPCU	Upper Paintbrush confining unit	mUPCUd	Modified upper Paintbrush confining unit–deep	UPCU south of Ribbon Cliff structural zone is composed of nonwelded tuffs and is conceptualized as a confining unit. The mUPCUs and mUPCUd are shallow and deep UPCU, respectively, in borehole *PM-3*. The mUPCUs has a higher transmissivity (4 ft^2/d) compared to the deeper mUPCUd (0.2 ft^2/d) based on aquifer-test data (Frus and Halford, 2018). The mUPCUd is the intervening unit between mUPCUs and TCA and is used to maintain a 2-foot, downward vertical-head difference between wells in borehole PM-3.
		mUPCUs	Modified upper Paintbrush confining unit–shallow	
LCA	Lower carbonate aquifer	LCA	Lower carbonate aquifer	LCA is conceptualized as a confining unit in the numerical models because the LCA occurs 3,000–6,000 feet below the water table and a transmissivity with depth analysis (Halford and Jackson, 2020) suggests that deep saturated rocks typically have low transmissivity.

The UPCU, LPCU, CHZCM, and BFCU are composed of nonwelded or bedded tuffs and are conceptualized to function as confining units (U.S. Department of Energy, 2020). The large vertical gradient of 0.3 ft/ft (260 ft vertical-head difference) between wells *ER-20-12 p4* and *ER-20-12 p3* supports the UPCU functioning as a confining unit (fig. 2). The 0.04 ft/ft vertical gradient (17-ft vertical-head difference) between wells *ER-20-12 p2* and *ER-20-12 p1* indicates that the intervening CHZCM functions as a confining unit (fig. 2). Between the Ribbon Cliff structural zone and the northern end of section *A–A'*, the UPCU, LPCU, BFCU, and most of the CHZCM (fig. 6*B*) were grouped into a modified unit, referred to as the modified CHZCM (mCHZCM; fig. 6*C*). South of the Ribbon Cliff structural zone, the LPCU, CHZCM, and BFCU also are grouped into the mCHZCM (fig. 6*C*). The UPCU south of the structural zone was not grouped into the mCHZCM to allow for potential variability between the UPCU and mCHZCM when estimating hydraulic and transport properties. Hydraulic- and transport-property distributions may differ between the UPCU and mCHZCM because available information is contradictory on groundwater flow and tritium migration patterns between boreholes *ER-20-12* and *PM-3*. Tritium concentrations and vertical gradients at borehole *PM-3* suggest a permeable shallow flow path, at least partly through the UPCU. However, transmissivity estimates and drawdown observations in wells *PM-3-1* and *PM-3-2* indicate that the hydraulic connection occurs through deeper units near borehole *ER-20-12* and propagates into shallower units toward borehole *PM-3*.

The UPCU south of the Ribbon Cliff structural zone was split into shallow and deep units, based on water-level and aquifer-test data (fig. 6*C*). To maintain the small, downward, vertical gradient of 0.004 ft/ft (2-ft vertical-head difference) between the UPCU and TCA at borehole *PM-3* (fig. 2), the recharge rate to the top of the UPCU must exceed the vertical hydraulic conductivity of the UPCU. This can be accomplished if the lower part of the UPCU that separates wells *PM-3-1* and *PM-3-2* has a low transmissivity. Slug-test results of packer-isolated intervals in borehole *PM-3* indicate that the upper 200 ft of UPCU, open to well *PM-3-2*, has a transmissivity of 4 ft^2/d and the lower 300 ft has a transmissivity of 0.2 ft^2/d (fig. 3*B*; Frus and Halford, 2018). Accordingly, the UPCU was split into a shallow and deep UPCU, referred to as mUPCUs and mUPCUd, respectively (fig. 6*C*).

The TCA is a hydraulically significant unit that remained unchanged between the PMOV HFM and mHFM (fig. 6). The TCA is the most transmissive HSU (600 ft^2/d) in borehole *PM-3*, based on slug-test results of packer-isolated intervals in the borehole (fig. 3*B*; Frus and Halford, 2018). As a result, the TCA is the likely pathway to propagate the hydraulic response between boreholes *ER-20-12* and *PM-3* that resulted from the removal of water during drilling of borehole *ER-20-12*.

The BRA is a hydraulically significant unit that remained unchanged between the PMOV HFM and mHFM (fig. 6). The BRA is the second-most transmissive unit in borehole *UE-20j* based on aquifer-test results (fig. 3*A*; Frus and Halford, 2018) and has an estimated transmissivity of 80 ft^2/d in well *ER-20-12 p1* (fig. 3*C*). The BRA provides a pathway for a deeper tritium plume to migrate from the HANDLEY nuclear test to well *ER-20-12 p1*. A high measured tritium concentration (26,000 pCi/L) in well *ER-20-12 p1* during 2017 indicates that tritium from the HANDLEY test migrated through the BRA to well *ER-20-12 p1* (fig. 2).

The PBRCM north of the Ribbon Cliff structural zone was split into three units (fig. 6) based on aquifer-test results (fig. 3*A*). Interpretation of slug-test data in borehole *UE-20j* indicates that the upper 530 ft, middle 800 ft, and lower 2,000 ft of PBRCM have transmissivities of 9.5, 618, and 30 ft^2/d, respectively (fig. 3*A*; Frus and Halford, 2018; Jackson, 2021). The upper and lower part of the PBRCM are predominantly nonwelded tuff, whereas the middle part is mostly lava flow (U.S. Department of Energy, 2020). Transmissivity estimates from slug tests suggest that PBRCM should be split into three modified units: (1) a shallow, low-transmissivity confining unit (mPBRCUs); (2) a middle high-transmissivity lava-flow aquifer (mPBRLFA); and (3) a deep, low-transmissivity confining unit (mPBRCUd). The modified units are extended southward to borehole *ER-20-12*, assuming each unit has relatively uniform thickness. All PBRCM south of the Ribbon Cliff structural zone was assigned to the mPBRCUd because of lateral continuity and the assumption that deep, saturated rocks likely have low transmissivity (Jackson and others, 2021; see section, "Transmissivity Variations with Depth," for details).

Low-transmissivity units must occur between HSUs open to wells at borehole *ER-20-12* to provide hydraulic separation and induce vertical-head differences. For example, low-transmissivity mPBRCUs is inferred to occur between wells *ER-20-12 m1* and *ER-20-12 p1* (fig. 6*C*) to cause an upward vertical gradient of 0.01 ft/ft (9-ft vertical-head difference) from the PBRCM (*ER-20-12 m1*) to the BRA (*ER-20-12 p1*). Likewise, an upward vertical gradient of 0.04 ft/ft (17-ft vertical-head difference) from the BRA (*ER-20-12 p1*) to the mCHLFA5 (*ER-20-12 p2*) is caused by the mCHZCM, which provides hydraulic separation between the BRA and mCHLFA5 (fig. 6*C*).

The LCA remained unchanged between the PMOV HFM and mHFM (fig. 6). The LCA is conceptualized as a confining unit in the study area because this unit occurs 3,000–6,000 ft below the water table and a transmissivity-with-depth analysis (Jackson and others, 2021) suggests that deep saturated rocks typically have low transmissivity. Furthermore, the LCA is not expected to be an aquifer because, even though no wells in the PMOV basin intersect the LCA, this discontinuous unit likely has been altered by volcanic activity (U.S. Department of Energy, 2020).

A new conceptual unit, referred to as a modified brecciated zone (mBZ), was incorporated into the modified HFM based on hydraulic connections inferred during model calibration (fig. 6*C*). The mBZ incorporates predominantly lava flows with lesser amounts of nonwelded and bedded tuff between the Ribbon Cliff structural zone and borehole *ER-20-12*. At borehole *ER-20-12*, there are upward, vertical-head differences between the mCHLFA5, BRA, and mPBRLFA. Based

on the PMOV HFM without the mBZ, groundwater flows sub-parallel through the BRA and mPBRLFA, and continues across the Ribbon Cliff structural zone because of overlying and underlying confining units. There is no hydraulic feature in the PMOV HFM that induces upward flow at borehole *ER-20-12*. Upward flow can be induced by assuming that the Ribbon Cliff structural zone is a hydraulic barrier. However, assigning a low hydraulic conductivity (1×10^{-6} ft/d) along the structural zone during calibration of the numerical flow and transport models was not sufficient to generate the large, upward vertical-head differences farther north at borehole *ER-20-12*. A permeable pathway that extends through previously mapped aquifers and confining units downgradient from borehole *ER-20-12* is necessary to allow groundwater to flow upward. Delineating the permeable mBZ close to or at the Ribbon Cliff structural zone induces upward flow, but this permeable unit needs to be closer to borehole *ER-20-12* to induce the large, upward, vertical-head differences at this borehole. Furthermore, as borehole *ER-20-12* was drilled into the CHLFA5 and BRA, the drilling (pumping) signal propagated through the TCA to borehole *PM-3*. A permeable unit that connects the BRA and mCHLFA5 is required to simulate the pumping response at well *PM-3-1*, which was achieved by introducing a new unit, the mBZ.

The mBZ feature can be explained by (1) an incorrect interpretation of the mapped location of the Ribbon Cliff structural zone in the PMOV HFM; or (2) the structural zone consisting of more than one fault. The Ribbon Cliff structural zone is an inferred buried feature that does not have an observed surface expression. The structural zone is inferred to exist based on evidence from surface geologic mapping, lithologic logs, and geophysical data (U.S. Department of Energy, 2020, p. 40). Therefore, the location of the structural zone could be several thousand feet farther north than currently mapped. The Ribbon Cliff structural zone is interpreted as a single normal fault; however, the structural zone may consist of a series of faults within several thousand feet that create permeable pathways for upward flow between HSUs. Regardless of the geologic explanation, the mBZ is a generalized feature (fig. 6*C*) that was delineated to create a hydraulic connection for upward flow south of borehole *ER-20-12*.

Numerical Model Development and Calibration

Recharge, hydraulic-conductivity, specific-yield, and specific-storage distributions were estimated by coupling one steady-state and one transient three-dimensional groundwater model using the computer code MODFLOW-2005 (Harbaugh, 2005). An effective-porosity distribution was estimated by coupling the three-dimensional, steady-state groundwater model (MODFLOW) to a three-dimensional multispecies transport model (MT3DMS; Zheng and Wang, 1999)[3]. The models are documented in a separate USGS data release (Jackson, 2021).

The steady-state groundwater model simulates predevelopment flow (prior to the HANDLEY nuclear detonation) and was used to estimate recharge and hydraulic-conductivity distributions between boreholes *UE-20j* and *PM-3*. The transient groundwater model simulated water-level changes in wells *PM-3-1* and *PM-3-2* from groundwater withdrawals during drilling of borehole *ER-20-12*. The transient groundwater model was used during model calibration to refine estimates of hydraulic conductivity, specific yield, and specific storage between boreholes *PM-3* and *ER-20-12*. The transient transport model simulated tritium migration sourced from the HANDLEY nuclear test between the date of detonation (March 26, 1970) and 50 years later (March 26, 2020). The transport model was used during model calibration to refine estimates of longitudinal dispersivity and the effective-porosity distribution. The use of separate, but coupled, models introduces fewer errors compared to simulating predevelopment flow, pumping responses, and tritium migration with a single generalized model.

The groundwater-flow and transport models have the same domain extent, mHFM, spatial discretization, and hydraulic and transport properties. The numerical models simulate groundwater flow and tritium migration along a northeast-to-southwest cross section that represents a groundwater-flow path from borehole *U-20m* (HANDLEY) through boreholes *ER-20-12* and *PM-3* (fig. 2). The model domain extends from 2,000 ft upgradient from borehole *U-20m* to about 2,600 ft downgradient from borehole *PM-3*.

Spatial Domain and Discretization

The numerical flow and transport models have the same spatial grid as the mHFM, where one HSU and associated hydraulic and transport properties are estimated for each model cell in the mHFM. The orientation and geometry of HSUs from the PMOV HFM were used to select an appropriate spatial discretization for the numerical models and mHFM. A spatial discretization of 200-ft (X) by 131-ft (Y) (61-m by 40-m) was selected (Y-dimension is vertical dimension in fig. 6*B*). This discretization minimizes the number of cells in the numerical models while preserving most of the lateral continuity and top and bottom contacts between HSUs (fig. 6*A*). The vertical (Y) dimension discretization of 131 ft causes minor discontinuities in relatively thin, hydraulically

[3]The USGS computer program, SEAWAT (Langevin and others, 2007), was used to couple the steady-state (MODFLOW) groundwater model to the MT3DMS transport model. SEAWAT simulates three-dimensional, variable-density groundwater flow coupled with multi-species solute and heat transport. SEAWAT packages simulating variable density, variable viscosity, and heat transport were not used. The SEAWAT program was used because its numerical solver converges faster compared to solving the groundwater-flow equation and advection-dispersion equation with radioactive decay by directly coupling MODFLOW and MT3DMS models with batch files.

significant HSUs, such as the UPCU and TCA north and south of the Ribbon Cliff structural zone, respectively (fig. 6*B*). These discontinuities were removed by manually altering HSUs in individual cells within the mHFM to form laterally continuous HSUs (fig. 6*C*). HSUs in the PMOV HFM (fig. 6*A*) also were modified in the mHFM (fig. 6*C*) by grouping HSUs that, conceptually, are hydraulically similar and splitting HSUs based on water-level, aquifer-test, and tritium data (see section, "Modified Hydrostratigraphic Framework," for details).

The lateral (X) dimension of the model domain coincides with the *A*–*A*′ section trace shown in figure 6*C*. Section *A*–*A*′ extends from 0 to 28,400 ft (fig. 7*A*). The model domain X reference at 0 ft corresponds to X and Y coordinates of 541,303 and 4,128,903 m, respectively, in Universal Transverse Mercator (UTM), zone 11, North American Datum of 1983 (NAD 83) projection. The X reference at 28,400 ft corresponds to X and Y coordinates of 538,606 and 4,120,686 m, respectively, in UTM, zone 11, NAD 83 projection. The model grid is in units of feet.

The three-dimensional, numerical model grid (and mHFM grid) was rotated 90 degrees about the x-axis so that two-dimensional arrays of hydraulic- and transport-property distributions coincided with the vertical distribution of HSUs shown in the cross section (figs. 6*C* and 7*A*). Rotating the grid causes the horizontal dimension to be represented by columns (X) and layers (Y) and the depth (Z) dimension to be represented by rows (fig. 7*B*; Halford and Yobbi, 2006; Garcia and others, 2013).

The horizontal dimension of the model grid, which coincides with section *A*–*A*′ (fig. 6*C*), was divided into 142 columns (X) and 37 layers (Y) (fig. 7*A*). The 142 uniform, 200-ft-long columns extend from 0 to 28,400 ft. The 37 uniform, 131-ft-thick layers extend from 0 to 4,888 ft above NGVD 29 (fig. 7*A*). The top of the uppermost, active model cell in each layer coincides with the water table, which encompasses the uppermost occurrence of saturation, including semi-perched intervals. The saturated thickness of each layer was specified and did not change in response to simulated pumping because a maximum drawdown of less than 10 ft in borehole *ER-20-12* was small compared to cell thickness. Therefore, the simulated water table does not move through layers.

The third dimension of the model grid was constructed by projecting the cross section into the page (fig. 7*B*). The projected part of the model domain extends from 0 to 2,000 ft and was divided into 10 uniform, 200-ft-thick rows (fig. 7*B*). The horizontal section plane shown in figure 7*A* is the top of the projected row at 2,000 ft. The numerical models in this study are quasi-three-dimensional models because of the projected third dimension.

The quasi-three-dimensional construction of the numerical models was done to account for: (1) flow convergence to borehole *ER-20-12* from groundwater withdrawals during drilling; and (2) lateral dispersion of tritium migration along the cross-sectional path. Because the model domain only was projected in one direction (into the page), only one-half of the groundwater system was simulated explicitly. Symmetry was assumed about the cross section, where the cross section in figure 7*A* was the plane of symmetry.

Estimating Recharge, Hydraulic Properties, and Transport Properties

Heterogeneous hydraulic-property (hydraulic conductivity, specific yield, and specific storage) and effective-porosity distributions were estimated with PEST, the Parameter ESTimation code (Doherty, 2010a), using pilot points (RamaRao and others, 1995). The locations of pilot points were user-specified. More pilot points occurred in areas where more data are available to constrain hydraulic-property and effective-porosity estimates. Estimated hydraulic-property and effective-porosity values at user-specified locations were translated into continuous hydraulic-property and effective-porosity fields by interpolation with kriging using variograms (Doherty, 2010b).

Isotropic, exponential variograms defined spatial variability of log-hydraulic properties and log-effective porosities, where spatial correlation was specified with user-defined ranges (distances). Spatial correlation is assumed non-existent where distances between the interpolated location (cell center) and known value (pilot point) exceed the user-defined range (RamaRao and others, 1995). A hydraulic-property or effective-porosity value at a cell functionally was an inverse-distance weighted average of the eight nearest pilot-point values if all distances between cell center and pilot points were less than the range (RamaRao and others, 1995). A hydraulic-property or effective-porosity value at a cell is a simple average if distances between a cell center and the eight nearest pilot points all exceed the range.

Interpolated hydraulic properties and effective porosities varied spatially along the cross section for each HSU (fig. 6*C*). For example, in this study, each HSU was a unique zone in MODFLOW and the pilot points were grouped by zone. This means that only pilot points within the HSU (zone) were used in the interpolation of hydraulic-property and effective-porosity values at model cells within the HSU. Therefore, hydraulic properties and effective porosities are estimated at pilot points, interpolated laterally within each HSU, and then assigned the same value for all projected rows where the HSU occurs. Heterogeneous hydraulic-property and effective-porosity fields were uniform with the projected depth (into the page).

Hydraulic properties have assigned anisotropy ratios of 1, indicating that hydraulic properties are laterally and vertically isotropic along the cross-section plane. However, this does not mean that anisotropy is not simulated. Heterogeneity and anisotropy are correlated, where large degrees of anisotropy can be simulated with large contrasts in hydraulic properties (Halford and Jackson, 2020). Heterogeneity is simulated entirely by contrasts in hydraulic properties within and between HSUs. Lateral and vertical contrasts (along the cross

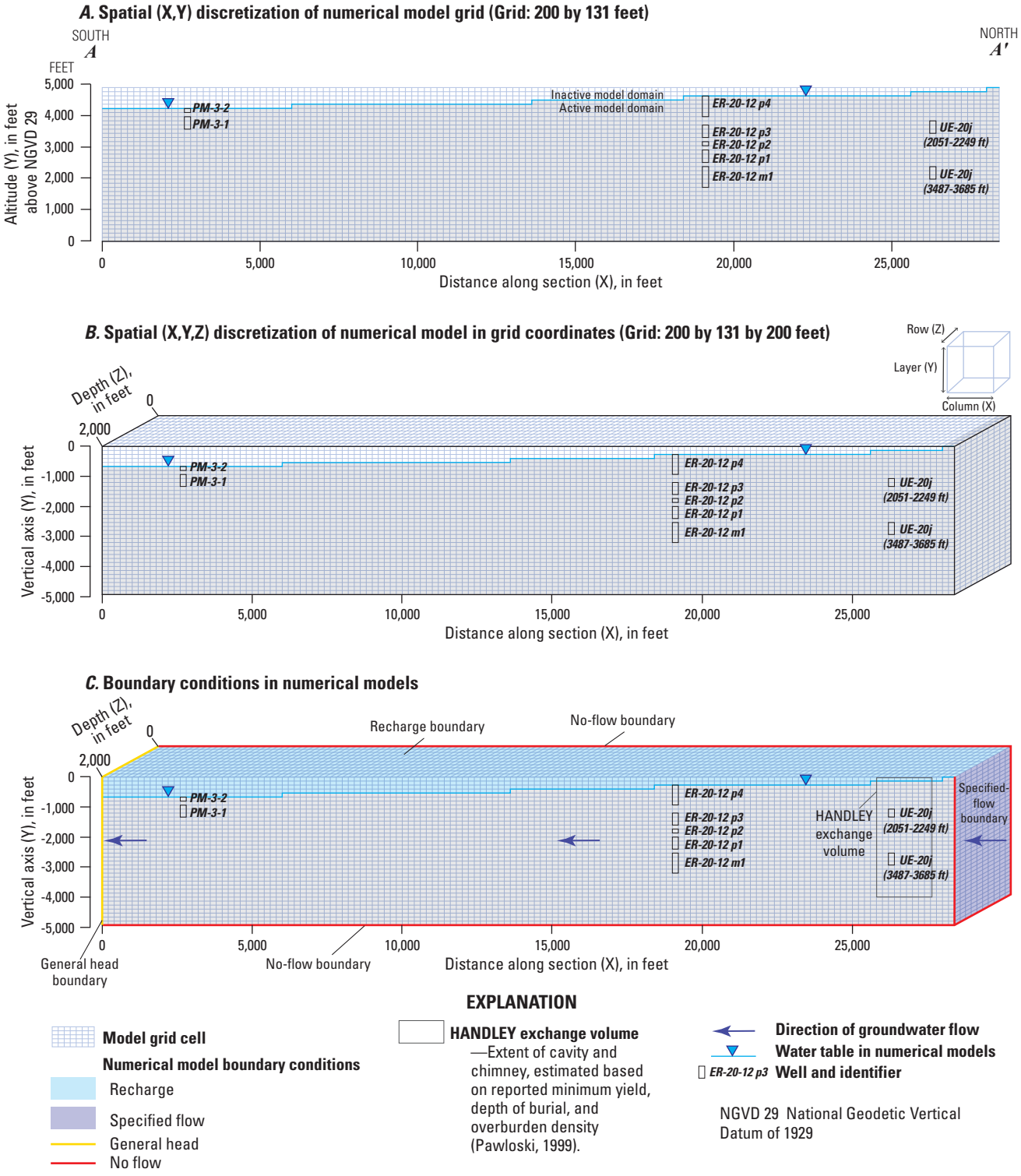

Figure 7. Cross sections showing numerical model spatial discretization, boundary conditions, and well locations in boreholes *PM-3*, *ER-20-12*, and *UE-20j*, Pahute Mesa, southern Nevada. *A*, Spatial (X,Y) discretization of numerical model grid. *B*, Spatial (X,Y,Z) discretization of numerical models in grid coordinates. *C*, Boundary conditions of numerical models.

section) were simulated by adding pilot points to HSUs, where greater pilot-point density allows for increased heterogeneity (and anisotropy).

Unique hydraulic properties were not estimated for the Ribbon Cliff structural zone. Instead, the structural zone was simulated as an interface where HSUs were offset and juxtaposed in the PMOV HFM. The hydraulic properties of juxtaposed HSUs on each side of the Ribbon Cliff structural zone determined the degree of hydraulic connection across the structural zone.

Recharge, longitudinal dispersivity, and matrix diffusion were estimated without the use of pilot points. Instead, individual parameters were defined in MODFLOW and MT3DMS package files, and these parameters were estimated with PEST.

Hydraulic Conductivity

Hydraulic conductivities were assigned with the Layer-Property Flow package in MODFLOW (Harbaugh, 2005). Hydraulic conductivities were distributed with 145 pilot points so that spatial variability could be simulated in HSUs. Isotropic, exponential variograms were used to define spatial variability of log-hydraulic conductivities with a specified range of 2,000 ft (RamaRao and others, 1995). Distributed hydraulic conductivities in HSUs were mapped to the mHFM and parsed to a two-dimensional array for each model row. All groundwater-flow and transport models used the same arrays of hydraulic conductivity.

Specific Yield and Specific Storage

Specific yields and specific storages were assigned with the Layer-Property Flow package in MODFLOW (Harbaugh, 2005). Specific-yield values typically range from 0.01 to 0.05 in fractured volcanic rocks (Winograd and Thordarson, 1975). Specific-storage values typically range from 1×10^{-6} to 5×10^{-6} 1/ft, regardless of HSU. Specific-yield and specific-storage values only were estimated (with PEST) between boreholes *PM-3* and *ER-20-12* because these storage values only could be estimated where saturated rocks were affected by pumping. In areas where HSUs were unaffected by pumping, a specific yield of 0.02 was assigned and specific storage of 2×10^{-6} 1/ft was assigned.

Specific-storage values estimated with PEST ranged from 1×10^{-7} to 5×10^{-5} 1/ft, which are beyond the expected range from 1×10^{-6} to 5×10^{-6} 1/ft. Underestimation of specific storages likely compensated for overestimating contributing thicknesses of HSUs. Specific storage is estimated in the numerical model assuming that the HSU thickness and contributing thickness are the same, and compensating errors result when these thicknesses are not equivalent. For example, suppose a 10-ft-thick interval contains all permeable, flowing fractures within a 100-ft-thick HSU. In this case, the actual HSU thickness is 100 ft, but the contributing thickness is 10 ft. If the 10-ft-thick permeable interval has a true specific storage of 2×10^{-6} 1/ft, but this permeable interval was simulated as a homogeneous 100-ft-thick layer, then the correct storage coefficient would be simulated if a specific storage of 2×10^{-7} 1/ft is estimated. Therefore, estimated specific storages are effective specific storages.

Specific yields and specific storages were estimated with 146 pilot points so that spatial variability could be simulated in HSUs. Interpolated specific yields were estimated in the first active cell in each model layer, whereas specific storages were estimated from the second active cell in each model layer to the bottom of the model domain (fig. 7*C*). Isotropic, exponential variograms defined spatial variability of log-specific yields and log-specific storages with a specified range of 2,000 ft (RamaRao and others, 1995). Distributed specific yields and specific storages were mapped to the mHFM and parsed to two-dimensional arrays for each MODFLOW model row as was done with hydraulic conductivities.

Effective Porosity

Effective porosities were assigned with the basic transport package in MT3DMS (Zheng and Wang, 1999). Effective porosities were distributed with 145 pilot points so that observed spatial variability could be simulated in HSUs. Isotropic, exponential variograms were used to define spatial variability of log-effective porosities with a range of 2,000 ft (RamaRao and others, 1995). Distributed effective porosities in HSUs were mapped to the mHFM and parsed to a two-dimensional array for each model row. Effective porosity was used only in the transport model.

Tritium migration was simulated assuming a single-porosity aquifer system. Therefore, model-estimated effective porosities account for the mobile (advective) porosity within the fracture network and rock matrix. The range of expected, model-estimated effective porosities was computed a priori using a thickness-porosity product (bn). Thickness-porosity product is a lumped term that accounts for the average effective porosity (n) and thickness (b) of rock contributing to groundwater flow without requiring the knowledge of either factor independently. For example, a porosity of 2 percent and a thickness of 2,000 ft or a porosity of 5 percent and a thickness of 800 ft both have a thickness-porosity product of 40 ft. The thickness-porosity product is derived using Darcy's law (eq. 1) and the average linear velocity (eq. 2).

$$Q = -KA\frac{dh}{dL} = -\left[\frac{T}{b}\right]wb\frac{dh}{dL} \quad (1)$$

$$v = \frac{Q}{An} = \frac{Q}{(wb)n} \quad (2)$$

In equations 1 and 2, Q is the volumetric flow rate, or discharge [L^3/T]; K is the hydraulic conductivity [L/T]; A is the cross-sectional area [L^2]; dh/dL is the hydraulic gradient [L/L]; T is transmissivity [L^2/T]; b is the aquifer thickness [L];

w is the width of aquifer perpendicular to flow [L]; and v is the average linear velocity [L/T]. The thickness-porosity product (bn) is defined in equation 3 by substituting Q equal to $-[T/b]\,wb[dh/dL]$ from equation 1 for Q in equation 2 and rearranging terms.

$$bn = -\left[\frac{T}{v}\right]\frac{dh}{dL} \tag{3}$$

Average linear velocity (v) was estimated from a plot of tritium concentration versus distance (Jackson, 2021, app. E). This method requires nuclear-test-derived tritium concentrations measured during the same year from wells downgradient from the nuclear test. The average linear velocity from the HANDLEY nuclear test is uncertain because of limited data. However, the average linear velocity estimated from the BENHAM nuclear test can be used as a proxy because (1) the BENHAM nuclear test occurred less than 6 mi from the HANDLEY test; (2) BENHAM and HANDLEY were both large-yield (greater than 1 megaton) nuclear tests that were detonated in volcanic rocks within the Pahute Mesa area (U.S. Department of Energy, 2015); and (3) tritium was detected in seven boreholes downgradient from the BENHAM nuclear test, which was sufficient to estimate an average linear velocity. The BENHAM test average linear velocity is about 145 ft/yr, which was estimated from a tritium migration distance of 7,200 ft in 50 years (Jackson, 2021, app. E).

Hydraulic gradient (dh/dL) and transmissivity (T) were estimated near the HANDLEY test. The estimated hydraulic gradient is about 0.036 ft/ft. Hydraulic gradient was estimated using water-level altitudes measured in boreholes *UE-20j* and *ER-20-12* because these two boreholes are about 7,200 ft apart. Transmissivity was estimated from the calibrated groundwater-flow model, where the geometric mean transmissivity is about 430 ft^2/d between the HANDLEY nuclear test and borehole *ER-20-12*. Substituting these estimated parameters in equation 3, the thickness-porosity product is about 40 ft. The ratio of the thickness-porosity product (40 ft) to the total model thickness (4,888 ft) is the average effective porosity, which is 0.008. The average effective porosity is the expected, average value of effective porosity for volcanic rocks outside the cavity-chimney system of HANDLEY. Within the cavity-chimney system, the expected range of effective porosity is between 0.05 and 0.3, and depends on the degree of rubblization (Pawloski, 1999).

Recharge

Recharge was simulated across the entire top surface of the model domain with the river package in MODFLOW (Harbaugh, 2005). The river package was used, instead of the recharge package, because model rows and layers were inverted. In the recharge package, the inverted rows and layers would have caused recharge to be simulated along the plane of symmetry, instead of on top of the model domain. In the river package, river stage and river bottom altitudes were assigned large values of 9,999 and 9,998 ft, respectively, so that river cells always simulate a loss of water and recharge occurs.

Recharge only could be estimated reliably in areas where water-level data constrain recharge-rate estimates. Therefore, recharge rates only were estimated with PEST at 19 river-cell locations that are within 2,000 ft of boreholes *PM-3*, *ER-20-12*, and *UE-20j*. The steady-state groundwater model and transport model used the same recharge distribution.

Dispersivity and Matrix Diffusion

In the transport model, longitudinal, transverse, and vertical dispersivity were assigned in the dispersion package in MT3DMS (Zheng and Wang, 1999). Longitudinal dispersivity was estimated manually, whereas transverse and vertical dispersivities were assigned as ratios of longitudinal dispersivity. The ratios of transverse-to-longitudinal and vertical-to-longitudinal dispersivity were assigned constant values of 0.1 and 0.01, respectively (Zheng and Wang, 1999). The longitudinal dispersivity was adjusted manually until simulated tritium concentrations were the same order of magnitude as measured tritium concentrations. During manual estimation of longitudinal dispersivity, a homogeneous effective-porosity field of 0.008 was specified as an initial condition throughout the model domain.

A longitudinal dispersivity equal to 500 ft was assigned and is reasonable because tritium migration is relatively fast from the HANDLEY nuclear test, where the leading front of tritium has migrated at least 23,800 ft in 40 years (about 600 ft/yr). A longitudinal dispersivity of 500 ft also is supported by results from a review paper that compiled longitudinal-dispersivity estimates from 109 studies of laboratory experiments, aquifer tests, and numerical models (Schulze-Makuch, 2005). The scale of HANDLEY tritium migration is on the order of 25,000 ft, which correlates to a longitudinal dispersivity between 330 and 1,640 ft for basalts (see figure 2 of Schulze-Makuch [2005]). Schulze-Makuch (2005, p. 443) concludes that "*no clear evidence exists for the presence of an upper bound or asymptotic behavior on the relationship for any of the analyzed media*."

An effective tritium matrix-diffusion coefficient of 1.86×10^{-4} ft^2/d was assigned. The matrix diffusion coefficient is the product of tortuosity (0.1) and the tritium free-water molecular diffusion coefficient (1.86×10^{-3} ft^2/d). The assigned matrix diffusion coefficient is based on laboratory and field tracer studies in fractured volcanic rocks at the NNSS (Reimus and Haga, 1999; Reimus and Callahan, 2007; Stoller-Navarro Joint Venture, 2009).

Boundary Conditions

The top surface of the groundwater-flow and transport models is the water table (fig. 7*A*). The steady-state groundwater model and transport model simulate recharge to the top

surface of the first active cell in each model layer (fig. 7*C*). Total recharge to the top of the model domain is 0.1 acre-ft/yr (12.5 ft^3/d), which is equivalent to recharge rates on the order of 1×10^{-5} ft/d. The lower surface of the models, at -4,888 ft below the top of the model domain, is a no-flow boundary in all groundwater-flow and transport models (fig. 7*C*).

Groundwater flows from right to left in the model domain (fig. 7*C*). For all models, the right model domain boundary is a specified flow and the left domain boundary is a general-head boundary (fig. 7*C*). Total specified flow at the upstream (right) boundary is 30 acre-ft/yr (3,600 ft^3/d). This specified-flow rate was obtained from a previously published PMOV groundwater-flow model (Fenelon and others, 2016; Halford, 2016a). Because the PMOV model was published prior to completion of borehole *ER-20-12*, the model was recalibrated after incorporating the steady-state water-level altitude and aquifer-test transmissivity estimates at borehole *ER-20-12* (Jackson, 2021, app. F). Simulated flow rates were extracted from the recalibrated PMOV model, where flow rates within 4,000 ft of the HANDLEY nuclear test averaged 30 acre-ft/yr (Jackson, 2021, app. F).

The water budget of the flow and transport models in this study was qualitatively checked by comparing to water budgets calculated in other studies. The model domain of the flow and transport models occurs in the western Pahute Mesa–Black Mountain area of the PMOV groundwater basin (fig. 1). The recalibrated PMOV groundwater model (Fenelon and others, 2016) and a numerical model of the Death Valley regional flow system (Halford and Jackson, 2020) indicate that 700–800 acre-ft/yr of groundwater flows through the 10-mi-wide, southern outflow boundary of the western Pahute Mesa–Black Mountain area (fig. 1). The flow and transport models in this study have a projected width of 2,000 ft, meaning that these models are simulating 30 acre-ft/yr through 2,000-ft-wide streamtubes. A total of 26, 2,000-ft-wide streamtubes can fit along the 10-mi-wide boundary and, if each streamtube is 30 acre-ft/yr, then the total outflow across the 10-mi-wide boundary is about 800 acre-ft/yr (Jackson, 2021).

Temporal Discretization

Only the transient groundwater-flow and transport models required temporal discretization. Temporal discretization of the transient groundwater-flow model was used to simulate groundwater withdrawals from borehole *ER-20-12* during drilling operations. Temporal discretization of the transport model was used to simulate 50 years of tritium migration from the date of detonation of the HANDLEY test (March 26, 1970) to March 26, 2020.

Transient Groundwater Model

The transient groundwater model is a superposition model. A superposition model simulates relative water-level changes from an arbitrary datum in response to one or more applied stresses. In this study, the transient groundwater model simulates water-level changes from predevelopment (steady-state) conditions in response to groundwater withdrawals (pumping) in borehole *ER-20-12*.

The top surface of the model domain is the predevelopment water table. The transient superposition model has an initial head of 0 ft, which is conceptualized as no water-level change, or drawdown, from predevelopment conditions. Simulated water-level changes in the transient model are relative to predevelopment heads.

The transient groundwater model simulated water-level changes in wells *PM-3-1* and *PM-3-2* from groundwater withdrawals during drilling of borehole *ER-20-12*. The simulation period spanned from November 22, 2015 at 01:14 a.m. to July 1, 2016 at midnight (00:00 a.m.). Seven withdrawal periods were simulated in the transient superposition model: four pumping and three non-pumping periods (table 1). Because symmetry was assumed about the cross-sectional models, one-half of the groundwater-withdrawal rates listed in table 1 were simulated in the transient superposition model.

Transient Transport Model

The transient transport model simulated tritium migration sourced from the HANDLEY nuclear test between the date of detonation (March 26, 1970) and March 26, 2020, a total of 18,264 days. Radioactive decay of tritium was simulated, where tritium has a half-life of 12.3 years (Lucas and Unterweger, 2000). An initial tritium source concentration of 1×10^8 pCi/L was assigned to the HANDLEY cavity-chimney system (Pawloski and others, 2001; U.S. Department of Energy, 2018b) using a computed exchange volume equal to three cavity radii (fig. 7*C*; Stoller-Navarro Joint Venture, 2009). The exchange volume for HANDLEY, assuming three cavity radii of 974 ft based on a minimum of the announced yield, extends from the water table to about 3,700 ft below the water table (fig. 7*C*; Pawloski, 1999; Stoller-Navarro Joint Venture, 2009, table 4-3).

Uniformly distributing the initial tritium source concentration within the cavity-chimney system assumes that thermal-buoyancy effects that drive upward flow through the chimney are instantaneous. This assumption is reasonable because the HANDLEY test was detonated in transmissive rock (see borehole *UE-20j* on fig. 3*A*), which causes the upward and outward movement of tritium through the cavity-chimney system to occur relatively fast (within 1 year) (Carle and others, 2003).

Calibration

Groundwater-flow equations in the steady-state and transient groundwater models were solved using the U.S. Geological Survey (USGS) finite-difference model, MODFLOW-2005 (Harbaugh, 2005). In the transport model, the groundwater-flow equation and advection-dispersion

equation with radioactive decay were solved using SEAWAT (Langevin and others, 2007). Groundwater flow and transport models were calibrated using PEST (Doherty, 2010a). Recharge, hydraulic-conductivity, specific-yield, specific-storage, and effective-porosity distributions were estimated by minimizing a weighted composite, sum-of-squares objective function. The objective function was informed by measurement and regularization observations.

Recharge was estimated at 19 river-cell locations, and hydraulic-conductivity, specific-yield, specific-storage, and effective-porosity distributions were defined with 436 pilot points, where about 75 percent of the parameters were adjusted with PEST (Doherty, 2010a). Differences between measured observations and simulated responses formally defined the goodness-of-fit or improvement of calibration.

Model parameters were estimated using a two-step process (fig. 8). First, steady-state and transient groundwater models were calibrated simultaneously using PEST (fig. 8*A*; Doherty, 2010a). Batch files initially translated estimated hydraulic conductivities, specific yields, and specific storages at pilot points into two-dimensional MODFLOW arrays. Steady-state and transient groundwater models were executed sequentially, where both models used the same hydraulic-property arrays stored in a common directory (Jackson, 2021, app. G). Simulated responses from both models were compared to measured observations. Results from both models simultaneously informed PEST, and parameter changes were estimated iteratively until the objective function had been minimized, resulting in calibration of the groundwater model.

A coupled groundwater-flow and transport model was developed that uses the best-fit estimated recharge and hydraulic-conductivity field from the calibrated groundwater models (fig. 8*B*). Recharge and hydraulic conductivities were assigned in the transport model. Batch files initially translated estimated effective porosities at pilot points into two-dimensional MODFLOW arrays. Measured tritium concentrations were compared to simulated equivalents and results informed PEST. Effective porosities were estimated iteratively until the objective function had been minimized, resulting in calibration of the transport model (Jackson, 2021, app. G).

Measurement Observations

Measurement observations in the steady-state groundwater model include water-level altitudes, vertical-head differences, and aquifer-test transmissivities at boreholes *PM-3*, *ER-20-12*, and *UE-20j*. Steady-state measurement observations are assumed to have been unaffected by the HANDLEY nuclear test and represent predevelopment conditions. Measured water-level changes in wells *PM-3-1* and *PM-3-2* from November 22, 2015 to July 1, 2016 were used as measurement observations in the transient groundwater model. Tritium concentrations in boreholes *PM-3*, *ER-20-12*, and *U-20m PS-1D* were used as measurement observations in the transport model.

Predevelopment Observations—Steady-State Groundwater Model

Measurement observations used in the calibration of the steady-state groundwater model were categorized into three observation groups: (1) water-level altitudes (table 3); (2) vertical-head differences between wells (table 4); and (3) transmissivity estimates from aquifer-test results (discussed herein as measured transmissivities) (table 5). Measured and simulated water-level altitudes were compared from 10 wells in the study area (table 3). Water-level altitude differences between 5 well pairs constrained vertical-head differences between wells in boreholes *ER-20-12*, *PM-3*, and *UE-20j* (table 4). Log-transformed measured and simulated transmissivities were compared at 9 locations (table 5).

Weights were assigned to account for the range of measurement values between the three observation groups. Measured water-level altitudes and vertical-head differences were assigned weights equal to 1, and measured log-transformed transmissivities were assigned higher weights of 20. A higher weight was assigned to measured log-transmissivities that ranged from 0 to 2.9, compared to water-level altitudes that ranged from about 4,366 to 4,670 ft above NGVD 29. Transmissivity observations would be insensitive during calibration if log-transmissivities from aquifer-tests and water-level altitudes in wells were weighted equally. For example, if simulated and measured log-transmissivities are 1.8 and 2, respectively, the residual difference is 10 percent or 0.2. If simulated and measured water-level altitudes are 3,960 and 4,400 ft, respectively, then the residual difference is 10 percent or 440 ft. In both examples, the residual difference is 10 percent. However, a 10-percent difference in log-transmissivity of 0.2 would result in this observation having less sensitivity during model calibration compared to a 10-percent difference in water-level altitudes of 440 ft if both observation groups were weighted equally.

Simulated transmissivities were extracted from the groundwater-flow and transport models using the computer program T-COMP (Halford, 2016b). Simulated transmissivities were computed by defining the volume investigated by each aquifer test and averaging hydraulic conductivities of all model cells that occur within the volume investigated (Halford, 2016b). The volume investigated was set equal to the volume of model cells that intersected the open interval of each well because either the aquifer-test transmissivity was less than 1,000 ft^2/d or small volumes of water were removed during slug testing (Halford and others, 2006). In these cases, the volume investigated is limited to the open interval of the well (Halford and others, 2006). As an example, slug testing of packer-isolated intervals in borehole *UE-20j* indicates that the total transmissivity of the BRA is 177 ft^2/d. Because slug testing displaces relatively small volumes of water, the volume investigated is the three model cells classified as BRA that intersect borehole *UE-20j* in the mHFM of the numerical models.

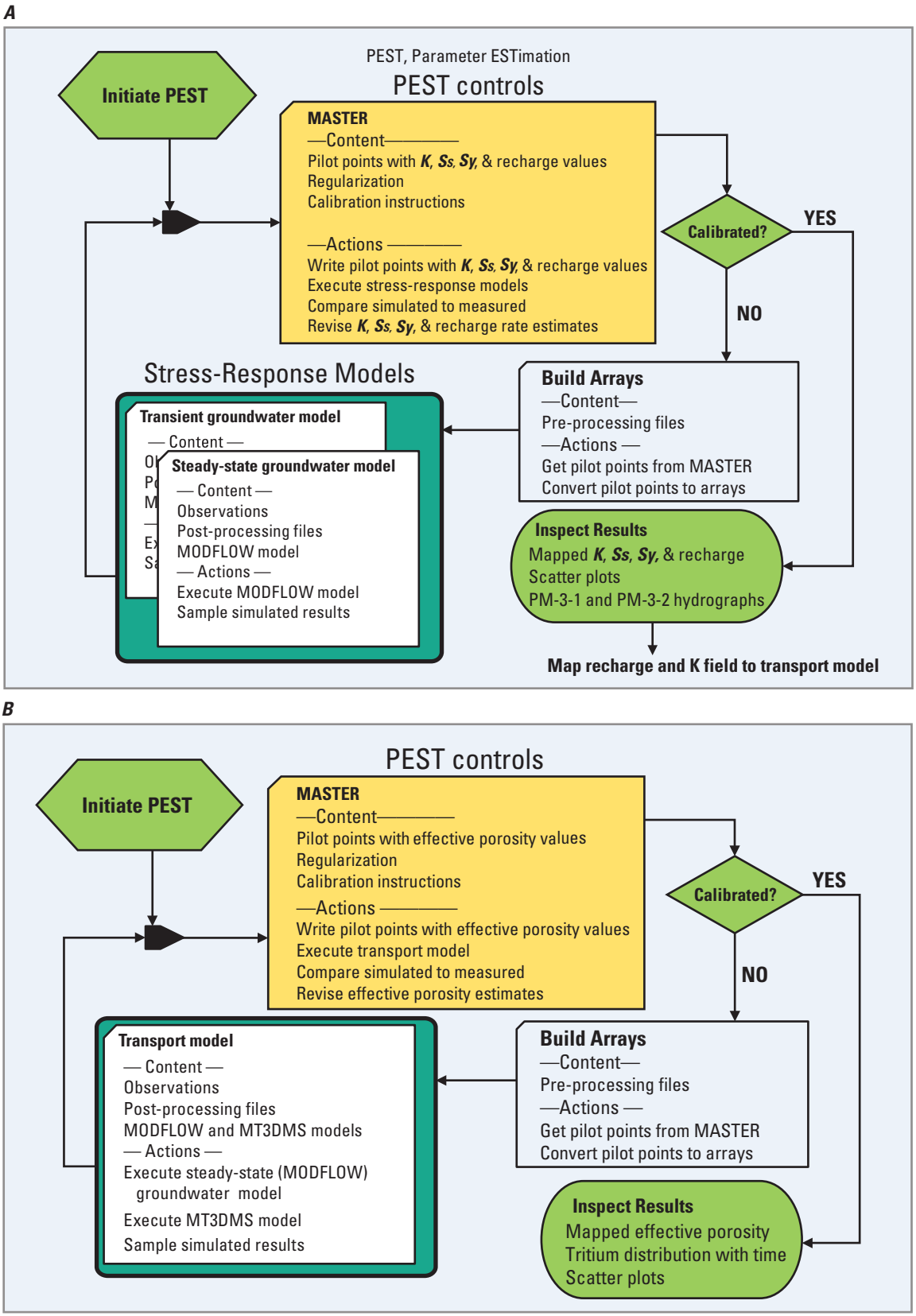

Figure 8. Model-run process of the (*A*) steady-state and transient groundwater-flow models and (*B*) transient transport model, Pahute Mesa, southern Nevada. MODFLOW, three-dimensional groundwater model; MT3DMS, three-dimensional multispecies transport model; *K*, hydraulic conductivity; *Ss*, specific storage; Sy, specific yield.

Table 3. Predevelopment water-level altitudes used as measurement observations and observation weights in the steady-state groundwater model, Pahute Mesa, southern Nevada.

[**USGS well name:** U.S. Geological Survey well name. **USGS site ID:** Unique, 15-digit, U.S. Geological Survey site identification number. NA, not applicable. **Water-level altitude**: Static water-level altitude, in feet above the National Geodetic Vertical Datum of 1929. **Modified HSU:** Primary hydrostratigraphic unit in open interval from modified hydrostratigraphic framework model. Hydrostratigraphic units are defined as follows: BRA, Belted Range aquifer; mCHLFA5, modified Calico Hills lava flow aquifer #5; mPBRLFA, modified pre-Belted Range lava flow aquifer; TCA, Tiva Canyon aquifer; TMWTA, Timber Mountain welded tuff aquifer; mUPCUs, modified upper Paintbrush confining unit–shallow. **Observation weight:** Weight assigned to static water-level altitude observation in numerical models]

USGS well name	USGS site ID	Water-level altitude	Modified HSU	Observation weight
UE-20j (TMWTA)	NA	[1]4,670.0	TMWTA	1
UE-20j (2051-2249 ft)	371801116320312	4,663.2	BRA	1
UE-20j (3487-3685 ft)	371801116320305	4,637.3	mPBRLFA	1
ER-20-12 p4	371652116321805	4,638.3	TMWTA	1
ER-20-12 p3	371652116321804	4,378.0	mCHLFA5	1
ER-20-12 p2	371652116321803	4,378.2	mCHLFA5	1
ER-20-12 p1	371652116321802	4,395.3	BRA	1
ER-20-12 m1	371652116321801	4,404.3	mPBRLFA	1
PM-3-2	371421116333704	4,368.2	mUPCUs	1
PM-3-1	371421116333703	4,366.2	TCA	1

[1]Water-level altitude in TMWTA at borehole *UE-20j* was not measured; water-level altitude is an approximation that is used in model to constrain simulated head.

Table 4. Computed vertical-head differences for five well pairs used as measurement observations in the steady-state groundwater model, Pahute Mesa, southern Nevada.

[**Well pair names:** Wells in the same borehole selected for paired well analysis. Shallow well listed on top. **Open interval depths (feet bls):** Depths, in feet below land surface, to top of uppermost and bottom of lowermost openings in wells. **Water-level measurement dates**: Dates water levels measured, in month-day-year. **Water-level altitudes (ft above NGVD 29):** Altitude of measured water level in feet above the National Geodetic Vertical Datum of 1929. **Vertical-head difference (feet):** Absolute value of water-level altitude in the deep well minus water-level altitude in the shallow well. **Gradient direction:** "Up" and "Down" indicate that calculated vertical-head difference is upward or downward, respectively. **Observation weight:** Weight assigned to vertical-head difference observations in numerical models]

Well pair names	Open interval depths (feet bls)	Water-level measurement dates (mm-dd-yyyy)	Water-level altitudes (ft above NGVD 29)	Vertical-head difference (feet)	Gradient direction	Observation weight
ER-20-12 p4 *ER-20-12 p3*	1,612–2,287 2,510–2,947	01-17-2018 01-17-2018	4,638.3 4,378.0	260	Down	1
ER-20-12 p2 *ER-20-12 p1*	3,053–3,157 3,343–3,725	05-13-2019 05-13-2019	4,378.2 4,395.3	17	Up	1
ER-20-12 p1 *ER-20-12 m1*	3,343–3,725 3,916–4,543	05-13-2019 05-13-2019	4,395.3 4,404.3	9	Up	1
PM-3-2 *PM-3-1*	1,455–1,687 1,872–2,192	06-02-2015 06-02-2015	4,368.2 4,366.2	2	Down	1
UE-20j (2051-2249 ft) *UE-20j (3487-3685 ft)*	2,051–2,249 3,487–3,685	10-25-1964 10-26-1964	4,663.2 4,637.3	26	Down	1

Table 5. Transmissivities estimated from aquifer-test results that were used as measurement observations in the steady-state groundwater model, Pahute Mesa, southern Nevada.

[**USGS well name:** U.S. Geological Survey well name. **T (ft^2/d):** Single-well aquifer-test estimate of transmissivity, in feet squared per day. **Log-T:** log-transformed, single-well aquifer-test estimate of transmissivity, dimensionless. **Modified HSU:** primary hydrostratigraphic unit in open interval from modified hydrostratigraphic framework model. Hydrostratigraphic units are defined as follows: BRA, Belted Range aquifer; mCHZCM, modified Calico Hills zeolitic composite unit; mPBRCUd, modified pre-Belted Range confining unit–deep; mPBRLFA, modified pre-Belted Range lava flow aquifer; mUPCUs, modified upper Paintbrush confining unit–shallow; TCA, Tiva Canyon aquifer; TMWTA, Timber Mountain welded tuff aquifer. **Observation weight:** Weight assigned to log-transformed transmissivity observation in numerical models. **Source:** Reference to aquifer-test analysis and transmissivity estimate]

USGS well name	T (ft^2/d)	Log-T	Modified HSU	Observation weight	Source
UE-20j (TMWTA)	164	2.65	TMWTA	20	Jackson (2021)
UE-20j (2051-2249 ft)	177	2.18	BRA	20	Jackson (2021)
UE-20j (3487-3685 ft)	618	2.88	mPBRLFA	20	Jackson (2021)
ER-20-12 p4	270	2.43	TMWTA	20	Jackson (2021)
ER-20-12 p1	80	1.90	BRA	20	Jackson (2021)
ER-20-12 m1	20	1.30	mPBRLFA	20	Jackson (2021)
PM-3-2	4	0.60	mUPCUs	20	Frus and Halford (2018)
PM-3-1	600	2.78	TCA	20	Frus and Halford (2018)
PM-3	1	0.00	mCHZCM, BRA, mPBRCUd	20	Frus and Halford (2018)

Drawdown Observations—Transient Groundwater Model

Measurement observations used in the calibration of the transient groundwater model were estimated drawdowns in wells *PM-3-1* and *PM-3-2* during the drilling of borehole *ER-20-12*. Estimated and simulated drawdowns were compared in both wells, where each well had 447 drawdown observations that were assigned a weight equal to 10. The weighting assigned to drawdown observations is relatively high, compared to water-level altitude and vertical-head difference observations, because of the small range in estimated drawdowns (0–0.75 ft). The assigned drawdown weight of 10 was selected so that all three steady-state observation groups (water-level altitude, vertical-head difference, and transmissivity) and the drawdown observation group equally contribute to model calibration.

Tritium Observations—Transport Model

Measurement observations used in the calibration of the transport model were tritium concentrations in 7 wells (table 6). Tritium concentrations have been measured in borehole *ER-20-12* only during 2017. However, tritium concentrations have been measured at least 10 times in wells *PM-3-1* and *PM-3-2* from 2010 to 2018 (fig. 5). Because of the large variability (noise) in measured tritium concentrations (fig. 5), which cannot be simulated in the transport model, only tritium concentrations in 2016 were used as measurement observations for wells *PM-3-1* and *PM-3-2*. Measured tritium concentrations in wells *PM-3-1* and *PM-3-2* that were not used in the transport model were qualitatively compared to simulated concentrations as a qualitative assessment of goodness of fit.

Tritium observations were divided into three groups because measured tritium concentrations span five orders of magnitude. Tritium concentrations within the transport model are in units of gram per foot cubed (g/ft^3). The "Large" tritium concentration group contains four tritium observations. The largest concentration (412 g/ft^3; 9,700,000 pCi/L) is the measured concentration in the HANDLEY nuclear test cavity, as measured from post-shot hole *U-20m PS-1D* on January 4, 2012 (table 6; Jackson, 2021, app. C). Large tritium concentrations of 1–2.5 g/ft^3 (25,600–58,000 pCi/L) were measured in wells *ER-20-12 p4*, *ER-20-12 m1*, and *ER-20-12 p1* during July 2017 (table 6). The "Medium" tritium concentration group contains one estimated tritium measurement of 0.018 g/ft^3 (420 pCi/L) in well *ER-20-12 p3*. The "Small" tritium concentration group contains the low measured concentrations of 0.008 g/ft^3 (190 pCi/L) and 0.005 (120 pCi/L) in wells *PM-3-2* and *PM-3-1*, respectively.

Weights assigned to measured tritium observations were adjusted iteratively so all observations in each of the three observation groups affected model calibration. For example, the tritium observation at well *U-20m PS-1D* was assigned a weight of 1, whereas the other three large tritium observations were assigned weights of 50 so that all observations have sensitivity during model calibration (table 6). A low weight (20) was assigned to well *PM-3-2* because a structural error in the model precludes matching tritium concentrations in both wells *PM-3-1* and *PM-3-2* (see section, "Data Incongruencies at Borehole PM-3," for details).

Table 6. Tritium concentrations used as measurement observations in the transport model, Pahute Mesa, southern Nevada, 2012–17.

[**Observation group:** Observation group name used to categorize and assign weights to high (Large), moderate (Medium), and low (Small) tritium concentration observations during model calibration. **USGS well name:** U.S. Geological Survey well name. **Measured tritium (g/ft^3):** Measured tritium concentration, in grams per cubic feet. **Measured tritium (pCi/L):** Measured tritium concentration, in picocuries per liter. **Measurement date:** Date tritium concentration measured, in month (mm)-day (dd)-year (yyyy). **Observation weight:** Weight assigned to measured tritium concentration observation in numerical models. **Source:** Reference to report with measured tritium concentration]

Observation group	USGS well Name	Measured tritium (g/ft^3)	Measured tritium (pCi/L)	Measurement date (mm-dd-yyyy)	Observation weight	Source
Tritium–Large	*U-20m PS-1D*	412	9,700,000	01-04-2012	1	Jackson (2021)
	ER-20-12 p4	2.47	58,000	07-06-2017	50	U.S. Department of Energy (2018a)
	ER-20-12 m1	1.75	41,000	07-12-2017	50	U.S. Department of Energy (2018a)
	ER-20-12 p1	1.09	25,600	07-17-2017	50	U.S. Department of Energy (2018a)
Tritium–Medium	*ER-20-12 p3*	0.018	420	07-24-2017	2,000	U.S. Department of Energy (2018a)
Tritium–Small	*PM-3-2*	0.008	190	09-13-2016	20	U.S. Department of Energy (2018c)
	PM-3-1	0.005	120	09-13-2016	20,000	U.S. Department of Energy (2018c)

Regularization Observations

Tikhonov regularization informed pilot-point values of hydraulic conductivity (foot per day), specific yield (decimal fraction), specific storage (1 per foot), and effective porosity (decimal fraction) that were insensitive to measurement observations (Doherty, 2010a). Tikhonov regularization observations were equations that defined either a preferred value at a pilot point or a preferred relation between pilot points. In the preferred-value approach, a single equation is provided for each adjustable parameter (pilot point) that equates the parameter to the preferred value. Preferred relations between pilot points were specified as ratios of preferred (or expected) values between pilot points, which guided relative differences rather than absolute values.

If the preferred relation is homogeneity, then the preferred ratio between pilot points within an HSU is 1. By invoking homogeneity, Tikhonov regularization limits differences between pilot points by penalizing sharp differences, thereby ensuring relatively continuous distributions (Doherty and Johnston, 2003). Contrasts within HSUs were penalized minimally in areas where data informed the objective function.

Homogeneity was the preferred relation between pilot points for hydraulic conductivity, specific yield, specific storage, and effective porosity. About 150 regularization observations constrained hydraulic-conductivity estimates with preferred relations of 1 between pilot points in each HSU. Preferred values of specific yield, specific storage, and effective porosity were 0.02, 2×10^{-6} 1/ft, and 0.008, respectively. About 15, 50, and 175 regularization observations constrained specific-yield, specific-storage, and effective-porosity values, respectively, with these preferred relations.

Regularization observations were weighted so that preferred relations were emphasized where measurement observations were few. Regularization observations were weighted relative to separation distances between pilot points and the nearest measurement sites. Regularization-observation weights between pilot-point pairs were equal to 1 where the distance between the two pilot points was less than the separation between a measured observation location and the nearest pilot point. Weights between pilot-point pairs decreased as the distance between the pilot points was more than the distance between a measured observation location and the nearest of the two pilot points.

Unrealistic hydraulic-property distributions were avoided partially by preventing overfitting of measurement observations (Fienen and others, 2009). Goodness-of-fit was limited so that the weighted, sum-of-squares error could not be reduced to less than irreducible measurement and numerical model errors. This expected measurement error is a weighted, sum-of-squares error and is the variable PHIMLIM in a PEST control file (Doherty, 2010a). A PHIMLIM of 60 ft^2 was specified for the groundwater models, which is equivalent to root-mean-square errors of 1 and 0.02 ft for water-level measurements and drawdowns, respectively. A PHIMLIM of 5 (g/ft^3) was specified for the transport model, which is equivalent to a root-mean-square errors of 0.01, 0.0001, and 0.0001 g/ft^3 for “Large,” “Medium,” and “Small” tritium concentrations in wells, respectively. These PHIMLIM and root-mean-square

errors approximate the average allowable misfit between the simulated and measured water levels, drawdowns, and tritium concentrations at each well.

Goodness of Fit

Goodness of fit was evaluated with scatter plots of measured and simulated observations, hydrographs of wells *PM-3-1* and *PM-3-2*, and hydraulic- and transport-property distributions. Steady-state calibration primarily was evaluated with scatter plots of simulated and measured water-level altitudes, vertical-head differences, and transmissivities. Calibration of the transient groundwater model was evaluated by agreement between hydrographs of estimated and simulated drawdowns in wells *PM-3-1* and *PM-3-2*. Calibration of the transport model was evaluated primarily with a scatter plot of simulated and measured tritium concentrations.

Predevelopment Observations

Simulated water levels compare favorably to measured water levels in the steady-state groundwater model simulating predevelopment flow prior to the HANDLEY nuclear test (fig. 9). A root-mean-square water-level error of 1.5 ft is small relative to the 300-ft range of measured water levels (fig. 9). Measured water-level altitudes in wells *PM-3-1* and *UE-20j (TMWTA)* range from about 4,366 to 4,670 ft, respectively.

Simulated and measured vertical-head differences compare favorably in the steady-state groundwater model (fig. 10). The root-mean-square, vertical-head difference error is 0.7 ft (fig. 10). The maximum vertical-head difference is 260 ft between wells *ER-20-20 p4* and *ER-20-12 p3*.

Simulated and measured transmissivities agree, with all sites within the 95-percent confidence interval (fig. 11). Simulated and measured transmissivities geometrically average 64 and 80 ft^2/d, respectively. Simulated transmissivities range from 1 to 766 ft^2/d, or about two orders of magnitude, which is similar to the range of measured transmissivities.

Drawdown Observations

Calibration of the transient groundwater model primarily was evaluated with the hydrographs from wells *PM-3-1* and *PM-3-2*. Estimated and simulated drawdowns in wells *PM-3-1* and *PM-3-2* closely match, with root-mean-square errors of 0.04 ft (fig. 12). Estimated drawdowns in both wells were replicated closely, except for a slight under-recovery in the simulated drawdowns after May 2016.

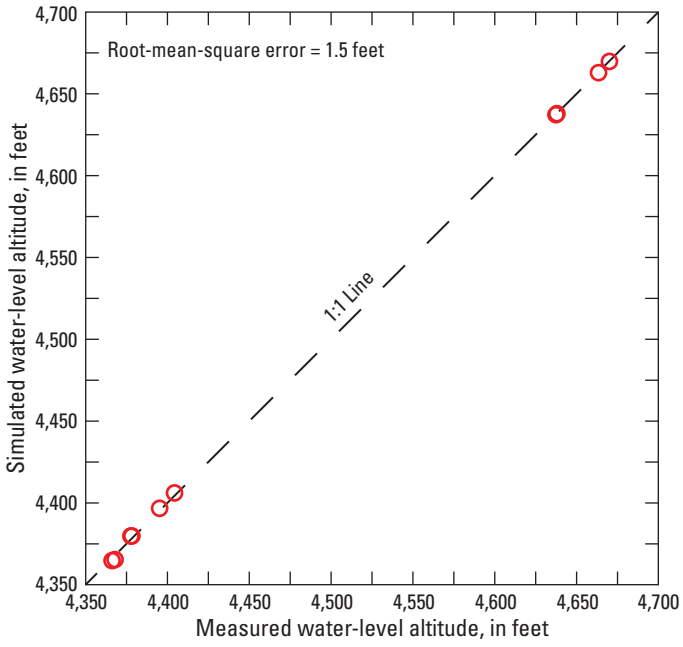

Figure 9. Comparison of measured and simulated water-level altitudes from the calibrated steady-state groundwater model, Pahute Mesa, southern Nevada.

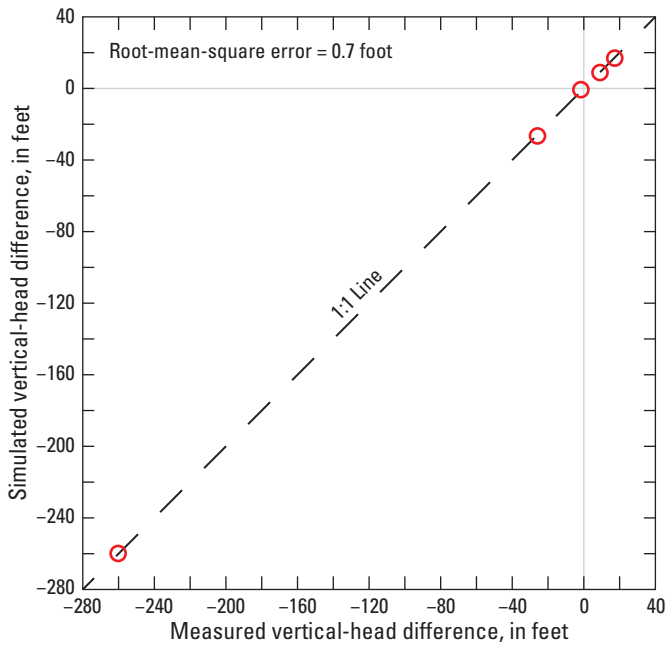

Figure 10. Comparison of measured and simulated vertical-head differences from the calibrated steady-state groundwater model, Pahute Mesa, southern Nevada.

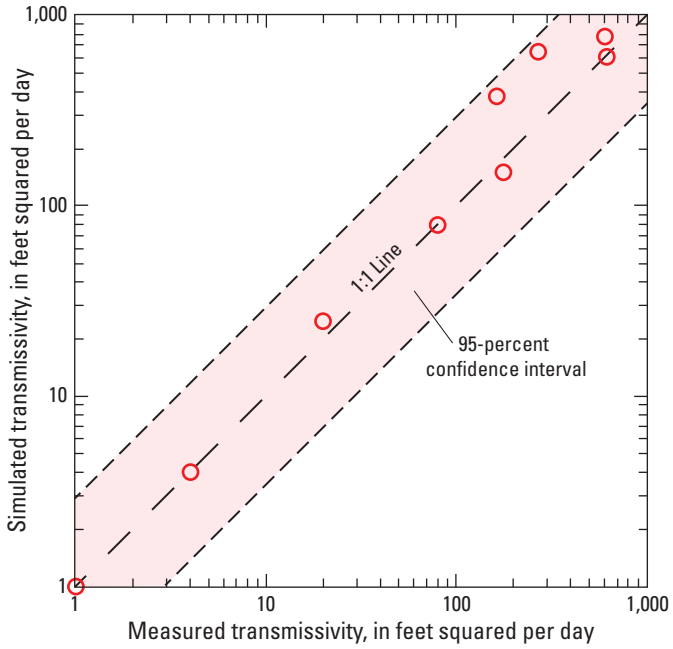

Figure 11. Comparison of measured and simulated transmissivities from the calibrated steady-state groundwater model, Pahute Mesa, southern Nevada. Dashed lines are 95-percent confidence intervals.

Tritium Observations

Calibration of the transport model primarily was evaluated with comparison of tritium concentrations. Simulated tritium concentrations compare favorably to measured tritium concentrations for all wells in the transport model, except well *PM-3-2* (fig. 13). Misfit between simulated and measured tritium concentrations in well *PM-3-2* are discussed in detail in section, "Data Incongruencies at Borehole PM-3." A root-mean-square error of 1 g/ft^3 for tritium concentrations is small relative to the 412 g/ft^3 range of tritium concentrations (fig. 13).

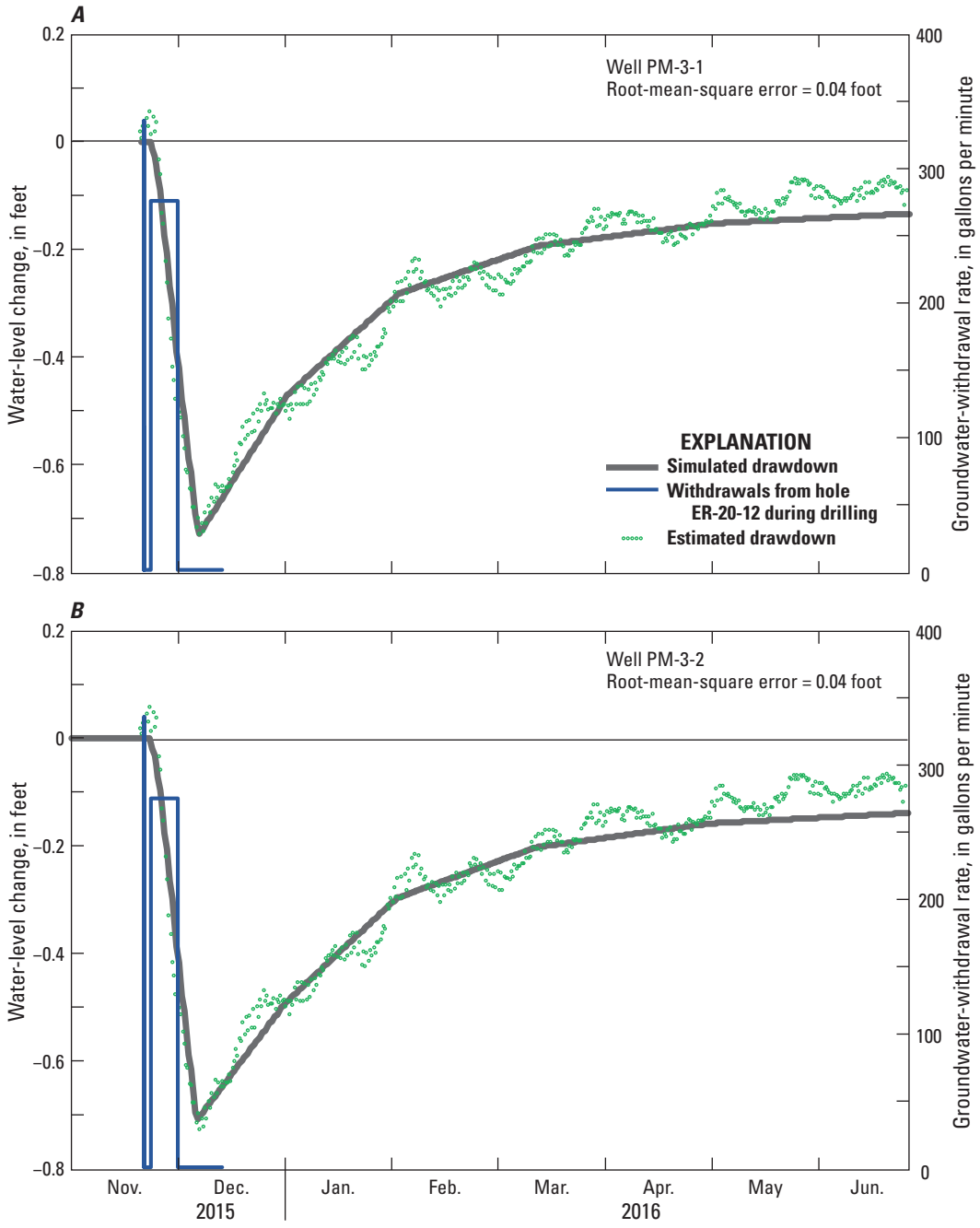

Figure 12. Comparison of estimated and simulated drawdowns in wells *PM-3-1* (A) and *PM-3-2* (B) from the calibrated transient groundwater model, Pahute Mesa, southern Nevada, November 2015–June 2016.

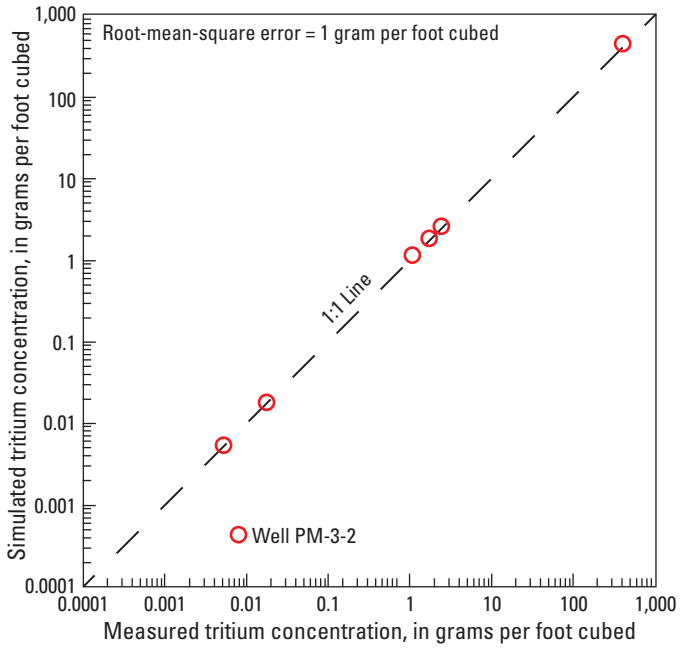

Figure 13. Comparison of measured and simulated tritium concentrations from the calibrated transport model, Pahute Mesa, southern Nevada.

Permeable Pathways from the HANDLEY Underground Nuclear Test

Permeable groundwater pathways from the HANDLEY nuclear test to borehole *PM-3* were discerned from model-simulated distributions of hydraulic conductivity, specific yield, and specific storage (fig. 14). These distributions are consistent with the expected distributions from the conceptual model. Permeable pathways occur within modified HSUs conceptualized as aquifers in the mHFM. The shallow permeable pathway occurs within the semi-perched TMWTA. Deeper permeable pathways occur within the BRA, mPBRLFA, mBZ, and TCA.

The semi-perched aquifer (TMWTA and TMVTA) has the highest geometric-mean hydraulic conductivity of continuous units between the HANDLEY nuclear test and borehole *ER-20-12*. The TMWTA forms the shallow permeable pathway from the HANDLEY test to well *ER-20-12 p4* (fig. 14*B*), where estimated hydraulic conductivities are between 0.01 and 2 ft/d, with a geometric average of 0.25 ft/d (fig. 15). The underlying TMLVTA has a uniform estimated hydraulic conductivity of 0.001 ft/d (fig. 15), which causes the unit to function as a leaky confining unit.

The mCHZCM has the lowest geometric-mean hydraulic conductivity between the HANDLEY nuclear test and borehole *ER-20-12* (fig. 14*B*). Estimated hydraulic conductivities range from 2×10^{-6} to 0.002 ft/d, with a geometric average of 1×10^{-4} ft/d (fig. 15). The mCHZCM directly underlies the semi-perched TMWTA and TMLVTA (fig. 14*A*). Hydraulic conductivities of 2×10^{-6} ft/d were estimated for the mCHZCM near borehole *ER-20-12* (fig. 14*B*). This low hydraulic conductivity isolates the semi-perched aquifer from the regional system and induces the 260-ft vertical-head difference between wells *ER-20-12 p4* and *ER-20-12 p3*.

Permeable pathways in the regional system between the HANDLEY nuclear test and borehole *ER-20-12* occur in the BRA and mPBRLFA (fig. 14*B*). The BRA and mPBRLFA are less permeable than the semi-perched TMWTA. The BRA has estimated hydraulic conductivities that range from 0.003 to 0.2 ft/d, with a geometric mean of 0.01 ft/d (fig. 15). The mPBRLFA has estimated hydraulic conductivities that range from 0.01 and 0.3 ft/d, with a geometric mean of 0.07 ft/d (fig. 15).

A permeable feature, simulated as the mBZ, exists between borehole *ER-20-12* and the Ribbon Cliff structural zone (fig. 14*A*). The mBZ hydraulically connects permeable intervals in the mCHLFA5, BRA, and mPBRLFA north of the Ribbon Cliff structural zone with the TCA south of the structural zone (fig. 14*B*). Estimated hydraulic conductivities within the mBZ range from 0.02 to 12 ft/d, with a geometric mean of 0.9 ft/d (fig. 15).

The permeable pathway between boreholes *ER-20-12* and *PM-3* occurs through the TCA (fig. 14*B*). Aquifer-test results indicate that the TCA is the most likely pathway for the fast propagation of drawdown to borehole *PM-3* from withdrawals in borehole *ER-20-12* (fig. 14*A*). The fast propagation of drawdown to well *PM-3-1* requires the TCA to have high hydraulic diffusivity, defined as the ratio of hydraulic conductivity to specific storage. Therefore, the TCA is expected to have high hydraulic conductivities and low specific storages. Numerical results indicate that the TCA is the most permeable unit in the study area, where estimated hydraulic conductivities range from 0.5 to 320 ft/d, with a geometric mean of 34 ft/d (fig. 15). The TCA and mBZ also have the lowest estimated specific storages (less than 1×10^{-6} 1/ft) in the study area (fig. 14*C*), which increase drawdown propagation through these units. Low specific-storage estimates result from assuming that the entire aquifer thickness is equal to the contributing thickness of permeable fractures in the TCA and mBZ. In actuality, only a few hydraulically connected, permeable fractures likely exist in the TCA that cause the fast propagation of drawdown to wells *PM-3-1* and *PM-3-2*.

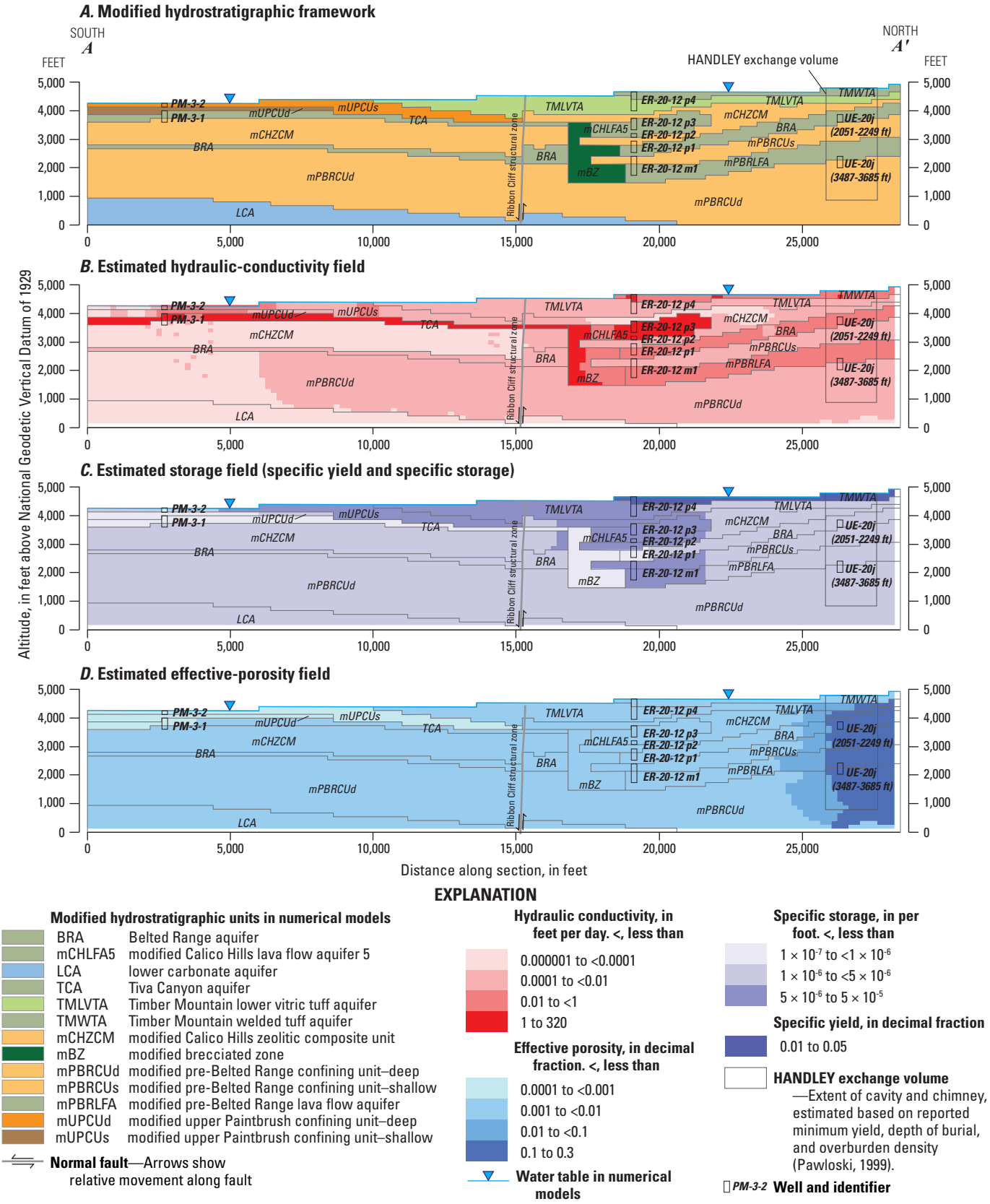

Figure 14. Cross sections showing modified hydrostratigraphic framework in numerical models (*A*), estimated hydraulic-conductivity distribution from steady-state groundwater model (*B*), combined specific-yield and specific-storage distribution from transient groundwater model (*C*), and effective-porosity distribution from transport model (*D*), Pahute Mesa, southern Nevada.

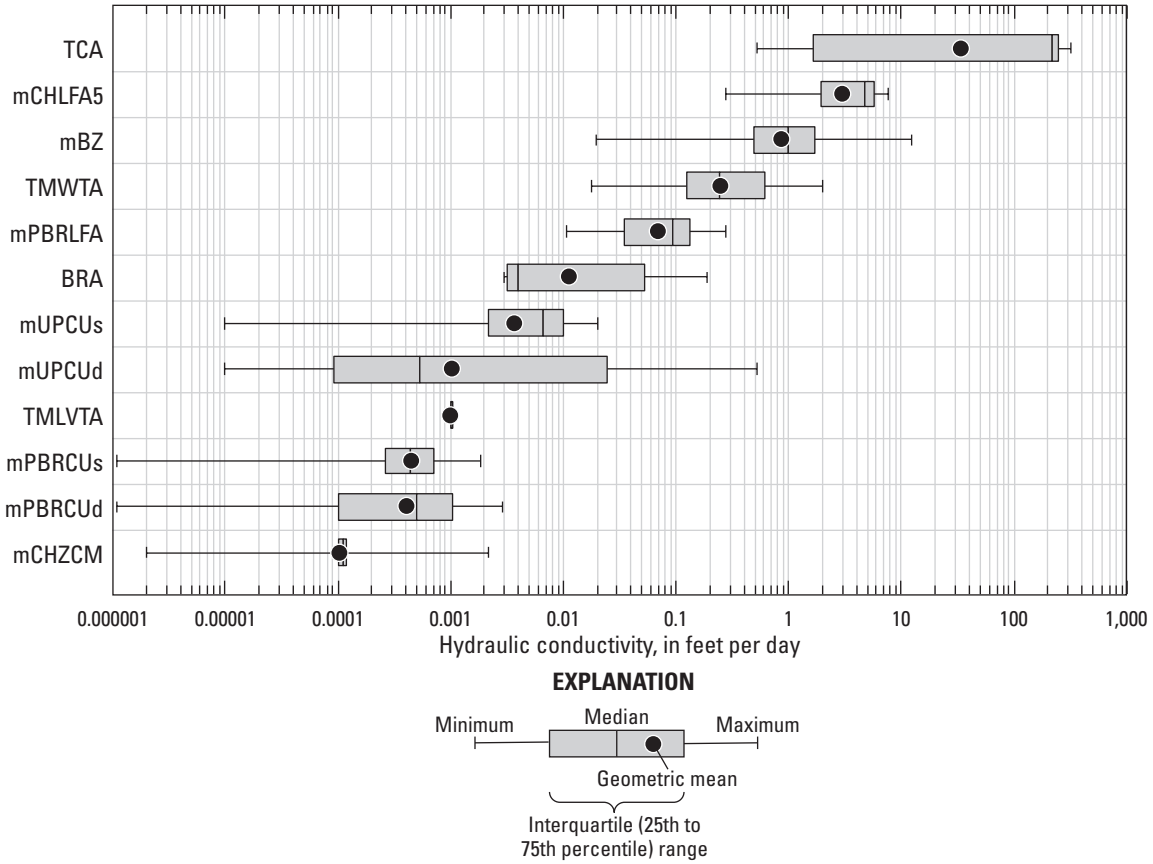

Figure 15. Model-estimated hydraulic-conductivity distributions for modified hydrostratigraphic units from the steady-state groundwater model, Pahute Mesa, southern Nevada.

Tritium Migration from the HANDLEY Underground Nuclear Test

Simulated tritium results suggest that boreholes *PM-3*, *ER-20-12*, and *U-20m* (HANDLEY) do not align along the same groundwater-flow path. Tritium concentrations could not be matched at boreholes *PM-3* and *ER-20-12* when all wells are simulated along the same groundwater-flow path (that is, along the section plane; fig. 7*A*). When all wells in boreholes *PM-3* and *ER-20-12* are simulated in the same plane, the simulated tritium concentration in well *PM-3-1* could be matched only if the simulated tritium concentrations in all wells within borehole *ER-20-12* were overestimated by more than a factor of 2. When borehole *ER-20-12* was shifted one row deeper into the numerical model (that is, into the page, or west), tritium concentrations could be matched in well *PM-3-1* and for all wells in borehole *ER-20-12*. This shift suggests that borehole *ER-20-12* is offset 200 ft east from the groundwater-flow path connecting HANDLEY to borehole *PM-3* (fig. 1). Therefore, model results suggest that the center of the tritium plume likely occurs west of borehole ER-20-12.

One shallow and two deeper tritium plumes are simulated that follow permeable pathways (fig. 16). The initial tritium source distribution is assumed to be well mixed in the cavity-chimney system (fig. 16*B*) and radioactively decays from 100,000,000 pCi/L in 1970 to about 6,000,000 pCi/L by the end of the simulation period in 2020 (fig. 17*A*). Between the HANDLEY test and borehole *ER-20-12*, the simulated shallow tritium plume moves through the semi-perched aquifer (TMWTA and TMLVTA), whereas the simulated deeper tritium plumes move predominantly through the BRA and mPBRLFA (fig. 16). Simulated tritium migration is fastest through the TMWTA (figs. 16*C*, 17*B*). Migration of the simulated deeper tritium plumes is faster through the mPBRLFA compared to the BRA (figs. 16*C*, 17*B*). The leading edges of the shallow and deeper tritium plumes reach borehole *ER-20-12* within 20 years of the detonation of the HANDLEY nuclear test, or by 1990 (fig. 16*D*). Downgradient from borehole *ER-20-12*, the shallow plume stagnates as water spreads slowly into low hydraulic conductivity (0.001 ft/d) and high-porosity TMLVTA (figs. 16*E*–16*G*). The deeper tritium plumes coalesce downgradient from borehole *ER-20-12* and move upward through the permeable mBZ into the TCA (fig. 16*E*). The leading edge of the deep tritium plume reaches well *PM-3-1* between 2000 and 2010, or between 30 and 40 years after the detonation of the HANDLEY nuclear test (figs. 16*E*–16*F*, 17*C*). From 1970 to 2020, the simulated tritium load mostly occurs between borehole *ER-20-12* and the HANDLEY test (fig. 16*G*).

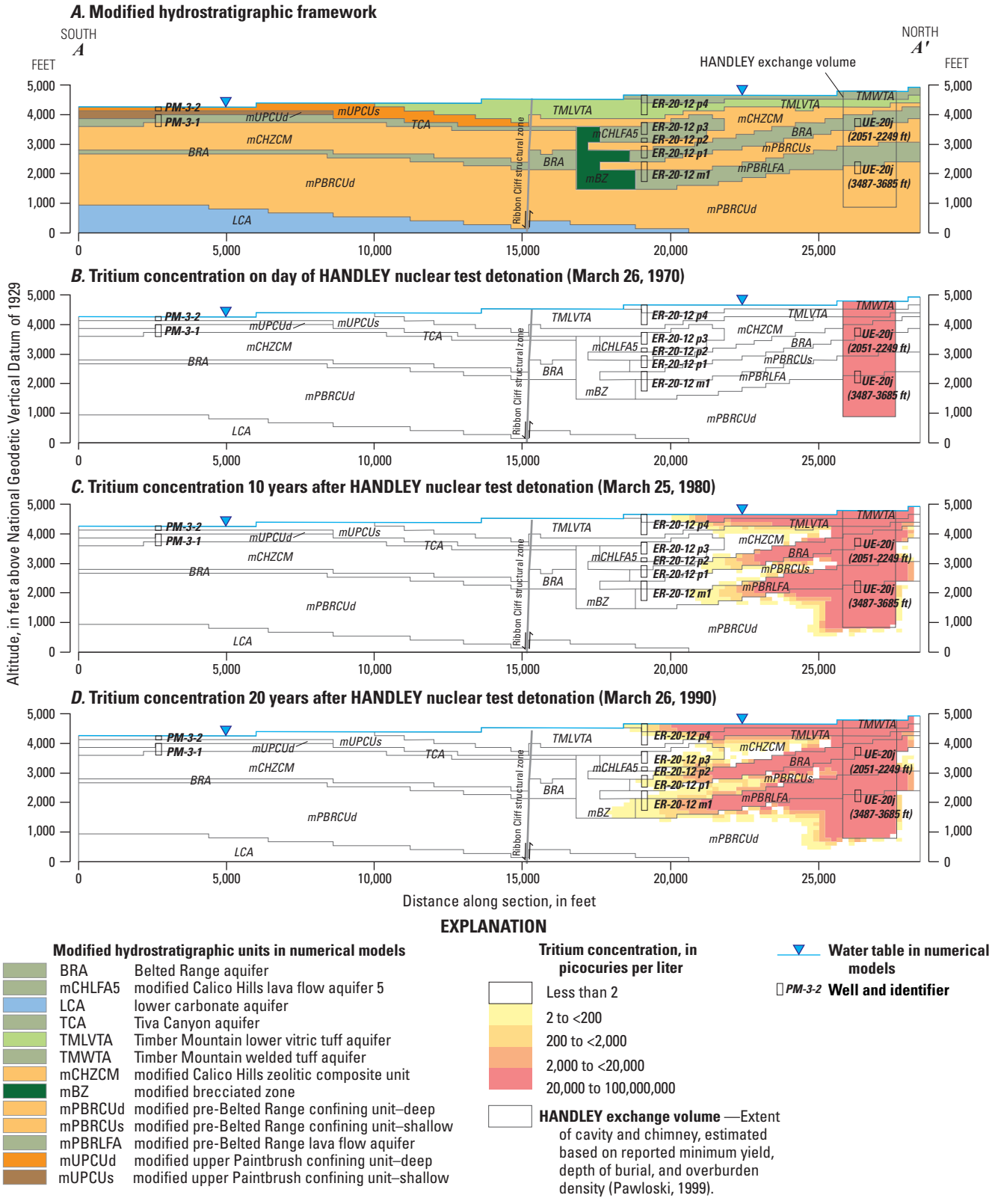

Figure 16. Cross sections showing modified hydrostratigraphic framework in numerical models (*A*); simulated tritium concentration distributions on day 1 of the HANDLEY nuclear test detonation (initial transport model concentration field) (*B*); and simulated tritium concentration distributions at 10 years (*C*), 20 years (*D*), 30 years (*E*), 40 years (*F*), and 50 years (*G*) after the HANDLEY nuclear test detonation, Pahute Mesa, southern Nevada.

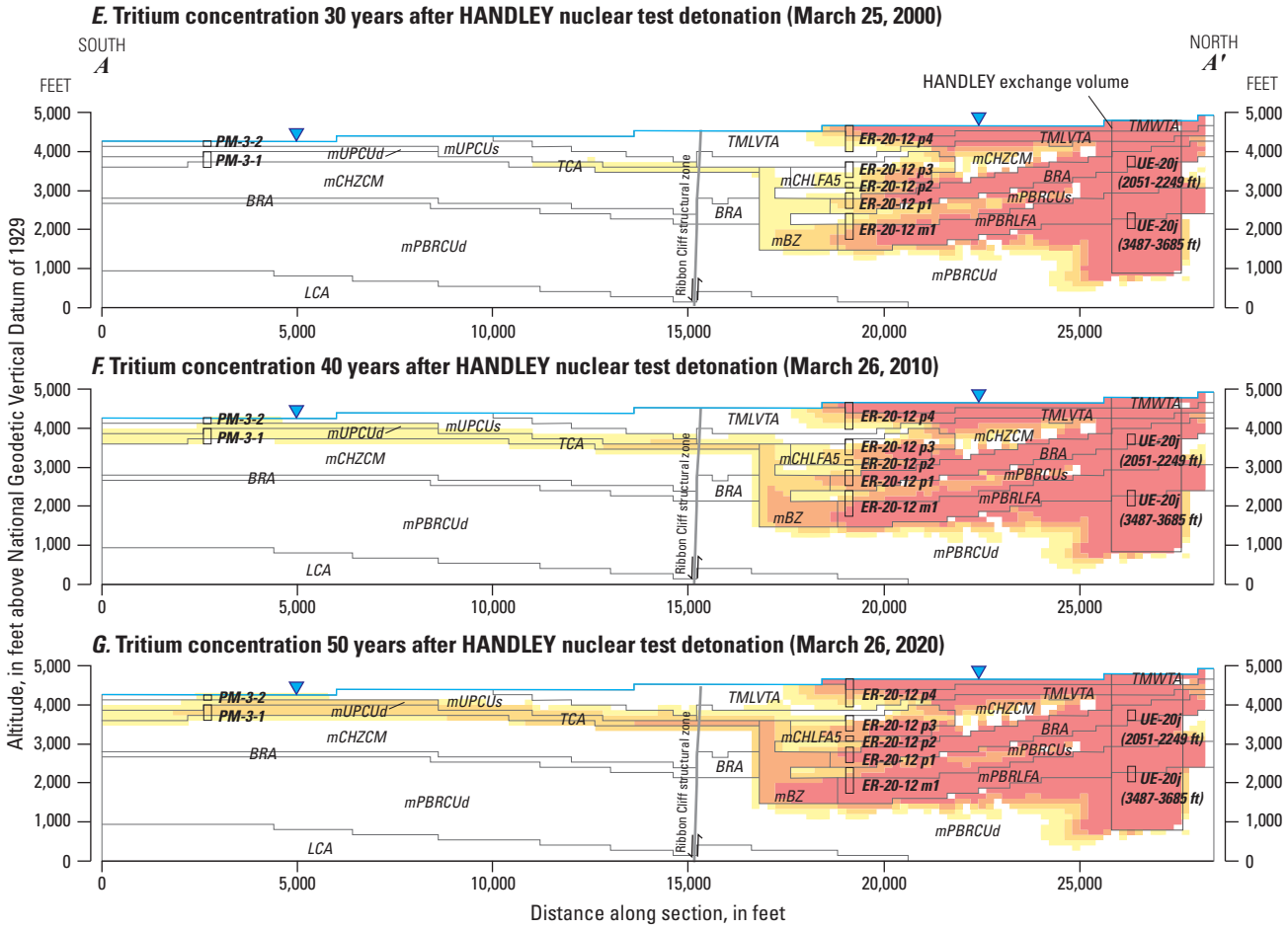

Figure 16.—Continued

From 2010 to 2020, simulated tritium concentrations in shallow well *PM-3-2* range from 0 to 27 pCi/L and cannot be matched to measured tritium concentrations ranging from 10 to 575 pCi/L (fig. 17*D*). A poor match occurs between simulated and measured tritium concentrations because the TMWTA in the mHFM pinches out into low-permeability modified HSUs such as the TMLVTA, mUPCUs, and mUPCUd, which impede shallow tritium plume migration (fig. 16*A*). Revising the mHFM by incorporating a permeable feature in the mUPCUs or mUPCUd is not reasonable because aquifer-test data in all study area boreholes indicate that these modified HSUs are low permeability. Furthermore, a geologic explanation currently is not available for including a permeable feature or new unit within or near the mUCPUs of the mHFM (see section, "Data Incongruencies at Borehole PM-3," for details).

Estimated effective porosities for modified HSUs outside the HANDLEY cavity-chimney system range from about 0.0004 to 0.012, with a geometric mean of 0.008 (fig. 18). The average, model-estimated effective porosity from the transport model is equal to the expected value of 0.008. The mUPCUs and mUPCUd have estimated effective porosities between 0.0004 and 0.0007, which are lower than all other modified HSUs (fig. 18). These low effective porosities were necessary in the model so that tritium concentrations greater than 0 pCi/L could be simulated in shallow well *PM-3-2* (fig. 14*D*). High effective porosities between 0.01 and 0.3 mostly occur within the cavity-chimney system (fig. 18) and are within the range of expected values because rubblization increases the effective porosity of the rock (Pawloski and others, 2001).

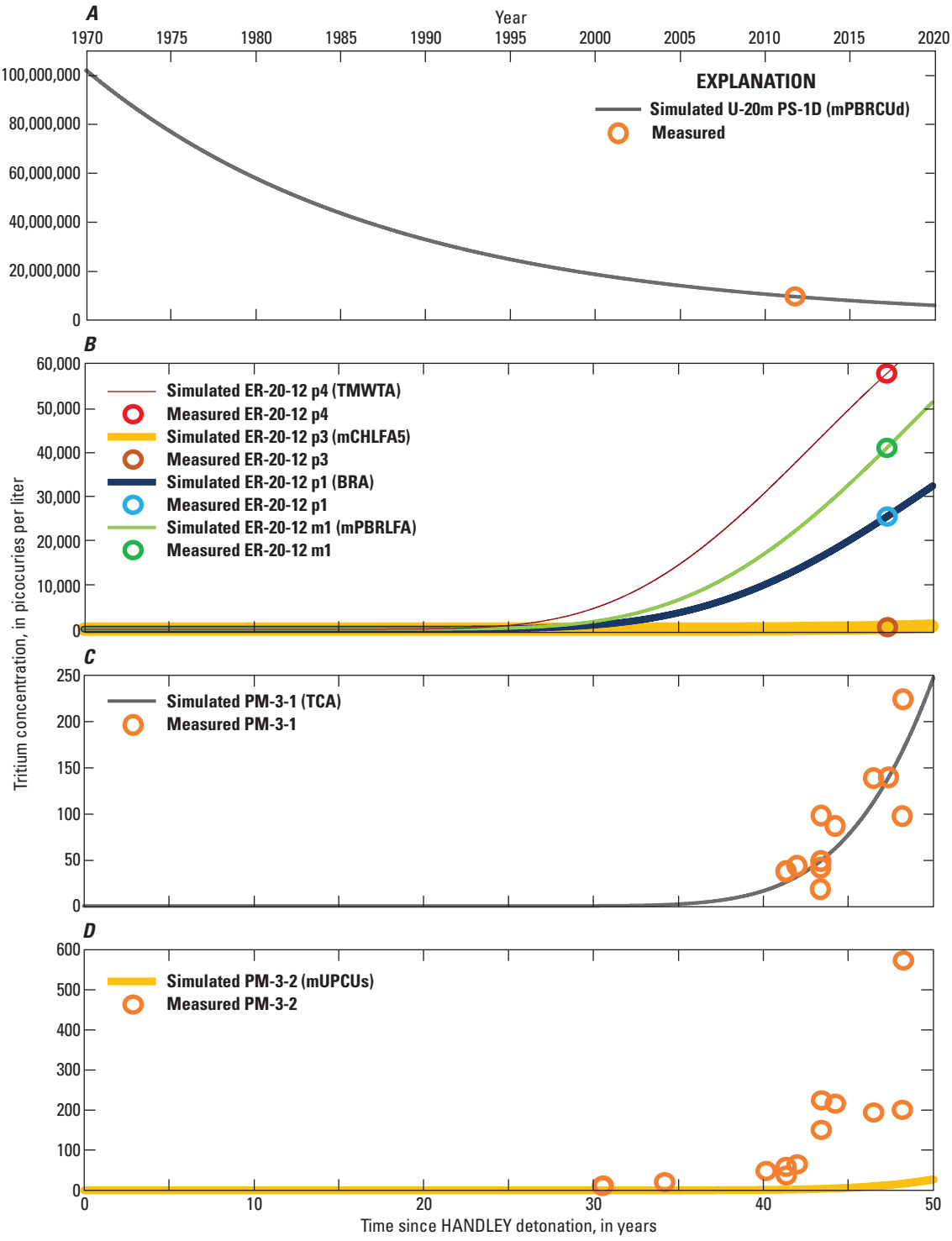

Figure 17. Measured and simulated tritium concentrations with time from the transport model for (*A*) post-shot hole *U-20m PS-1D*, (*B*) wells in borehole *ER-20-12*, and wells (*C*) *PM-3-1* and (*D*) *PM-3-2*, Pahute Mesa, southern Nevada, 1970–2020. Primary hydrostratigraphic units open to wells are shown in parentheses: BRA, Belted Range aquifer; mCHLFA5, modified Calico Hills lava flow aquifer #5; mPBRCUd, modified pre-Belted Range confining unit–deep; mPBRLFA, modified pre-Belted Range lava flow aquifer; mUPCUs, modified upper Paintbrush confining unit–shallow; TCA, Tiva Canyon aquifer; TMWTA, Timber Mountain welded tuff aquifer.

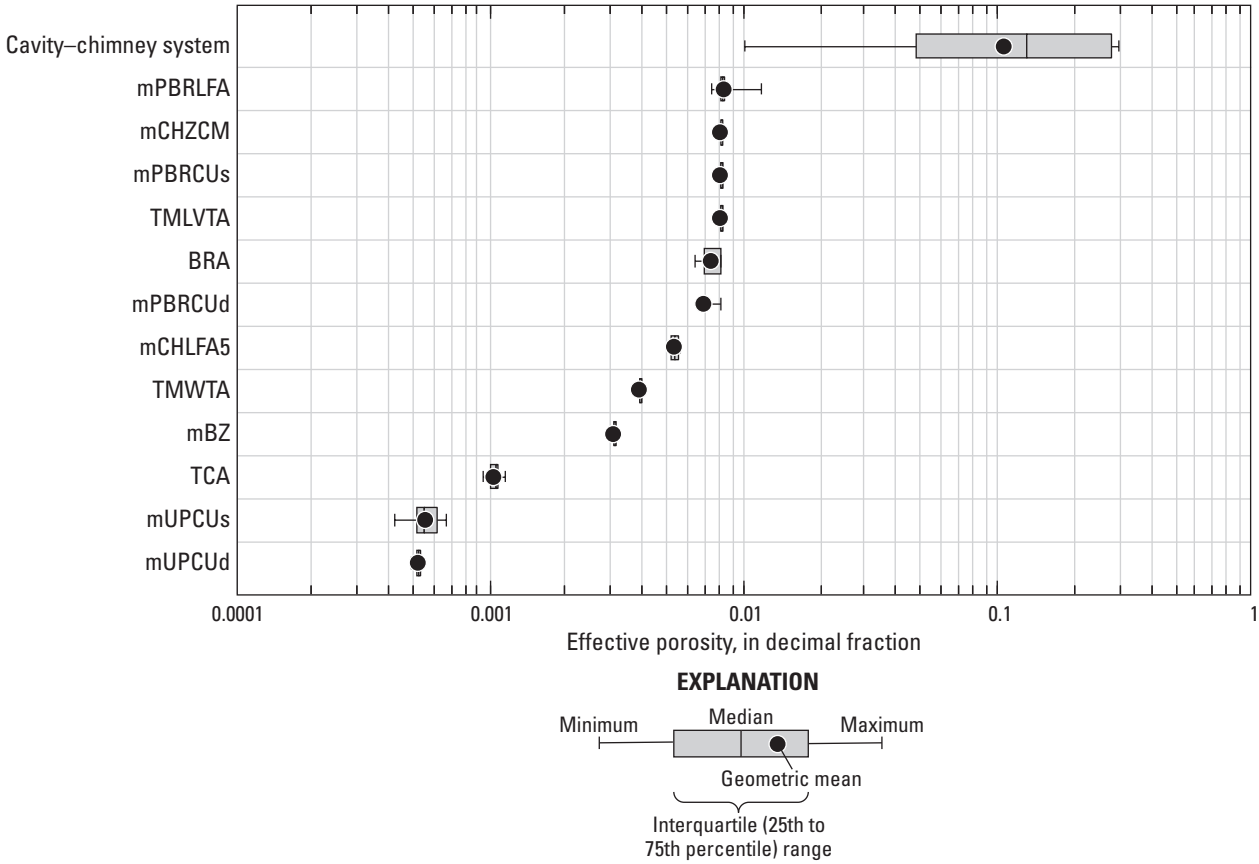

Figure 18. Model-estimated effective-porosity distributions for modified hydrostratigraphic units and the cavity-chimney system from the transport model, Pahute Mesa, southern Nevada.

Data Incongruencies at Borehole PM-3

Borehole *PM-3* was the only location where hydrologic and tritium data could not be reconciled with simulated estimates. Simulated and estimated drawdowns in wells *PM-3-1* and *PM-3-2* closely match, with root-mean-square errors of 0.04 ft (fig. 12). However, the good agreement between simulated and estimated drawdowns occurred at the expense of misfits between simulated and measured tritium concentrations in well *PM-3-2* as well as misfits in vertical-head differences and transmissivities in borehole *PM-3*.

Drawdowns in shallow well *PM-3-2* from withdrawals in borehole *ER-20-12* were simulated by allowing the mUPCUd to be more permeable than the mUPCUs, which contradicts transmissivity estimates. Simulated drawdown propagates from borehole *ER-20-12* through the BRA, mBZ, and TCA toward deep well *PM-3-1* (fig. 14*A*). The simulated drawdown propagates from the TCA into shallow well *PM-3-2* (mUPCUs) through the intervening mUPCUd (fig. 14*A*). Measured and simulated transmissivities match (4 ft^2/d) for the mUPCUs but do not match for the mUPCUd. The measured transmissivity for the mUPCUd is 0.2 ft^2/d (fig. 3*B*), but a high transmissivity of 66 ft^2/d was simulated to allow the hydraulic signal generated from drilling borehole *ER-20-12* to propagate from the deeper TCA into the shallower mUPCUs at well *PM-3-2* (fig. 14*A*). Misfit between measured and simulated transmissivities in the mUPCUd at borehole *PM-3* occurs because there is no permeable pathway in the mHFM (or PMOV HFM) to allow the propagation of simulated drawdown from deeper HSUs toward shallow well *PM-3-2*.

The necessity to simulate a high transmissivity of the mUPCUd causes a mismatch between measured and simulated vertical-head differences at borehole *PM-3*. A 0.5-ft, downward, vertical-head difference was simulated, compared to the measured 2-ft, downward, vertical-head difference. Vertical-head differences would match if the mUPCUd is simulated with a lower transmissivity, compared to the mUPCUs, but this would have caused no drawdown to be simulated in well *PM-3-2* from the drilling of borehole *ER-20-12*.

Simulated tritium concentrations in shallow well *PM-3-2* range from 0 to 27 pCi/L and do not match measured tritium concentrations ranging from 10 to 575 pCi/L (fig. 17*D*). Misfit between simulated and measured tritium in well *PM-3-2* occurs because simulated tritium is migrating from the TCA into shallow well *PM-3-2* (mUPCUs) through the intervening mUPCUd (fig. 16). This causes simulated tritium concentrations to be lower in shallow well *PM-3-2*, compared to

deeper well *PM-3-1*, whereas measured tritium concentrations are consistently higher in shallow well *PM-3-2* than deeper well *PM-3-1*.

A strong hydraulic connection must be present between wells *PM-3-1* and *PM-3-2*. The strong connection is supported by the drawdown responses in the two wells, which were nearly synchronous and had the same drawdown magnitudes (fig. 4). A strong connection also is supported by the presence of tritium in both wells. Two possible sources of the hydraulic connection are an artificial breach in the annulus between wells *PM-3-1* and *PM-3-2* or a natural permeable pathway that connects the TCA and the UPCUs.

Leakage through the annulus of borehole *PM-3* does not explain the hydraulic connection between wells *PM-3-2* and *PM-3-1*. At first glance, annulus leakage may seem like a reasonable explanation for the nearly identical estimated drawdowns in wells *PM-3-2* and *PM-3-1* from groundwater withdrawals during the drilling of borehole *ER-20-12* (fig. 12). If annulus leakage explains the nearly identical drawdowns, then aquifer-test results suggest that the hydraulic response likely propagated from the BRA at borehole *ER-20-12* into the TCA, and then propagated upward from the TCA at well *PM-3-1* through the annulus breach to well *PM-3-2*. However, upward propagation of the hydraulic response from drilling borehole *ER-20-12* does not explain measured tritium concentrations. If a breach in the annulus hydraulically connects the two wells in borehole *PM-3*, then leakage must be downward, based on vertical-head data. Downward annulus leakage means that tritium entering the deeper well through the TCA might be induced into the shallow well during well sampling, but measured tritium in the shallow well could not be higher than in the deep well, which contradicts the measured tritium data.

The argument for annulus leakage also can be rejected based on water levels in wells *PM-3-2* and *PM-3-1*. There is a downward, 2-ft, vertical-head difference between wells *PM-3-2* and *PM-3-1*. If there was a hydraulic connection between these wells through annulus leakage, then the vertical-head difference likely would have changed with time. Long-term water-level trends in wells *PM-3-2* and *PM-3-1* show that the 2-ft, downward, water-level difference is maintained from 1992 to 2016 (fig. 19). Maintaining a 2-ft water-level difference for decades suggests that, if there was annulus leakage, the leakage rate would have been constant with time. Moreover, a constant leakage rate for decades is not likely because constant leakage means that there was no enlargement of the breach to increase leakage and the breach did not seal with time to decrease leakage.

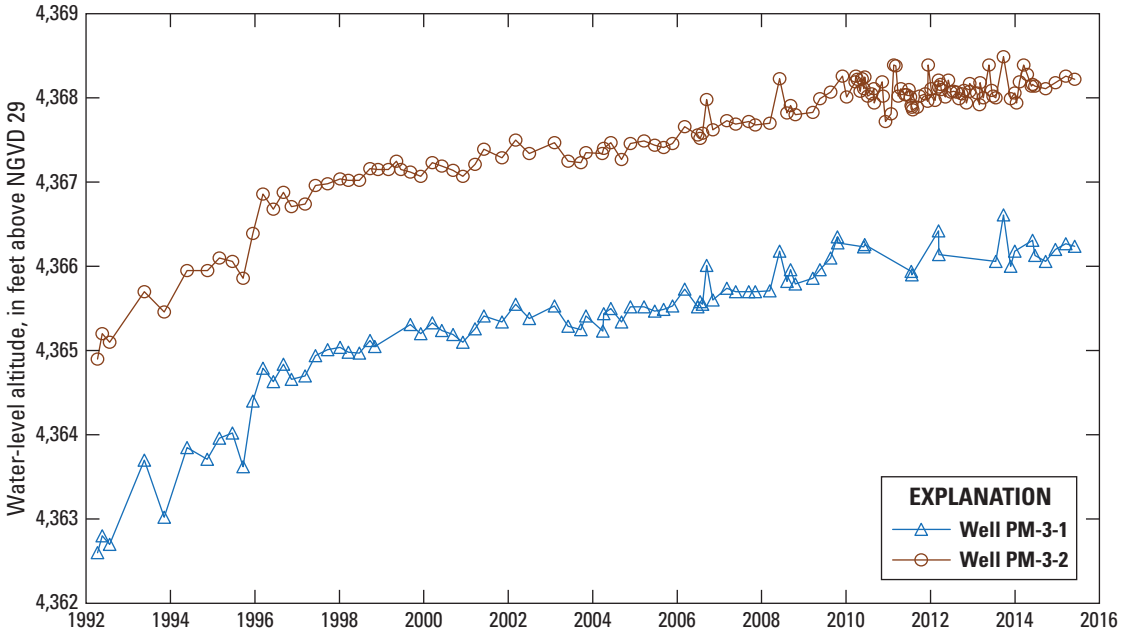

Figure 19. Measured water-level altitudes in wells *PM-3-1* and *PM-3-2*, Pahute Mesa, southern Nevada, 1992–2016.

The mHFM and PMOV HFM do not have a permeable HSU at the water table near borehole *PM-3*, which is necessary to match measured tritium concentrations in well *PM-3-2* and transmissivities and vertical-head differences in borehole *PM-3*. Consistently higher measured tritium in shallow well *PM-3-2*, compared to deeper well *PM-3-1*, and a downward vertical gradient between these wells indicates that a permeable feature exists near the water table that causes faster tritium migration toward the shallow well. This permeable feature is postulated to be near the low-transmissivity UPCU in borehole *PM-3*. The distribution of HSUs at the water table in the PMOV HFM is shown in figure 20. The nearest shallow feature in the PMOV HFM to the UPCU is the TMLVTA, which functions as a leaky confining unit based on aquifer-test data (fig. 20; Jackson and others, 2021). Aquifer-test data do not support the TMLVTA functioning as a transmissive aquifer. No geologic interpretations are available to support modifications to the PMOV HFM that incorporate a permeable HSU at the water table near borehole *PM-3*. For example, the shallow permeable HSU at borehole *ER-20-12* is the TMWTA, but this unit is unsaturated at borehole *PM-3* (fig. 2). Incorporating a permeable feature at the water table would not resolve the other issue of drawdown propagating from the BRA at borehole *ER-20-12* to well *PM-3-2*. Drawdowns were not observed in wells *PM-3-1* or *PM-3-2* from groundwater withdrawals during the advancement of borehole *ER-20-12* through the TMWTA, TMLVTA, and UPCU (fig. 3*C*), which indicates that the hydraulic connection (drawdown propagation) between boreholes *ER-20-12* and *PM-3* primarily occurs through deeper HSUs. Reevaluation of the PMOV HFM and geologic investigations, such as drilling another well, are needed to better understand the shallow permeable pathway to well *PM-3-2*.

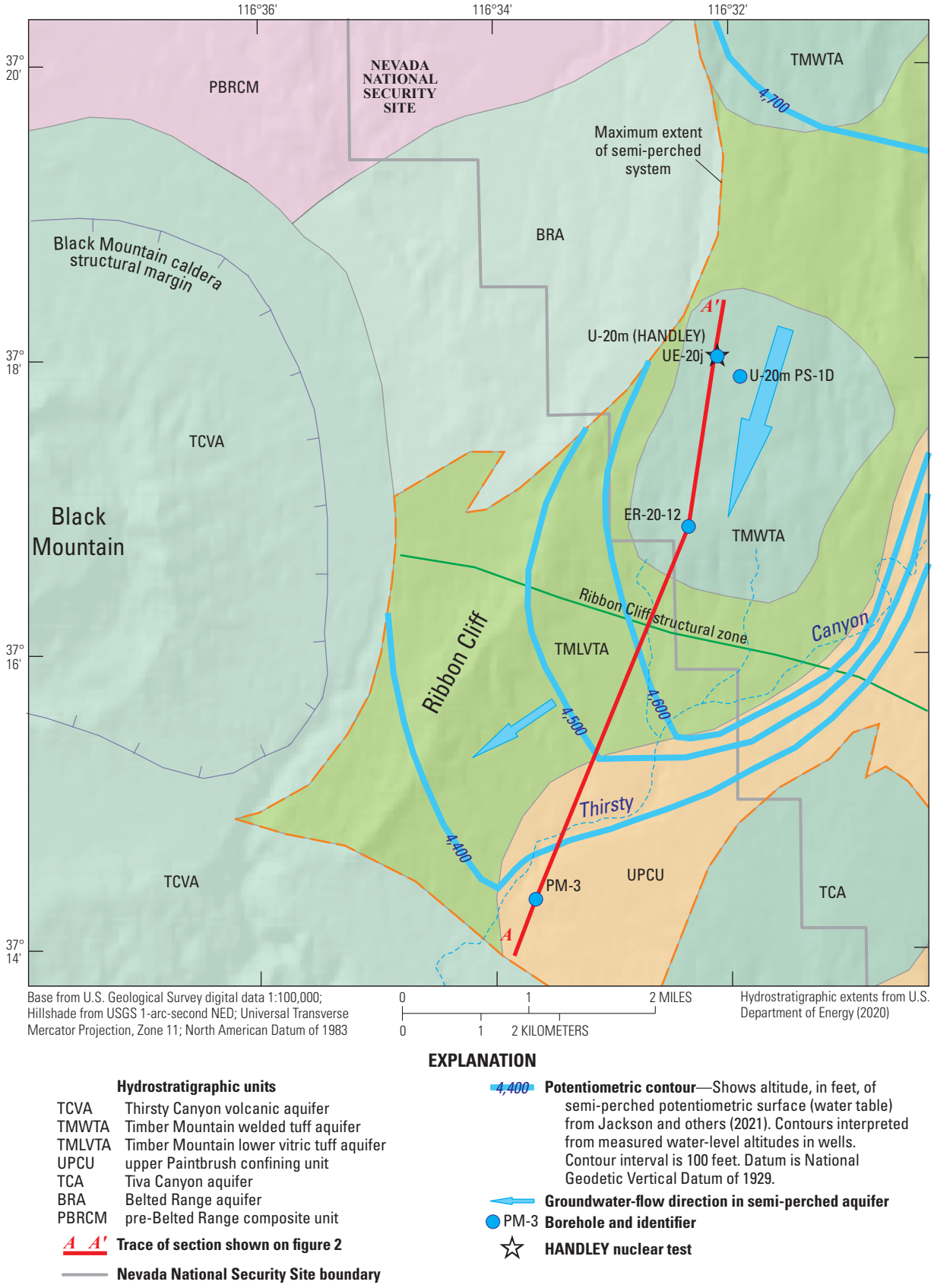

Figure 20. Hydrostratigraphic units and potentiometric contours at the water table, Pahute Mesa, southern Nevada (modified from Jackson and others, 2021).

Model Limitations

Permeable pathways and tritium migration patterns in the groundwater system downgradient from the HANDLEY nuclear test were discerned from model-simulated distributions of hydraulic and transport properties. The plausibility of these estimated hydraulic and transport properties depends on the goodness of fit of simulated water-level altitudes, vertical-head differences, transmissivity estimates, drawdowns, and tritium concentrations to measured equivalents. Model results are limited by (1) simulation of the groundwater system as quasi-three-dimensional; (2) structural errors in the PMOV HFM; and (3) uncertainty in groundwater-withdrawal estimates from the drilling of borehole *ER-20-12*. These limitations result from simplifying assumptions and insufficient data. Spatial and temporal discretization also affect results, but these numerical limitations are minor.

The numerical models were constructed as quasi-three-dimensional models. That is, the third dimension of the model domain was constructed by projecting cross-section plane *A–A′* (fig. 7*A*) 2,000 ft into the page (fig. 7*B*). Projection into the page causes the section plane in figure 7*A* to be the plane of symmetry and allows only one-half of the groundwater system to be simulated explicitly. Use of quasi-three-dimensional models was appropriate for the study purpose, which was to infer the location of permeable pathways between the HANDLEY test and downgradient boreholes *ER-20-12* and *PM-3*. Numerical results along the section *A–A′* are meaningful where geologic, hydrologic, and tritium data have been reconciled. However, the simulated tritium distribution in the X-Z plane (fig. 7*B*) is not realistic because HSUs along section *A–A′* are assumed to be continuous in the projected 2,000-ft third (Z) dimension, rather than honoring the distribution of HSUs in the PMOV HFM.

Estimates of groundwater-withdrawal rates during drilling of borehole *ER-20-12* have low accuracy. Groundwater-withdrawal rates were computed by subtracting injection rates from water-production rates during the drilling of borehole *ER-20-12*. Water-production rates were estimated by Navarro (2016) by differencing lithium-bromide concentrations between injected and discharged drilling fluid at each sample time. Measured lithium-bromide concentrations have uncertainty, especially for highly productive intervals, because increased flow to the borehole diluted the measured concentration in the discharge line and caused concentrations to be below the detection limit within parts of the CHLFA5 and BRA (Navarro, 2016). These unquantifiable uncertainties resulted in maximum groundwater-withdrawal rates that are biased low because water-production rates are biased low. Bias in groundwater-withdrawal rates likely caused the mBZ and TCA between boreholes *ER-20-12* and *PM-3* to have hydraulic conductivities that are biased high and specific storages that are biased low. However, the bias in groundwater-withdrawal rates does not affect the simulated pathways for tritium transport between boreholes *ER-20-12* and *PM-3*.

Spatial discretization of the model domain into a rectangular grid of cells causes hydraulic and transport properties to be averaged in each cell. Each cell was assumed to represent a homogeneous block of a modified HSU. Hydraulic-conductivity, specific-yield, specific-storage, and effective-porosity estimates are effective averages of the properties of the rock matrix and fractures in each model cell. These effective averages do not affect the location of permeable pathways for groundwater flow and tritium transport between the HANDLEY nuclear test and downgradient boreholes.

Hydraulic conductivities estimated between the HANDLEY nuclear test and borehole *ER-20-12* are plausible because these estimates are constrained by transmissivity estimates from aquifer tests. Furthermore, simulated water-level altitudes, vertical-head differences, and tritium concentrations matched measured equivalents in all wells within boreholes *UE-20j* and *ER-20-12*. Hydraulic and transport properties near borehole *PM-3* likely are incorrect because of structural errors in the mHFM. Estimated hydraulic conductivities are erroneously high in the mUPCUd (figs. 14*B*, 15) to allow simulated drawdown to propagate to well *PM-3-2*. Hydraulic-conductivity estimates are biased high in the TCA because of low-accuracy groundwater-withdrawal rates, but the TCA likely is a permeable pathway. Estimated specific storages for the mUPCUs, mUPCUd, and TCA (fig. 14*C*) may be erroneously low from fitting simulated drawdowns to drawdowns estimated from low-accuracy groundwater-withdrawal rates. Estimated effective porosities for the mUPCUs and mUPCUd (figs. 14*D*, 18) are erroneously low to allow simulated tritium to migrate into well *PM-3-2*.

Summary

The HANDLEY nuclear test was detonated at about 2,700 feet (ft) below the water table on March 26, 1970, in Pahute Mesa, south-central Nevada. Measured tritium in boreholes *ER-20-12* and *PM-3* indicates that a shallow tritium plume has migrated more than 1 mile (mi) downgradient from the HANDLEY test within a semi-perched aquifer and deeper tritium plumes have migrated 4.5 mi within underlying regional aquifers. Boreholes *ER-20-12* and *PM-3* are in an area of moderate-to-low transmissivity, but observation of tritium moving 4.5 mi within 40 years of the detonation indicates that high-transmissivity intervals exist. However, the location of these permeable pathways is unknown.

This report integrates geologic, hydrologic, and tritium data to infer the location of permeable pathways downgradient from the HANDLEY nuclear test. Geologic data were obtained from a preexisting Pahute Mesa–Oasis Valley hydrostratigraphic framework model (PMOV HFM). Hydrologic data include water-level altitudes; vertical-head differences; transmissivities estimated from single-well aquifer tests in boreholes *UE-20j*, *ER-20-12*, and *PM-3*; and drawdowns in

wells *PM-3-1* and *PM-3-2*. Tritium data include tritium concentrations measured in boreholes *U-20m PS-1D*, *ER-20-12*, and *PM-3*.

Geologic, hydrologic, and tritium data were integrated to develop a conceptual framework of groundwater flow and tritium migration near and downgradient from the HANDLEY nuclear test. Transmissivities were estimated for hydrostratigraphic units (HSUs) in boreholes *UE-20j*, *PM-3*, and *ER-20-12* from single-well aquifer tests. Drawdowns were estimated in wells *PM-3-1* and *PM-3-2*, where water levels in these wells only responded to groundwater withdrawals during the drilling of borehole *ER-20-12*. Transmissivity estimates from aquifer tests, estimated drawdowns, water-level altitudes, vertical gradients, and measured tritium concentrations were used to infer permeable HSUs and tritium-migration pathways within semi-perched and regional aquifers near and downgradient from the HANDLEY nuclear test. A modified hydrostratigraphic framework model (mHFM) was developed that incorporates HSUs from the PMOV HFM. HSUs from the PMOV HFM were modified by grouping HSUs that, conceptually, are hydraulically similar and splitting HSUs based on water-level, aquifer-test, and tritium data.

Numerical groundwater-flow and tritium-transport models were developed to estimate hydraulic and transport properties between the HANDLEY test and boreholes *UE-20j*, *ER-20-12*, and *PM-3*. Recharge, hydraulic-conductivity, specific-yield, specific-storage, and effective-porosity distributions were estimated with the numerical models by fitting simulated water-level altitudes, vertical-head differences, aquifer-test transmissivities, tritium concentrations, and drawdowns in wells *PM-3-1* and *PM-3-2* to measured equivalents. Simulated and measured observations were matched with root-mean-square errors of 1 ft, 0.02 ft, and 0.0001–0.01 grams per foot cubed for water-level measurements, drawdowns, and tritium concentrations, respectively.

Permeable pathways from the HANDLEY nuclear test to borehole *ER-20-12* occur in the Timber Mountain welded tuff aquifer (TMWTA), Belted Range aquifer (BRA), and the modified pre-Belted Range lava flow aquifer (mPBRLFA), which is a high-transmissivity lava flow in the middle of the pre-Belted Range composite unit. A simulated shallow tritium plume moves through the semi-perched TMWTA, whereas simulated deeper tritium plumes move predominantly through the BRA and mPBRLFA. Simulated tritium concentrations with time indicate that the leading edge of the shallow and deeper tritium plumes reached borehole *ER-20-12* within about 20 years of the detonation of the HANDLEY nuclear test, or by 1990.

An unmapped permeable feature was simulated between borehole *ER-20-12* and the downgradient Ribbon Cliff structural zone. This permeable feature, referred to as the modified brecciated zone (mBZ), hydraulically connects permeable intervals in the modified Calico Hills lava flow aquifer #5, BRA, and mPBRLFA north of the Ribbon Cliff structural zone with the Tiva Canyon aquifer (TCA) south of the structural zone. The mBZ feature can be explained by (1) an incorrect interpretation of the mapped location of the Ribbon Cliff structural zone in the PMOV HFM, where the structural zone is assumed to be provide a permeable pathway; or (2) the structural zone consisting of more than one fault, where one of the faults is assumed to provide a permeable pathway.

The deeper tritium plumes move upward through the permeable mBZ downgradient from borehole *ER-20-12* and then migrate toward well *PM-3-1* through the TCA. The TCA is the most transmissive unit in the study area. The leading edge of the simulated deeper tritium plumes reach well *PM-3-1* between 30 and 40 years after the detonation of the HANDLEY nuclear test, or by 2010. From 1970 to 2020, the simulated tritium load mostly occurs between borehole *ER-20-12* and the HANDLEY test.

Simulated tritium results suggest that boreholes *PM-3*, *ER-20-12*, and *U-20m* (HANDLEY) do not align along the same groundwater-flow path. Tritium concentrations could be matched at well *PM-3-1* and all wells in borehole *ER-20-12* when borehole *ER-20-12* was offset 200 ft east from a straight-line connecting HANDLEY to borehole *PM-3*. This shift suggests that borehole *ER-20-12* is offset 200 ft east from the groundwater-flow path connecting HANDLEY to borehole *PM-3*. Therefore, the center of the plume likely is west of borehole *ER-20-12*.

The mHFM and PMOV HFM do not have a permeable HSU at the water table near borehole *PM-3*, which is necessary to match measured water levels, transmissivities, and tritium concentrations in well *PM-3-2*. Consistently higher measured tritium in shallow well *PM-3-2*, compared to deeper well *PM-3-1*, and a downward vertical gradient between these wells indicates that a permeable feature exists near the water table that causes faster tritium migration toward the shallow well. This permeable feature is postulated to be near low-transmissivity, modified upper Paintbrush confining unit–shallow and modified upper Paintbrush confining unit–deep, which are near the water table in borehole *PM-3*. No permeable unit exists at the water table near borehole *PM-3* in the PMOV HFM and no geologic interpretations are available to support modifying the PMOV HFM by incorporating a permeable HSU. Reevaluation of the PMOV HFM and geologic investigations, such as drilling another well, are needed to better understand the shallow permeable pathway to well *PM-3-2*.

Results of this numerical study will aid in the understanding of tritium migration in a complex hydrologic setting that can be applied to flow and transport modeling at a groundwater-basin scale. Hydraulic- and transport-property estimates from this study can be used to forecast transport from nuclear tests in other areas of Pahute Mesa where data are limited.

Acknowledgments

The author gratefully acknowledges Kevin Day (GeoHydros, LLC), Ken Rehfeldt (Navarro Research and Engineering, Inc.), and Jeff Wurtz (Navarro Research and Engineering, Inc.) for providing data from the Pahute Mesa–Oasis Valley hydrostratigraphic framework model. The author thanks Keith Halford (U.S. Geological Survey, retired) for providing hydrologic expertise and guidance throughout the project. The author also gratefully acknowledges the reviewers of this report for their helpful comments: Tim deBues (Navarro Research and Engineering, Inc.), Joseph M. Fenelon (U.S. Geological Survey, retired), Linzy Foster (U.S. Geological Survey), and Philip M. Gardner (U.S. Geological Survey).

References Cited

Blankennagel, R.K., 1967, Hydraulic testing techniques of deep drill holes at Pahute Mesa, Nevada Test Site: U.S. Geological Survey Open-File Report 67–18, 50 p., https://doi.org/10.3133/ofr6718.

Blankennagel, R.K., and Weir, J.E., Jr., 1973, Geohydrology of the eastern part of Pahute Mesa, Nevada Test Site, Nye, County, Nevada: U.S. Geological Survey Professional Paper 712-B, 35 p., https://doi.org/10.3133/pp712B.

Bouwer, H., and Rice, R.C., 1976, A slug test for determining hydraulic conductivity of unconfined aquifers with completely or partially penetrating wells: Water Resources Research, v. 12, no. 3, p. 423–428, https://doi.org/10.1029/WR012i003p00423.

Carle, S.F., Maxwell, R.M., and Pawloski, G.A., 2003, Impact of test heat on groundwater flow at Pahute Mesa, Nevada Test Site: Lawrence Livermore National Laboratory, Report UCRL-ID-152599, 144 p.

Carroll, R.D., 1981, Seismic velocities and postshot properties in and near chimneys, Proceedings of the Monterey Containment Symposium, Monterey, California, 1981: Los Alamos National Laboratory, Report LA-9211-C, v. 1, p. 379–396.

Cooper, H.H., Jr., and Jacob, C.E., 1946, A generalized graphical method for evaluating formation constants and summarizing well field history: Transactions - American Geophysical Union, v. 27, no. 4, p. 526–534, https://doi.org/10.1029/TR027i004p00526.

Doherty, J., 2010b, Addendum to the PEST manual: Brisbane, Australia, Watermark Numerical Computing, 235 p.

Doherty, J., 2010a, PEST, Model-independent parameter estimation—User manual (5th ed., with slight additions): Brisbane, Australia, Watermark Numerical Computing, 336 p.

Doherty, J., and Johnston, J.M., 2003, Methodologies for calibration and predictive analysis of a watershed model: Journal of the American Water Resources Association, v. 39, no. 2, p. 251–265, https://doi.org/10.1111/j.1752-1688.2003.tb04381.x.

Faunt, C.C., Sweetkind, D.S., and Belcher, W.R., 2010, Three-dimensional hydrogeologic framework model, chap. E *of* Belcher, W.R., and Sweetkind, D.S., eds., Death Valley regional ground-water flow system, Nevada and California—Hydrogeologic framework and transient ground-water flow model: U.S. Geological Survey Professional Paper 1711, p. 161–249, https://doi.org/10.3133/pp1711.

Fenelon, J.M., Halford, K.J., and Moreo, M.T., 2016, Delineation of the Pahute Mesa–Oasis Valley groundwater basin, Nevada (ver. 1.1, May 2016): U.S. Geological Survey Scientific Investigations Report 2015–5175, 40 p., https://doi.org/10.3133/sir20155175.

Fenelon, J.M., Sweetkind, D.S., and Laczniak, R.J., 2010, Groundwater flow systems at the Nevada Test Site, Nevada—A synthesis of potentiometric contours, hydrostratigraphy, and geologic structures: U.S. Geological Survey Professional Paper, v. 1771, https://doi.org/10.3133/pp1771.

Fienen, M., Muffels, C., and Hunt, R., 2009, On constraining pilot point calibration with regularization in PEST: Ground Water, v. 47, no. 6, p. 835–844, https://doi.org/10.1111/j.1745-6584.2009.00579.x.

Freeze, R.A., and Cherry, J.A., 1979, Groundwater: Englewood Cliffs, New Jersey, Prentice-Hall, Inc., 604 p.

Frus, R.J., and Halford, K.J., 2018, Documentation of single-well aquifer tests and integrated borehole analyses, Pahute Mesa and vicinity, Nevada: U.S. Geological Survey Scientific Investigations Report 2018–5096, 22 p., https://doi.org/10.3133/sir20185096.

Garcia, C.A., Halford, K.J., and Fenelon, J.M., 2013, Detecting drawdowns masked by environmental stresses with water-level models: Ground Water, v. 51, no. 3, p. 322–332. https://doi.org/10.1111/gwat.12042.

Halford, K.J., 2016a, Model archive of Pahute Mesa-Oasis Valley groundwater flow model: U.S. Geological Survey data release, https://dx.doi.org/10.5066/F7N58JFQ.

Halford, K.J., 2016b, T-COMP—A suite of programs for extracting transmissivity from MODFLOW models: U.S. Geological Survey Techniques and Methods, book 6, chap. A54, 17 p., https://doi.org/10.3133/tm6A54.

Halford, K., Garcia, C.A., Fenelon, J., and Mirus, B., 2012, Advanced methods for modeling water-levels and estimating drawdowns with SeriesSEE, an Excel add-In, (ver. 1.1, July 2016): U.S. Geological Survey Techniques and Methods, book 4, chap. F4, 28 p., https://dx.doi.org/10.3133/tm4F4.

Halford, K.J., and Jackson, T.R., 2020, Groundwater characterization and effects of pumping in the Death Valley regional groundwater flow system, Nevada and California, with special reference to Devils Hole: U.S. Geological Survey Professional Paper 1863, https://doi.org/10.3133/pp1863.

Halford, K.J., Weight, W.D., and Schreiber, R.P., 2006, Interpretation of transmissivity estimates from single-well pumping aquifer tests: Ground Water, v. 44, p. 467–471, https://doi.org/10.1111/j.1745-6584.2005.00151.x.

Halford, K.J., and Yobbi, D.K., 2006, Estimating hydraulic properties using a moving-model approach and multiple aquifer tests: Ground Water, v. 44, no. 2, p. 284–291, https://doi.org/10.1111/j.1745-6584.2005.00109.x.

Harbaugh, A.W., 2005, MODFLOW-2005, the U.S. Geological Survey modular ground-water model—The ground-water flow process: U.S. Geological Survey Techniques and Methods, book 6, chap. A16, https://doi.org/10.3133/tm6A16.

Harrison, J.C., 1971, New computer programs for the calculation of earth tides: Cooperative Institute for Research in Environmental Sciences, 58 p.

Hasler, J.W., 1965, Preliminary report of the lithology of drill hole UE20j, Pahute Mesa, Nevada Test Site: U.S. Geological Survey Technical Letter Special Studies-I-035, 13 p.

Jackson, T.R., 2021, MODFLOW-2005 and MT3DMS models and supplemental data used to simulate groundwater flow and tritium transport from the HANDLEY underground nuclear test, Pahute Mesa, southern Nevada: U.S. Geological Survey data release, https://doi.org/10.5066/P9YRDQSN.

Jackson, T.R., Fenelon, J.M., and Paylor, R.L., 2021, Groundwater flow conceptualization of the Pahute Mesa–Oasis Valley Groundwater Basin, Nevada—A synthesis of geologic, hydrologic, hydraulic-property, and tritium data: U.S. Geological Survey Scientific Investigations Report 2020–5134, 100 p., https://doi.org/10.3133/sir20205134.

Kilroy, K.C., and Savard, C.S., 1996, Geohydrology of Pahute Mesa-3 test well, Nye County, Nevada: U.S. Geological Survey Water-Resources Investigations Report 95–4239, 37 p., https://pubs.usgs.gov/wri/1995/4239/report.pdf.

Laczniak, R.J., Cole, J.C., Sawyer, D.A., and Trudeau, D.A., 1996, Summary of hydrogeologic controls on ground-water flow at the Nevada Test Site, Nye County, Nevada: U.S. Geological Survey Water-Resources Investigations Report 96–4109, 59 p., https://doi.org/10.2172/257364.

Langevin, C.D., Thorne, D.T., Jr., Dausman, A.M., Sukop, M.C., and Guo, W., 2007, SEAWAT Version 4—A computer program for simulation of multi-species solute and heat transport: U.S. Geological Survey Techniques and Methods, book 6, chap. A22, 39 p.

Lucas, L.L., and Unterweger, M.P., 2000, Comprehensive review and critical evaluation of the half-life of tritium: Journal of Research of the National Institute of Standards and Technology, v. 105, no. 4, p. 541–549, https://doi.org/10.6028/jres.105.043.

Navarro, 2016, Completion report for well ER-20-12—Corrective Action Units 101 and 102, Central and Western Pahute Mesa: U.S. Department of Energy Report DOE/NV--1549, 237 p, https://www.osti.gov/biblio/1295560-completion-report-well-er-corrective-action-units-central-western-pahute-mesa.

Navarro, 2018, Pahute Mesa Phase II well ER-20-12 well development, testing, and sampling data and analysis report: Navarro Report N/0002653--046, 269 p., https://www.osti.gov/biblio/1468441-pahute-mesa-phase-ii-well-er-well-development-testing-sampling-data-analysis-report-revision.

Navarro-Intera, LLC, 2015, Evaluation of PM-3 chemistry data and possible interpretations of 3H observations: Navarro-Intera Report N-I/28091--092, 159 p., https://www.osti.gov/biblio/1172309.

Pawloski, G.A., 1999, Development of phenomenological models of underground nuclear tests on Pahute Mesa, Nevada Test Site—BENHAM and TYBO: Lawrence Livermore National Laboratory Report UCRL-ID-136003, 46 p., https://www.osti.gov/biblio/822992-development-phenomenological-models-underground-nuclear-tests-pahute-mesa-nevada-test-site-benham-tybo.

Pawloski, G.A., Tompson, A.F.B., and Carle, S.F., 2001, Evaluation of the hydrologic source term from the underground nuclear tests on Pahute Mesa at the Nevada Test Site—The CHESHIRE Test: Lawrence Livermore National Laboratory Report UCRL-ID-147023, 507 p., https://www.osti.gov/biblio/15005874-evaluation-hydrologic-source-term-from-underground-nuclear-tests-pahute-mesa-nevada-test-site-cheshire-test.

Prothro, L.B., and Drellack, S.L., Jr., 1997, Nature and extent of lava-flow aquifers beneath Pahute Mesa, Nevada Test Site: U.S. Department of Energy Report DOE/NV/11718-156, 50 p., https://www.osti.gov/biblio/653925-nature-extent-lava-flow-aquifers-beneath-pahute-mesa-nevada-test-site.

Prothro, L.B., Drellack, S.L., Jr., and Mercadante, J.M., 2009, A hydrostratigraphic system for modeling groundwater flow and radionuclide migration at the Corrective Action Unit scale, Nevada Test Site and surrounding areas, Clark, Lincoln, and Nye Counties, Nevada: U.S. Department of Energy Report DOE/NV/25946--630, 145 p., https://www.osti.gov/biblio/950486-hydrostratigraphic-system-modeling-groundwater-flow-radionuclide-migration-corrective-action-unit-scale-nevada-test-site-surrounding-areas-clark-lincoln-nye-counties-nevada.

RamaRao, B.S., LaVenue, A.M., De Marsily, G., and Marietta, M.G., 1995, Pilot point methodology for automated calibration of an ensemble of conditionally simulated transmissivity fields—1, Theory and computational experiments: Water Resources Research, v. 31, no. 3, p. 475–493, https://doi.org/10.1029/94WR02258.

Reimus, P.W., and Callahan, T.J., 2007, Matrix diffusion rates in fractured volcanic rocks at the Nevada Test Site–Evidence for a dominant influence of effective fracture apertures: Water Resources Research, v. 43, no. 7, https://doi.org/10.1029/2006WR005746.

Reimus, P.W., and Haga, M.J., 1999, Analysis of tracer responses in the BULLION forced-gradient experiment at Pahute Mesa, Nevada: Los Alamos National Laboratory Report LA-13615-MS, 62 p, https://doi.org/10.2172/305939.

Russell, C.E., DeNovio, N.M., Farnham, I.M., and Wurtz, J.A., 2017, ER-20-12—A case-study of corrective action investigation in a challenging environment: Proceedings of the Waste Management 2017 Conference, Phoenix, Arizona, March 5–10, 2017, no. 17236, 15 p.

Sawyer, D.A., Fleck, R.J., Lanphere, M.A., Warren, R.G., Broxton, D.E., and Hudson, M.R., 1994, Episodic caldera volcanism in the Miocene southwestern Nevada volcanic field—Revised stratigraphic framework, 40Ar/39Ar geochronology, and implications for magmatism and extension: Geological Society of America Bulletin, v. 106, no. 10, p. 1304–1318, https://pubs.geoscienceworld.org/gsa/gsabulletin/article/106/10/1304/182886/Episodic-caldera-volcanism-in-the-Miocene.

Schulze-Makuch, D., 2005, Longitudinal dispersivity data and implications for scaling behavior: Ground Water, v. 43, no. 3, p. 443–456, https://doi.org/10.1111/j.1745-6584.2005.0051.x.

Soulé, D.A., 2006, Climatology of the Nevada Test Site: National Oceanic and Atmospheric Administration, Air Resources Laboratory, Special Operations and Research Division Technical Memorandum SORD 2006-3, 165 p.

Stoller-Navarro Joint Venture, 2009, Phase I transport model of Corrective Action Unit 101 and 102--Central and western Pahute Mesa, Nevada Test Site, Nye County, Nevada: Stoller-Navarro Joint Venture Report S-N/99205--111, Revision No. 1, 696 p., https://www.osti.gov/biblio/948559-phase-transport-model-corrective-action-units-central-western-pahute-mesa-nevada-test-site-nye-county-nevada-errata-sheet-revision.

Theis, C.V., 1935, The relation between the lowering of the piezometric surface and the rate and duration of discharge of a well using groundwater storage: Transactions - American Geophysical Union, v. 16, no. 2, p. 519–524, https://doi.org/10.1029/TR016i002p00519.

U.S. Department of Energy, 1996, Recompletion report and summary of well history for well PM-3: U.S. Department of Energy Report DOE/NV--437 UC-700, 55 p.

U.S. Department of Energy, 2015, United States nuclear tests, July 1945 through September 1992: U.S. Department of Energy Report DOE/NV--209-REV 16, 129 p., https://www.osti.gov/biblio/1351809-united-states-nuclear-tests-july-through-september-september.

U.S. Department of Energy, 2018a, Calendar year 2017 underground test area annual sampling report, Nevada National Security Site, Nevada: U.S. Department of Energy Report DOE/NV--1599-REV. 1, 156 p., https://www.osti.gov/biblio/1467682-calendar-year-underground-test-area-annual-sampling-report-nevada-national-security-site-nevada-revision.

U.S. Department of Energy, 2018b, Rainier Mesa/Shoshone Mountain flow and transport model report, Nevada National Security Site, Nevada: U.S. Department of Energy Report DOE/NV--1588, 908 p., https://www.osti.gov/biblio/1465819-rainier-mesa-shoshone-mountain-flow-transport-model-report-nevada-national-security-site-nevada-revision.

U.S. Department of Energy, 2018c, Underground Test Area calendar year 2016 annual sampling analysis report, Nevada National Security Site, Nevada: U.S. Department of Energy Report DOE/NV--1589, 123 p., https://www.osti.gov/biblio/1468440-underground-test-area-calendar-year-annual-sampling-analysis-report-nevada-national-security-site-nevada-revision.

U.S. Department of Energy, 2020, Pahute Mesa-Oasis Valley hydrostratigraphic framework model for Corrective Action Units 101 and 102—Central and western Pahute Mesa, Nye County, Nevada: U.S. Department of Energy Report DOE/EMNV--0014, 708 p.

U.S. Geological Survey, 2020, National Water Information System: U.S. Geological Survey web interface, accessed May 2020, at https://dx.doi.org/10.5066/F7P55KJN.

Winograd, I.J., and Thordarson, W., 1975, Hydrogeologic and hydrochemical framework, south-central Great Basin, Nevada-California, with special reference to the Nevada Test Site: U.S. Geological Survey Professional Paper 712-C, 126 p., https://doi.org/10.3133/pp712C.

Zheng, C., and Wang, P.P., 1999, MT3DMS—A modular three-dimensional 239multispecies transport model: U.S. Army Corps of Engineers, Contract Report SERDP-99, p.

Publishing support provided by the U.S. Geological Survey
Science Publishing Network, Tacoma Publishing Service Center

For more information concerning the research in this report, contact the

Director, Nevada Water Science Center
U.S. Geological Survey
2730 N. Deer Run Road
Carson City, Nevada 89701
https://www.usgs.gov/centers/nv-water

ISSN 2328-0328 (online)
https://doi.org/10.3133/sir20215032